APPLICATION OF COMPUTATIONAL FLUID DYNAMICS IN THE FORCED DISPERSION MODELING OF LNG VAPOR CLOUDS

A Dissertation

by

BYUNG KYU KIM

Submitted to the Office of Graduate Studies of
Texas A&M University
in partial fulfillment of the requirements for the degree of

DOCTOR OF PHILOSOPHY

Chair of Committee,	M. Sam Mannan
Committee Members,	Charles Glover
	Mahmoud El-Halwagi
	Andrew Duggleby
Head of Department,	M. Nazmul Karim

August 2013

Major Subject: Chemical Engineering

ABSTRACT

The safety and security of liquefied natural gas (LNG) facilities has prompted the need for continued study of LNG mitigation systems. Water spray systems are widely recognized as an effective measure for dispersing LNG vapor clouds. Currently, there are no engineering guidelines available for water curtain applications in the LNG industry due to a lack of understanding of the complex interactions between the LNG vapor cloud and water droplets.

This research applies computational fluid dynamics (CFD) modeling to investigate the forced dispersion of LNG vapor using upward-oriented full-cone spray nozzles. A Eulerian-Lagrangian approach was applied to simulate the energy and momentum exchange between the continuous (gas flow) and discrete (droplets) phases. Discussed are the physical parameters that are essential inputs to the CFD simulation of the water spray-LNG system. The experimental data collected from the Mary Kay O'Connor Process Safety Center's outdoor LNG spill work in March 2009 at the Brayton Fire Training Field were used to calibrate the physical parameters. The physical mechanisms of the water spray application were investigated using LNG forced dispersion modeling. The effects of momentum imparting from the droplets to the air-vapor mixture, thermal transfer between the two phases (droplet/vapor) and effects of various levels of air entrainment rates on the behavior of the LNG vapors are evaluated. Lastly, the key parametric dependences of the design elements for an effective water curtain system are investigated. The effects of different droplet sizes, droplet

temperatures, nozzle cone angles, and installation configurations of water spray applications on LNG vapor behavior are analyzed.

This work aims to investigate the complex interaction of the water droplet-LNG vapor system, which will serve in developing guidelines and establishing engineering criteria for a site-specific LNG mitigation system. Finally, the potentials of applying CFD modeling in providing guidance for setting up the design criteria for an effective forced mitigation system as an integrated safety element for LNG facilities are discussed.

DEDICATION

To my family and friends for all the endless supports and grateful encouragements in facing all the challenges in finishing this dissertation.

ACKNOWLEDGEMENTS

I would like to acknowledge and show my greatest appreciation to my advisor, Dr. M. Sam Mannan, for all his support and guidance throughout the course of this research. His professionalism and leadership has guided me to be ready for my next career, not only as an expert in process safety field, but as a professional team player as well. I also would like to thank my committee members, Dr. Charles Glover, Dr. Mahmoud El-Halwagi, and Dr. Andrew Duggleby, for their continuous supports and constructive suggestions.

I am very grateful to Dr. Ray Mentzer and Dr. Dedy Ng, for providing me with valuable guidance as team leader. Special thanks to the previous LNG team members, Dr. Geunwoong Yun, Dr. Morshed Rana, Dr. Ruifeng Qi, and Ms. Carolina Herrera, for providing me with great support during the initial stage of my research. I want to thank Ms. Valerie Green, Ms. Donna Startz, Ms. Tricia Hasan, and Ms. Towanna Arnold, for all their continuous supports. Finally, a great thanks also goes to all the friends and colleagues at the Mary Kay O'Connor Process Safety Center.

TABLE OF CONTENTS

Page

LIST OF FIGURES

Page

LIST OF TABLES

Page

CHAPTER I

INTRODUCTION AND LITERATURE REVIEW

1.1 Natural Gas

1.1.1 Natural Gas Overview

Natural gas is produced in conjunction with the crude oil or by its own (Mokhatab et al., 2006). It is mainly composed of methane, and depending on the conditions it was formed, natural gas also contains some heavier hydrocarbons, and toxic or acid contaminant materials. Natural gas is categorized as 'dry' if it is mainly composed of methane and 'wet' when it is combined with other heavier hydrocarbons.

The relative molar mass of natural gas is 17 to 20 and boiling temperature is around –162 °C. Natural gas becomes flammable between the ranges of 5 to 15 volume % and the properties vary depending on the composition of the mixture. Because the natural gas doesn't have any odors or colors, an odorant is added before reaching the final customers to detect any leaks. The value of the natural gas is converted and measured in British thermal units (Btu) and the quality requirement is provided in Btu-cubic foot.

1.1.2 Natural Gas Productions and Consumptions

The non-associated gas refers to the natural gas from the conventional gas fields, which can easily be extracted by allowing the gas to flow by its own pressure. The associated gas is extracted from the conventional oil production. The lighter

hydrocarbons are separated from the crude oil as they are extracted from the oil well. There are various forms of continuous gas (or unconventional gas), such as tight gas, coal bed methane (CBM), natural gas from geopressurized aquifers, gas hydrates, and deep gas. The unconventional gases are normally captured or dissolved in different forms, and may require further processing to extract the natural gas.

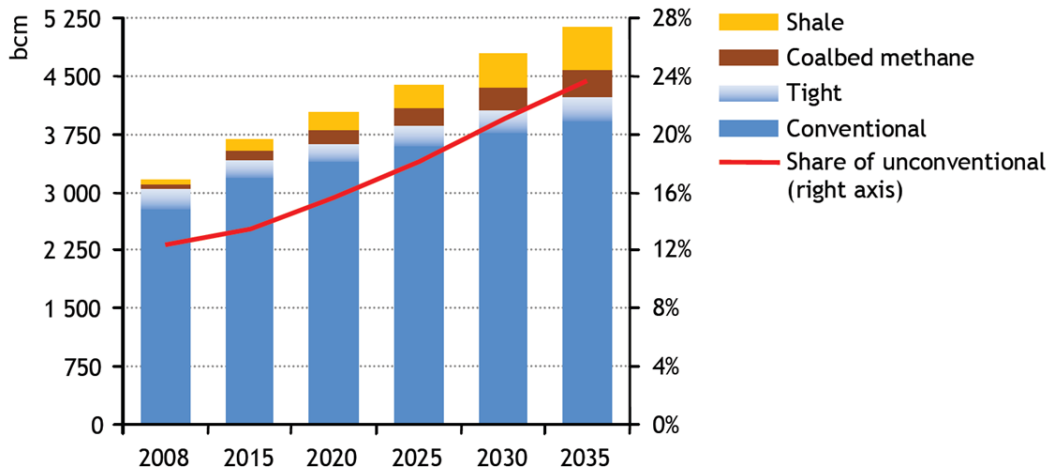

Fig. 1. Natural gas production by type worldwide (IEA, 2011)

The natural gas is expected to become the second largest energy source worldwide by 2030, supporting 25% of the total world energy demand (IEA, 2011). In keeping up with fast growing demands, the natural gas production will increase more than 50% by 2035, which will be more than double of the size compared to the production level in 2000 globally. Fig. 1 shows the expected natural gas production worldwide by its type. The share of conventional gas will decrease as the development of unconventional gas is expected to double by 2035.

Natural gas has been recognized as compatible energy source for the industry for having one of the cheapest heat content (dollar per Btu) compared to other fossil fuels (DOE, 2003b). It is widely used as an energy source supplied to boiler fuel or process heating equipment directly or converted chemically to raw materials for manufacturing other chemicals. It is considered one of the environmentally friendly fuels because of its low carbon, sulfur, and nitrous emissions when consumed, compared to coal or crude oil products.

Natural gas has played a significant role in providing a reliable energy source in US. The total share of natural gas in US energy consumption was approximately 25% in 2010 and is expected to grow gradually, mainly led by the increase of power generation (EIA, 2012). The natural gas was used mostly in the power generator sector (34%) and industrial applications (31%). The natural gas also provided heating and cooking for the residential (21%) and commercial usage (14%). More than 60 million US residential households rely on natural gas.

1.1.3 Transportation and Inter-regional Trade

The inter-regional gas trades will continue to grow as natural gas is expected to play a bigger role in the world energy consumption (EIA, 2011). It is difficult and expensive to store natural gas in large quantities; therefore, it is critical to develop an effective transportation chain of the natural gas (Dawe & Lucas, 2000). Fig. 2 shows the natural gas transportation illustrated for pipeline and LNG trade worldwide.

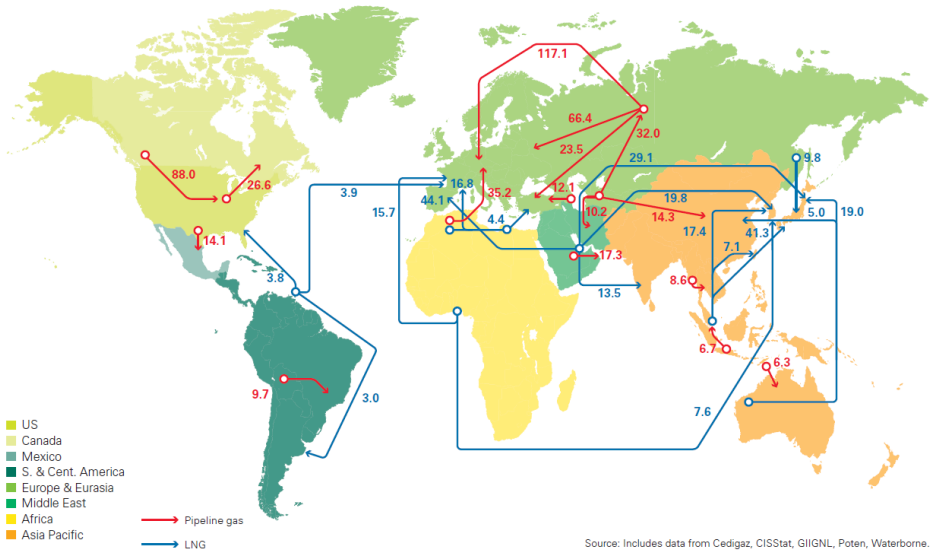

Fig. 2. Major trade movement of natural gas (BP, 2012)

Most of pipeline transportation had been limited to transnational because of the limited infrastructure. The natural gas can also be compressed at very high pressure to be transported through marine ships. The compressed natural gas (CNG) provides a flexible solution for inter-regional trade for short distance transportation. For longer distance transportation, liquefied natural gas (LNG) has been recognized as an economical transportation since mid-1970s. The natural gas is liquefied and transported through marine ships in large quantities. The recent expansions of LNG facilities are playing a significant role in boosting the natural gas trade globally (Kumar et al., 2011). The liquefaction capacity of natural gas is expected to double by 2035, providing the flexibility in diversifying the energy market worldwide.

1.2 Liquefied Natural Gas

1.2.1 LNG Overview

1.2.1.1 LNG Properties

There are significant discrepancies between the gas reserves and natural gas demand worldwide and an alternative means of transportation needed to support the inter-regional gas trade (DOE, 2003a). LNG was first introduced in 1964, and the LNG trade has dramatically been expanding to support the increasing demands of natural gas globally. The natural gas is liquefied by sub-cooling below its boiling temperature approximately around –162 °C (–260 °F) at an atmospheric pressure (BP, 2007).

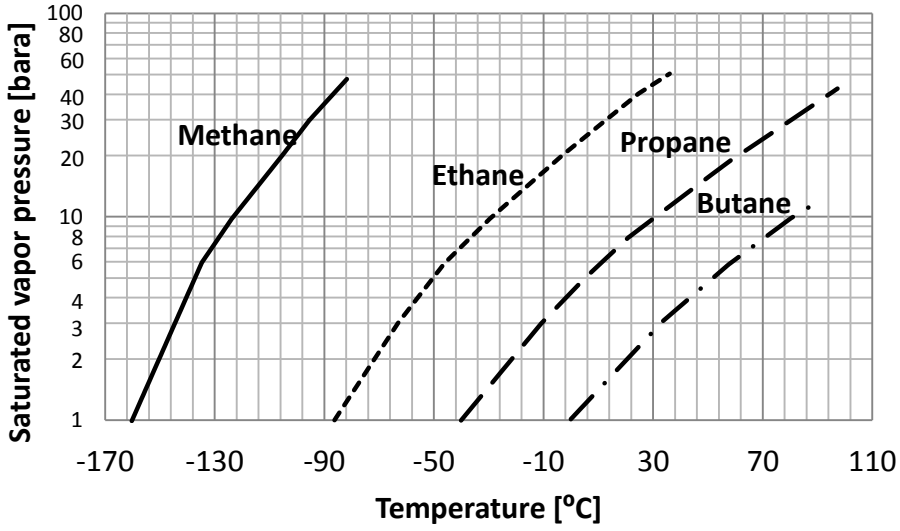

Fig. 3. Pressure/temperature curve for hydrocarbon gases [Adopted and modified from (ISGINTT, 2010)]

Fig. 3 shows the vapor pressure exerted by various hydrocarbons. The saturated vapor pressure is the pressure generated from the saturated vapor at a particular temperature. The point where the pressure intersects with the temperature axis indicates the atmospheric boiling temperature. The natural gas, which is mainly composed of methane, will liquefy to the volume that is 600 times less than at its gas phase around 111 K, allowing the transportation of bulk volume through specially designed marine vessel. Generally, LNG becomes more economical, when transporting the natural gas more than 1120 km (700 mi) (Foss, 2007). LNG is odorless, colorless, non-corrosive and non-toxic, and will initially be heavier than air and disperse at the ground level. When LNG vapors are warmed up to –107 °C (–160 °F), the vapor clouds will become positively buoyant and start dispersing to atmosphere.

1.2.1.2 LNG Supply Chain

In the LNG industry, there are four supply chains: exploration and production, liquefaction, shipping, and regasification and storage.

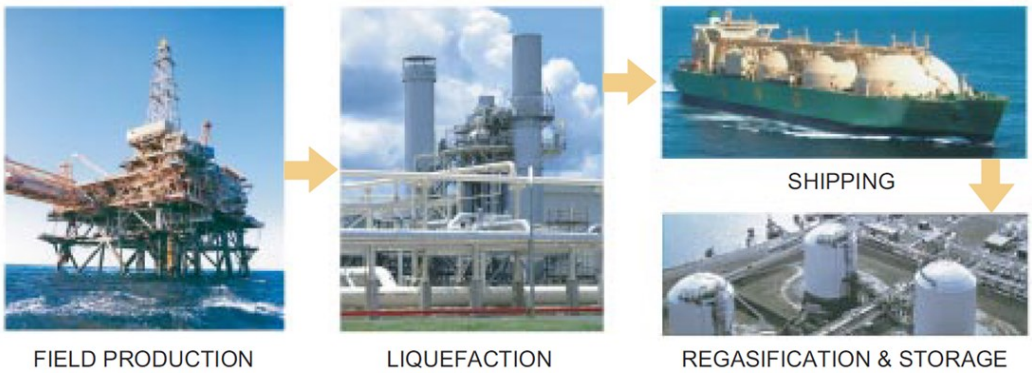

Fig. 4. LNG value chain (DOE, 2003a)

Fig. 4 shows the LNG supply chain, also known as value chain. In the first stage of exploration and production, the financial capitals are focused on the field development and production of the natural gas from the reservoir. After being processed, the natural gas goes through the liquefaction stage, where the volume is reduced to 600 times less than its gas state. The liquefaction facilities require massive investments, therefore, are limited to only certain region where the business can secure the global markets. Then, the LNG is loaded to the LNG tankers or tank trucks and shipped to its destination. The LNG tankers normally transport approximately 125,000–138,000 m^3 of LNG, which provide about 2.6–2.8 billion standard cubic feet of natural gas. The LNG transport trucks are used in the areas where the liquefaction facilities are located close by the regasification facilities. The final stage of LNG supply chain is the storage and regasification. The LNG tanker or tank truck unloads the LNG to the import terminal, and the LNG may be used directly as a transportation fuel or for power generation. The regasification stage allows the natural gas to return to the gas state, where it can be delivered to various sectors, such as the residential or industrial usage. If LNG is not used right away, it is transferred to storage tanks.

1.2.1.3 LNG Industry Trend

Since the first LNG batch was delivered to United Kingdom in 1964, the LNG industry has dramatically changed the climate of the natural gas business globally. The liquefaction capacity of natural gas is expected to double its size by 2020 as shown in Fig. 5.

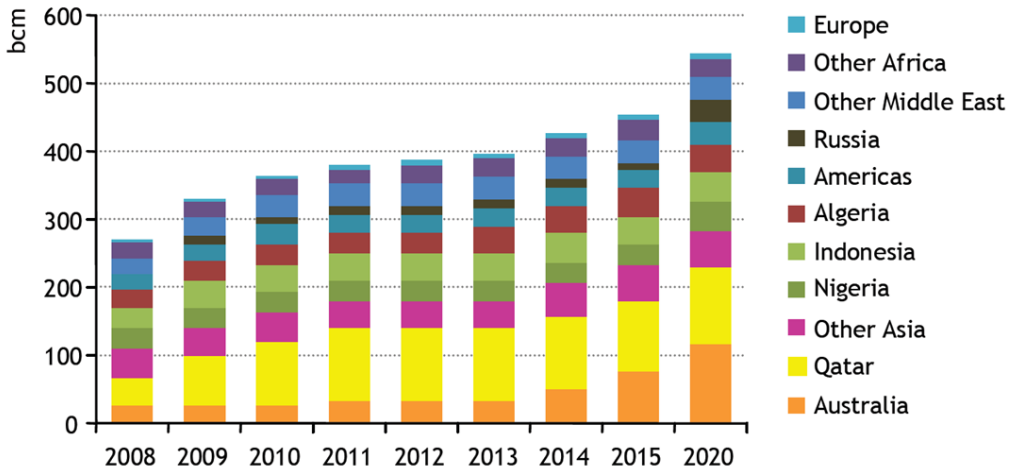

Fig. 5. Projected LNG liquefaction capacity by country (IEA, 2011)

LNG is expected to contribute to approximately half of worldwide natural gas trade by 2035. Over the next few decades, China, India, some parts of Middle East, and Latin America will become increasingly reliant on LNG import to meet the increasing demands from various sectors. LNG has been adopted in US gas market to minimize the uncertainties of the liquid hydrocarbon and to meet the environmental requirements. LNG has been supplying the energy in US as peak shaving, where the monthly demand exceeds 35–40% during the winter season for the heating and power generation. The recent unconventional gas development in North America has reshaped the energy portfolio in US significantly. Fig. 6 shows the natural gas imports and net imports in US.

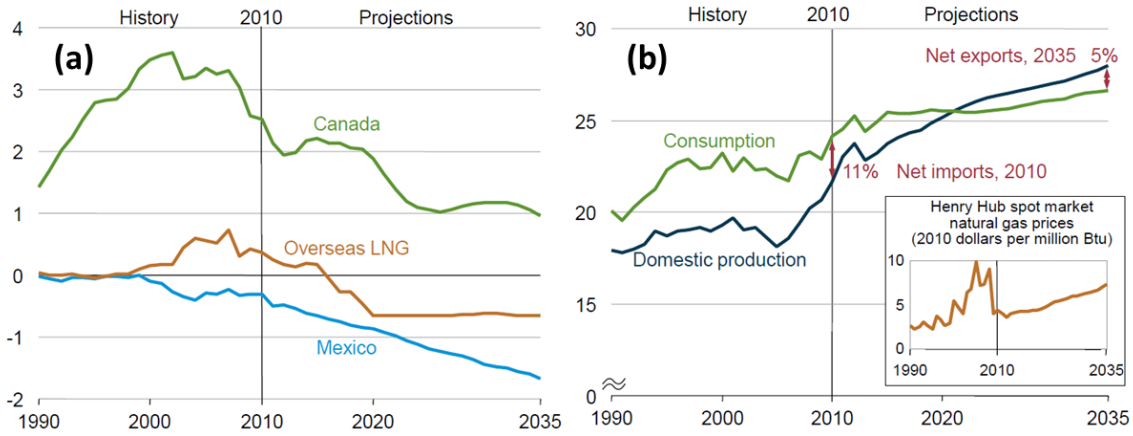

Fig. 6. (a) US net imports of natural gas by source, and (b) Total US natural gas production, consumption and net imports, 1990-2035 (trillion cubic feet) (EIA, 2012)

In 2010, the regasification capacity required dropped to approximately 6% in US (IEA, 2011). The LNG import terminals in US have not been utilized and some facilities had been proposed to be changed to export terminals. North America is expected to gradually become isolated from the LNG import business as the natural gas supply will exceed the self-sufficient level, and LNG export terminals are being planned in many parts of continent.

1.2.2 LNG Safety

1.2.2.1 LNG Hazards

One of the worst disasters recorded in the history of US LNG industry occurred in Cleveland, Ohio in 1944 (Mannan, 2012). The materials used for the LNG storage tanks were not appropriate to operate safely under the cryogenic temperature, and failed. This incident had a significant impact on the public safety, involving hundreds of

fatalities. After the Cleveland incident, the regulatory standards and research had advanced the technologies and practices, which made the US LNG industry one of the most reliable energy sectors in North America. Currently, the LNG industry has one of the best safety records throughout its decades of operation (Foss, 2003).

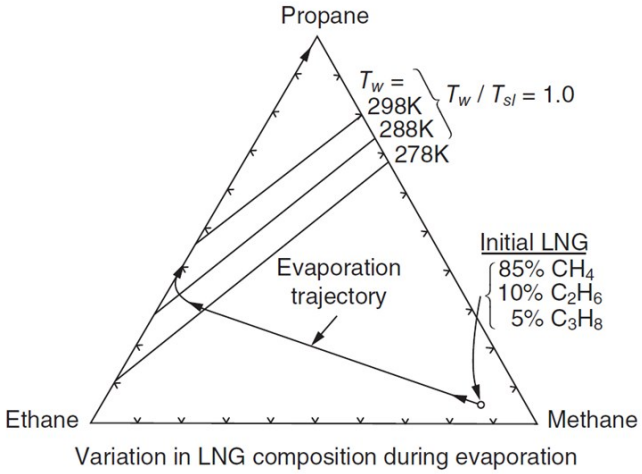

Fig. 7. LNG boil-off sequence showing residual liquid concentration (Reid, 1983)

During an LNG spill, the natural gas starts evaporating from the boiling pool (BP, 2007). A rupture or crack in the storage tank will not result in an immediate explosion, as LNG is not stored under pressure. During the initial flash, the methane will evaporate initially. Fig. 7 shows the evaporation trajectory for LNG composed of 85% methane, 10% ethane, and 5% propane. The methane will evaporate while the ethane–propane residual concentration remains constant. The LNG vapors are not toxic; however, there is a risk of asphyxiation in an unventilated or confined area release, when the methane concentration exceeds 50%.

LNG vapors are normally flammable between 5 and 15% when mixed with air. The vapors will ignite when they find an ignition source, and if ignited in a confined space, although less likely, an explosion may occur depending on the conditions. The partial confinement imposed by the process equipment may accelerate the flame and create higher-pressure front, resulting in a greater overpressure. The auto-ignition temperature of methane at its 10% mixture is above 540 °C (1004 °F), therefore, the LNG vapors are less likely to ignite by themselves. The minimum energy required to ignite the methane mixture is approximately 0.29 mJ (millijoule); therefore, any sparks in the facility will ignite the vapor clouds traveling from the LNG pool. The LNG vapors, when ignited in an open space, the flame will travel back to the LNG source, causing a flash fire. Normally, the flash fire lasts for only a few seconds, burning the flammable vapor present around the LNG pool. If the flash fire travels back and ignites the LNG pool, a pool fire occurs. The main hazard from the LNG pool fire is the radiant heat emitted from the pool. The LNG pool burns cleaner than the gasoline, producing less smoke. The typical heat radiated from the burning methane is approximately 220 kW/m^2 (12,000 $BTU/min/ft^2$), which is higher than the gasoline pool fire, which emits around 140 kW/m^2 (7,600 $BTU/min/ft^2$). The higher heat emitted from the LNG pool fire may impose greater risk to the equipment or personnel working within the facility.

The other hazards include boiling liquid expanding vapor explosion (BLEVE), rollover, and rapid phase transition (RPT). BLEVE occurs when fire heats up the pressurized storage tank. The pressure builds up inside the tank, and as the tank loses integrity, an explosion occurs as the storage tank ruptures. BLEVE normally results in

higher overpressure, compared to the explosion with the same amount of materials involved. The LNG storage tanks are required to be insulated and designed to withstand thermal degradation, thereby, BLEVE is less likely to be an actual hazard scenario (Drube, Haukoos, Thompson, & Williams, 2012). The rollover occurs when unstable layers of LNG form from mixing the LNG with different densities. A sudden vaporization may occur when the unstable layers starts to break and mix. If the amount of vaporized gas exceeds the designed safety pressure system, a structural failure on the storage tank may follow. The LNG storages tanks are designed with sensors and mixing systems to prevent rollovers. The RPT occurs when LNG comes in contact with the water. When LNG is released on the water, the LNG layer in direct contact with the water may vaporize rapidly, causing small blasts that could potentially damage the equipment or harm personnel around.

1.2.2.2 Layers of Protection

The LNG industry practices multiple layers of protection to ensure safe operations (Foss, 2003). The four main layers are primary containments, secondary containments, safeguard systems, and separation distances. These layers are integrated into the safety measures throughout the LNG supply chain with the standards and regulatory compliances.

The primary containment starts with selecting the proper materials for the storage tanks and equipment used in the facility. Also, an appropriate engineering design will ensure that the LNG is contained properly as intended. The secondary containment

includes dikes, berms, or double and full containment systems to prevent the LNG from spreading once an LNG leak occurs. This protection ensures that the LNG spill will be confined and consequences would be at the minimal. The safeguard systems are designed to actively engage to mitigate the consequence of an LNG spill. This system includes detection system, automatic shut-off systems, and operational system, such as the procedures, training, and emergency responses. Lastly, the separation distance is an element required by the federal regulations, which is intended to provide the last line of defense during an LNG release incident. The separation distance evaluated from the LNG dispersion modeling and radiation modeling must be considered to ensure that the hazards do not propagate beyond the facility boundary.

1.2.2.3 Safety Measures of LNG Industry

The engineering designs for the LNG facility mainly focus on preventing the loss of primary containments (Mannan, 2012). The integrity of the materials used in the equipment and storage tanks are critical factors and the inherent safety functions are incorporated throughout the LNG supply chains to ensure safe operations (Lom, 1974). The storage tanks must be designed to withstand the cryogenic state of LNG. The materials must be carefully chosen to have integrity below the boiling temperature of natural gas. The concentrate is used for constructing tank slab, and roof. The 9% nickel steel is used to reinforce the tank walls, and different types of insulations are applied to keep the integrity when operating near the cryogenic temperature. All the equipment

must be designed to handle the differential expansions that may occur from the temperature changes during the operation.

When an LNG release occurs, it is critical to have control over the vapor dispersion phenomena. Dikes are installed around the storage area to prevent the LNG from spreading, as the increase of the surface will result in more vapor cloud generation. The design intent of the confinements around the storage area are to restrict the LNG spill, reduce the vapor generation, and control the size of fire, if ignited by limiting the surface area. The regulatory requirement specifies dikes or bunds with either 100 or 110% of the total tank volume to be considered around the storage tank area. Applying particular material, such as insulating concrete, may help slow down the evaporation rate inside the confinement. The facility sitting can help mitigate any consequences from escalating and may protect the personnel in the facility when an unexpected release occurs.

Water curtain system can be applied outside the dikes to enhance the vapor dispersion to quickly remove the flammable gas from the ground level (BP, 2007). The water spray must be properly designed to limit the LNG vapor dispersion to above ignition source in the downwind region. Fig. 8 shows the outdoor experimental work conducted to investigate the effectiveness of water spray application on LNG vapors at the Brayton Fire Training Field. The concentration and temperature data were analyzed and various physical mechanisms involved in enhancing the vapor dispersion was investigated for different commercial spray nozzles. It was found that the conical spray

installed in upward direction was most effective in diluting LNG vapors at all elevations (Rana, Guo & Mannan, 2010).

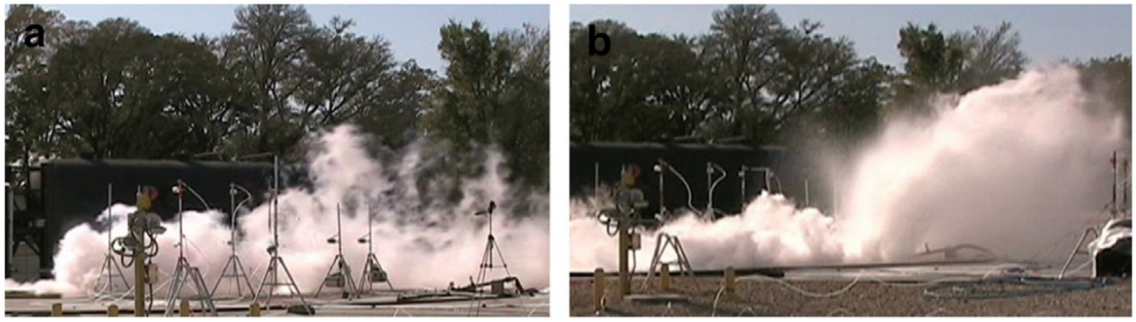

Fig. 8. LNG dispersion test: (a) without water curtain, (b) with water curtain (full cone) (Rana et al., 2010)

The expansion foams also had been used around the LNG facility for two different purposes. When LNG spill occurs, the expansion foams can be applied to cover the surface of LNG and suppress the vapor generation (Yun, Ng, & Mannan, 2011b). The mechanisms involved with vapor suppression using the expansion foam had been verified. It was concluded that the expansion foam application was effective in reducing the methane concentration. The expansion foam allows the control of vapor generation, and allows further emergency procedures to take place.

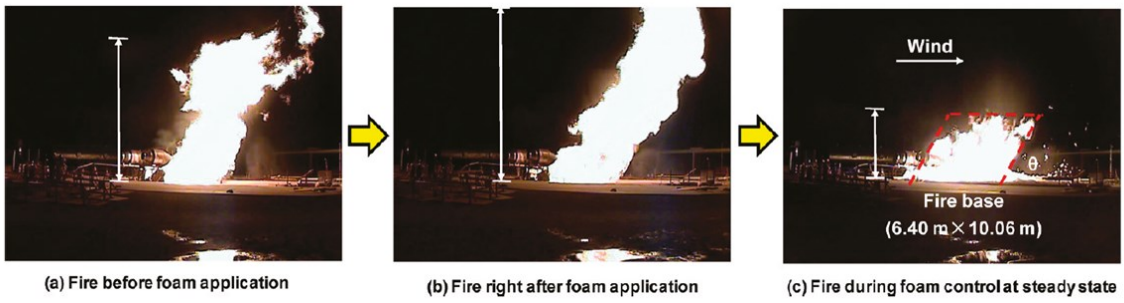

Fig. 9. Pictures of fire before and after foam application (Yun et al., 2011a)

In case of LNG pool fire, the expansion foam can be applied to reduce the radiation heat (Yun, Ng, & Mannan, 2011a). Fig. 9 shows the pool fire size being reduced after applying the high expansion foam. The outdoor experimental work on expansion foam had verified the essential parameters involved in the pool fire suppression, such as the mass-burning rate, effective foam depth, flame height, radiative heat flux, thermal exclusion zone, and LNG pool fire characteristics. It was evaluated that the expansion foam application reduced the flame heights by 61%, and with reduced mass burning rate. The thermal hazard distance reduced up to 52%.

1.2.3 Regulatory Requirements

For an LNG facility, the most catastrophic failure would be from the failure of the storage tanks. The hazards associated around the LNG facility may impose intolerable level of risk to the communities around. Extensive research has been carried out by the industry, academic scholars, and other government agencies to standardize the codes and regulations to ensure safe operation environments. The Federal Energy

Regulatory Commission (FERC) approves any onshore LNG facilities and inspects the operation. The US Coast Guard looks over all the offshore LNG facilities and LNG tanker ship operations.

The federal regulation, '49 CFR Part 193, Liquefied Natural Gas Facilities: Federal Safety Standards', provides detailed requirements on the facility siting, design requirement for safety measures, fire protection and materials, operations and maintenance activities (49CFR193, 2000). The 49 CFR Part 193 incorporates the industry standard, 'NFPA 59A, Standard for the Production, Storage, and Handling of Liquefied Natural Gas (LNG)', to clearly provide details on the siting requirement for any LNG facilities on US lands (NFPA, 2013). A vapor dispersion study must be submitted in advance that proves the vapor concentration of 2.5% (1/2 LFL) does not extend beyond the facility boundary. The vapor exclusion zone can be computed using the DEGADIS, or any alternative model that has been validated according to the requirements detailed in paragraphs (ii) through (iv) in CFR 193.2057(c).

The NFPA 59A outlines the requirements for a performance-based risk assessment applicable for any newly proposed facility or to a facility that goes through significant modifications. The analysis must ensure that the LNG facility does not impose any risk above the intolerable levels. An individual risk along with any further societal risk must be investigated with the ALARP (As Low as Reasonably Practicable) approach. For the cases where the risks are beyond the tolerable level, risk mitigation measures can be applied in meeting the criteria.

1.3 Statement of Problems and Significance

1.3.1 Research Motivation

The mitigating effects and efficiency of water curtain systems have made it possible for such systems to be used for preventing and minimizing the consequences of accidental releases of toxic and flammable gases. The water curtain system has also been recognized as an effective LNG mitigation measure. Because of the growing concerns over safety and security issues of LNG facilities and terminals, there is a need to explore the effectiveness of water curtain systems in mitigating the LNG hazards and identify the dominant mechanisms during the water curtain application.

Previous experimental studies investigating the effectiveness of water curtains on LNG vapor clouds are rather limited. Because of the limited data available, no conclusive findings on the physical mechanisms can be drawn from these studies. In addition, the modeling work for determining effectiveness of water spray application was not sufficient to draw a set of global design parameters.

To address the knowledge gap from the existing studies, the Mary Kay O'Connor Process Safety Center (MKOPSC) has performed a series of outdoor LNG spill tests at the Brayton Fire Training Field. Due to the large numbers of variables (e.g., droplet size and velocity, spray angle, flow rate, discharge angle, and duration of discharge) and complex physical phenomena of the droplet-vapor interaction, no engineering guidelines are currently available for an effective mitigation system. Therefore, further work, which includes numerical modeling, should be conducted to achieve a comprehensive assessment of the water curtain application in mitigating the LNG vapor clouds.

1.3.2 Research Objective

The integral-type modeling provided the prediction of LNG vapor mitigation effects that is bounded by the semi-empirical parameters and assumptions. The CFD tools have evolved significantly in providing solutions to the multiphase flow problems, which are also applicable to the water spray modeling. The Eulerian-Lagrangian approach assumes the gas (continuous) phase to be a continuum, whereas the water droplet (fluid/dispersed) phase is described as individual droplets. The momentum, heat, and mass transfer of the droplets are then calculated by considering various forces that are present in the gas phase using the Lagrangian approach. In addition, the influence of droplets on the gas phase is considered in the constitutive equations for the gas phase by selecting proper source terms.

Despite the increasing use of CFD codes to investigate the complex fluid flow problems, little work has been done so far to improve the understanding of LNG vapor cloud mitigation resulting from the water spray application. Driven by this motivation, the goal of this research is to apply the Eulerian-Lagrangian spray modeling using a CFD code to evaluate the forced dispersion effects of the water spray application on LNG vapor clouds.

1.3.3 Research Methodology

To understand the complex interaction between the LNG vapors and droplets, the LNG forced dispersion modeling was set up using the CFD codes. Fig. 10 outlines the overall research development for the LNG forced dispersion modeling work.

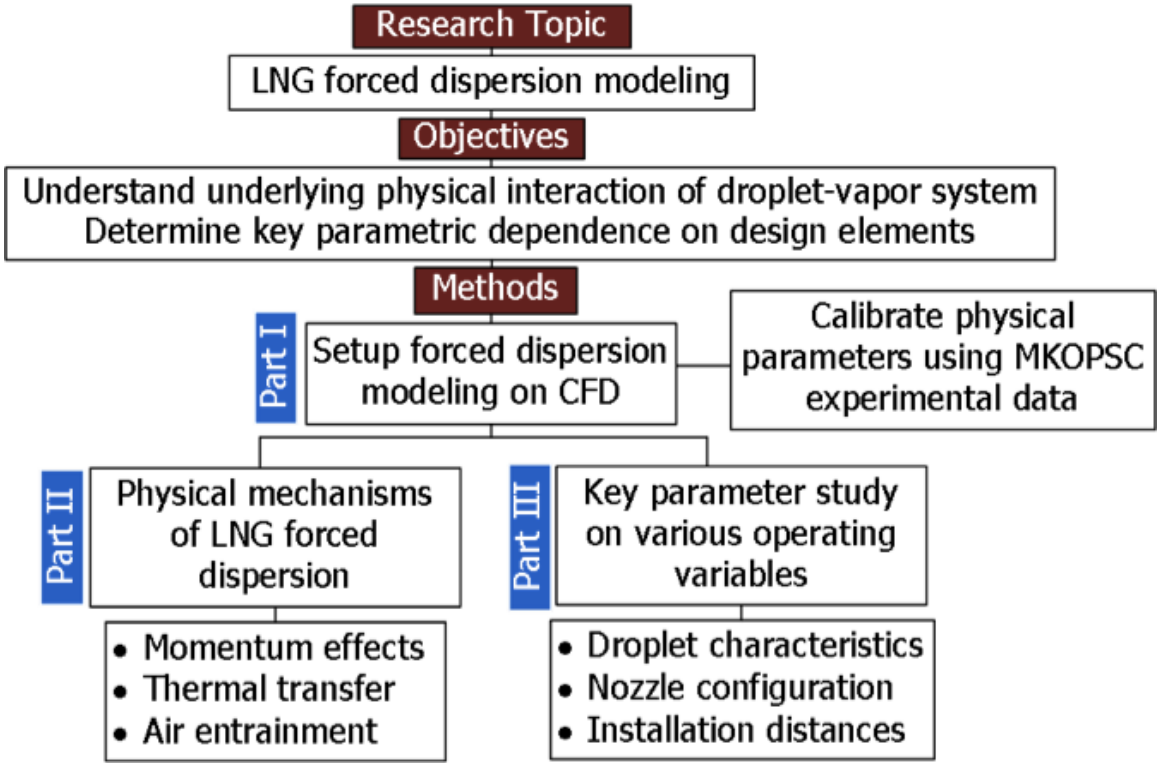

Fig. 10. Proposed research outline

The upward-full cone nozzle type was adopted in the simulations of the water curtain application. The essential physical parameters in describing the LNG dispersion phenomenon was calibrated using the March 2009 MKOPSC outdoor LNG spill experimental work. The simulation was setup to incorporate the two dominant mechanisms verified from previous experimental works: momentum effect and thermal transfer. The physical parameters essential in simulating the LNG forced dispersion modeling using the upward conical type nozzle application are discussed (Chapter III).

The LNG forced dispersion modeling is applied to verify various dominant mechanisms involved in the water spray application (Chapter IV). The mechanical

effects induced from the momentums imparted from the droplets to the air-vapor mixture are evaluated. The turbulence induced from the thermal transfer from the droplets is investigated and various air entrainment rates had been applied to determine the different level of dilution induced from various spray applications.

Lastly, the key parameters of the LNG forced mitigation have been investigated by modifying the operating variables (Chapter V). The thermal effects from the different droplet sizes and temperatures had been investigated. Also, the effects of various air entrainment rates and installation configurations had been compared.

CHAPTER II

WATER CURTAIN APPLICATIONS ON LNG VAPOR CLOUDS

2.1 Water Spray Systems and Modeling

2.1.1 Water Curtain Application

The main objective of water curtain system as a mitigation measure is to provide reliable risk reductions in case of an unexpected spill or release of hazardous materials. Water curtain is implemented in the facility as the post-release system in the last line of defense. Water spray provides mitigation effects by creating a barrier of water droplets in the pathway of prevailing winds to disperse the hazardous gas below the toxic or flammability limits (CCPS, 1997). Applying the water spray has been recognized as one of the most effective and economic methods in the chemical and petrochemical industries to alleviate the consequences of an unexpected release and prevent the escalation (Lopez, Badin, Lieto, & Grollier-Baron, 1989).

There are three different types of commercial nozzle commonly used in the industry (Hald, 2005). The full cone nozzle produces a circular cone with the spray angle of 30 to 130º depending on the nozzle design. The hollow cone nozzle produces water spray where the center part is free of droplets. The flat fan type nozzle creates a thin sheet of water barrier, which can provide wider coverage.

Water spray induces various physical and chemical mechanisms in the vicinity of the water spray (Rana, 2009). The momentum imparted from the water droplets induces the mechanical effects and air entrainments, which enhances the dilution and mixing of

the air-gas mixture. The thermal transfer from the droplets can provide heating to the cold gas or act as thermal barrier in case of fire. The mass transfer or physicochemical reaction can reduce the concentration significantly with the released material highly soluble in the water.

Some of the design elements of water spray application are water pressure, water flow rate, nozzle type, air flow rate into the water spray, and configuration of water curtain system (McQuaid, 1977). The nozzles produce different size distribution of water droplets and the mean diameters can be represented in many ways to describe the poly-dispersed droplet system. The Sauter mean diameter (SMD) is the ratio of total volume to total surface of the water droplets produced. The SMD represents the intrinsic characteristic of spray through the hydrodynamics of inertia and drag of water droplets.

2.1.2 Spray Modeling

2.1.2.1 Integral-Type Approach

The integral-type modeling for water spray application mainly involves the dilution effects from water curtain application. The models focus on the mitigation effects from the water spray by taking into account the air entrainment rates, and the detailed physical phenomena induced from the droplets were not considered.

McQuaid and Fitzpatrick (1981) proposed a simple 2-dimensional box model to evaluate the efficiency of water barrier (McQuaid & Fitzpatrick, 1981). The box model assumed simplified vapor behaviors by avoiding detailed vapor movement or concentration gradient, but rather averaging over the properties of cloud fields. The

mitigation effects are considered by providing the line source of additional air entrainments at the location of spray application. The air entrainment rates are mainly determined by semi-empirical correlations, and thermal effects from the water droplets are not considered. The mixing effects are assumed instantaneous that result in changes of vapor composition and behavior of cloud fields. The transition to passive vapor behavior was adopted in the downwind region from empirical correlation to describe the vapor movement in the post-spray region.

Moore and Rees (1981) have defined a forced dilution factor (FD) to describe the mixing effects of air by considering the turbulence from the wind and water spray (Moore & Rees, 1981). The semi-empirical model showed agreeable prediction of water spray application and concluded from theoretical study that the spray performs better dilution for smaller leaks with lower wind speed, closer to the source.

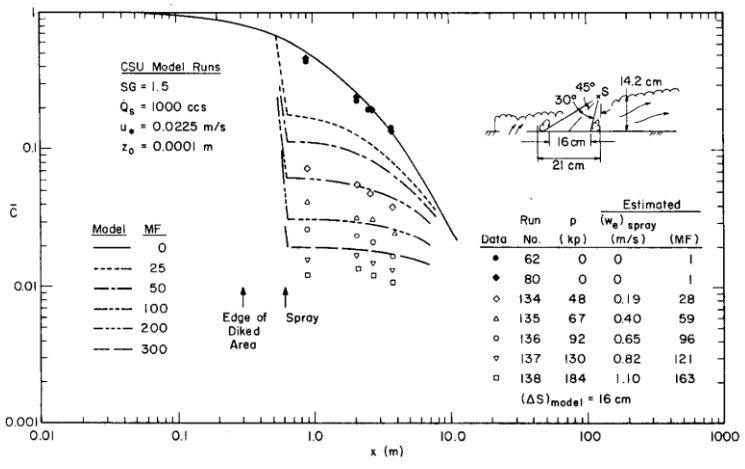

Fig. 11. Methane equivalent concentrations versus downwind distances, compared with box model using multiplicative factor (Meroney & Neff, 1985)

Meroney and Neff (1985) provided forced mitigation effects for both box and slab model assuming that the local entrainments increase with the application of water curtain (Meroney & Neff, 1985). Fig. 11 shows the vapor prediction of natural dispersion and with various spray settings applied. The enhanced air entrainment effects were incorporated into the model by applying the multiplicative or additive factor to the regular entrainment rates. These factors were determined empirically through previous experimental studies. The integral-models have provided a quick assessment method in evaluating the effects of alternative arrangements of water spray application and the spray performance using a single parameter.

2.1.2.2 Multi-phase Modeling Approach

The multiphase modeling of water spray application can provide rigorous solutions to complex interaction of gas-droplet flow by evaluating the effects of the mass, momentum and energy transfers (Crowe, Sharma, & Stock, 1977). As the multiphase flow exhibit various regime, it is critical to select proper model that could accurately describe the fluid flow phenomena (Ranade, 2002). Currently, two different approaches are available for water spray modeling using the multiphase interaction: the Eulerian continuous phase model and Lagrangian particle tracking models (Gant, 2006).

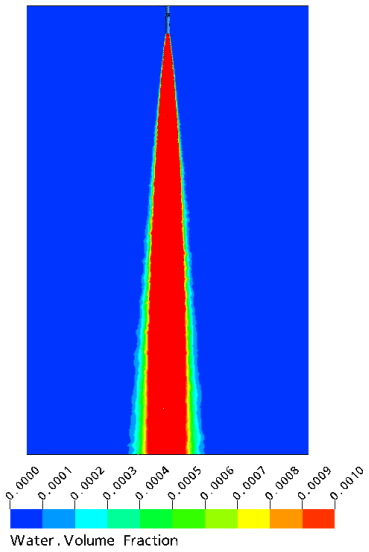

Fig. 12. Predicted water volume fraction on a slice through the flow domain for an Eulerian spray discharging vertically downwards (Gant, 2006). Crown Copyright, reproduced with permission of the Health and Safety Laboratory.

The Eulerian continuous phase modeling applies a static reference frame in the space of the fluid flow to derive the governing equations. Fig. 12 illustrates the water fraction of the Eulerian spray simulated in the vertical downward. The Eulerian phase treats the droplets as a fluid continuum, calculating the transport equations in the fraction that droplet consumes in a controlled volume. The droplets dispersed in the gas phase are treated as conceptual level, where the droplets are incorporated in the transport equation as volume fraction. It has the advantage of requiring less CPU time as the calculation solves the liquid-gas interface and droplet interactions in the expense of uncertainty in some properties. The Eulerian model, however, requires extremely fine mesh to model a small droplet, making it more appropriate where less resolution is required. This

approach is suitable for cases where the discrete phases take up significant fraction within the continuum.

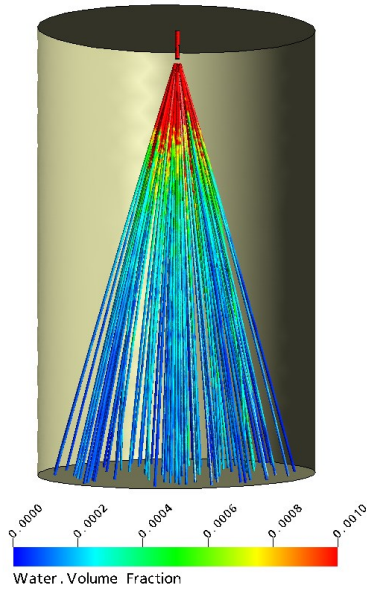

Fig. 13. Particle trajectories for the Lagrangian spray model colored with water volume fraction (100 droplet trajectories) (Gant, 2006). Crown Copyright, reproduced with permission of the Health and Safety Laboratory.

The Lagrangian particle-tracking model traces the droplets in discrete phase with a dynamic reference frame along the multi-parameter space and time. Fig. 13 illustrates the water volume fractions of 100-droplet trajectories using the Lagrangian spray modeling. The trajectories of the dispersed particles are tracked down in the continuum and the interaction between the particles and each computational cell in fluid continuum is processed to solve the influence of the droplets. Instead of tracking numerous particles in the domain, normally a large numbers of droplets with prescribed characteristics are

grouped in parcels to reduce the CPU cost. These parcels are tracked in the continuous gas phase and the mass, momentum, energy, and turbulence exchange between the droplets and continuum flow are considered. When the Lagrangian spray modeling is applied, a fine mesh setting is not required as the mass, momentum and energy conservation equation is calculated separately as the particles are tracked in the continuum phase. The Lagrangian model provides momentum, mass, and heat exchange more accurately, but becomes more CPU intensive as particle numbers increase.

Detailed analysis on the application of CFD in the simulation of the water spray barrier has been conducted by the Health and Safety Laboratory (Gant, 2006). A single non-impinging spray using the Eulerian and Lagrangian reference frame has been simulated and compared. The author concluded that the Lagrangian spray model is more flexible in the application of the spray model than the Eulerian spray model. The Lagrangian spray model integrated the multidimensional simulation models for the spray application research over the past few decades (Abraham, 1997). Alessandri, Buchlin, Cavallini, Patel, and Galea (1996) recommended the Lagrangian modeling as a more suitable approach for the application of dispersing dense gas (Alessandri, Buchlin, Cavallini, Patel, & Galea, 1996). The study on the effects of droplets on the gas flows using both spray models had been conducted by Nijdam, Guo, Fletcher, and Langrish (2004). The authors also preferred the Lagrangian model for its availability in different applications (Nijdam, Guo, Fletcher, & Langrish, 2004).

2.2 Experimental Work on LNG Forced Dispersion

2.2.1 Small-Scale LNG Spill Tests using Water Spray Screen

The US Coast Guard conducted a small-scale LNG spill experiment to simulate a spill on an LNG transport ship in 1976 (L. Brown, Martinsen, Muhlenkamp, & Puckett, 1976; Martinsen, Muhlenkamp, & Olson, 1977).

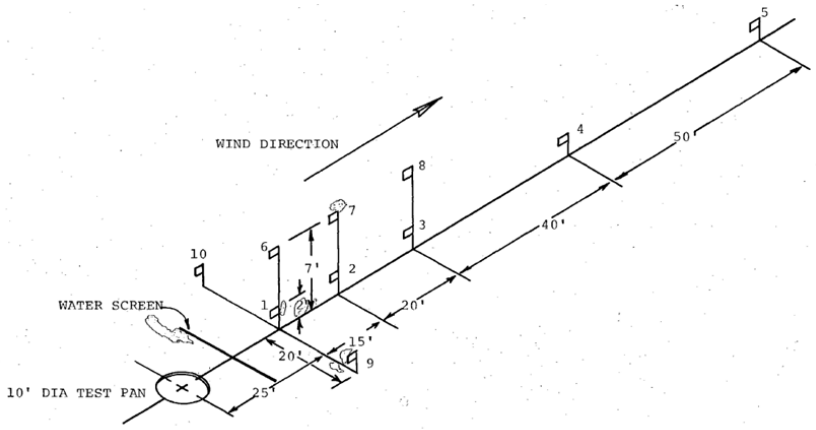

Fig. 14. Gas sensor layout for vapor dispersion tests (Martinsen et al., 1977)

Fig. 14 shows the schematic of the LNG spill experiments conducted by US Coast Guard. The tests were performed to investigate the effectiveness of applying the spray curtain in reducing the concentration of LNG vapors in the downwind region. The small scale of LNG pool (100 ft^2) was used to create the LNG hazard scenario, and flat-fan type, which produced circular radius ranging 2.44–3.05 m in 150–160°, was used. The flow rates were varied and vapor concentration was collected to compare the effectiveness of dilution of each application.

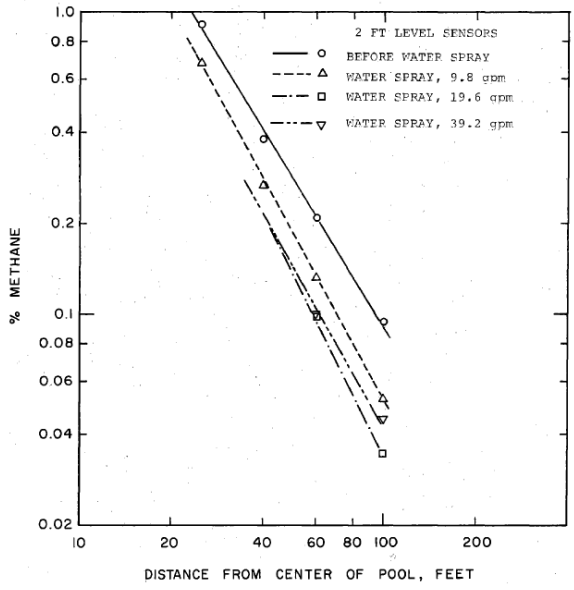

Fig. 15. Average concentration as a function of distance (Martinsen et al., 1977)

During the tests, the gas concentrations at ten different locations were collected, along with the wind velocity and water pressure at the spray nozzle. Fig. 15 shows the concentration plotted in the downwind region for water spray with various flow rates applied. The authors concluded that no quantitative analysis could be conducted from the experimental results, mainly because of the limited data acquired from the work. It was concluded from the test results that the water spray curtain was effective in reducing the methane concentration and that the mechanical turbulence induced from the water droplets improved the mixing of the LNG vapors. It was verified that the heating effects from the droplets played less significant role in vapor dilution. The authors did not provide any detailed recommendations on how to design an effective water curtain system.

2.2.2 Dispersal of LNG Vapors with Water Spray Curtain

The Gas Research Institute conducted three-phase research, which consisted of theoretical analysis, small-scale spill tests, and wind tunnel experiments (Heskestad, Meroney, Kothari, & Neff, 1983). This project aimed to determine the engineering designs and operating parameters for an effective dispersion of LNG vapors. The results were used to develop the design guidelines in applying the water spray barrier as an effective mitigation system in the LNG facilities (Atallah, Guzman, & Shah, 1988).

The layout of the experimental setup is illustrated in Fig. 16. The numbers in parentheses are the coordinates in meters. The LNG spill experimental work was setup with a confinement sized at 3 m x 3 m and the sprays were installed both upwards and downwards using 4 mm size nozzle.

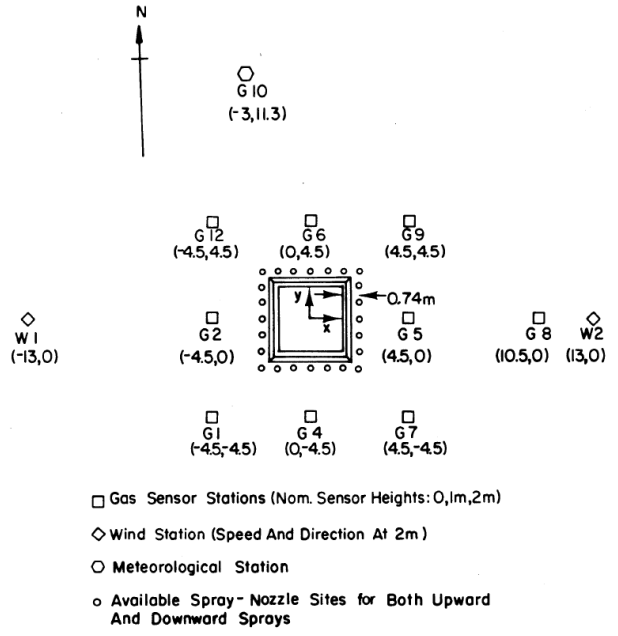

Fig. 16. Layout of instruments and spray nozzle sites (Heskestad et al., 1983)

A total of 11 experiments were analyzed among the 33 experiments conducted. It was concluded from the theoretical analysis that the downward sprays diluted the LNG vapors below 5%. The experimental results also provided agreeable data to the theoretical analysis, although the vapor concentration before the water spray was quite low. The downward spray application showed reduction of concentration to approximately 2 to 5% in the downwind region. The upward sprays had diluted vapor concentration approximately to 1 to 2%; however, the effectiveness of vapor concentration reduction was not consistent with the theoretical estimation.

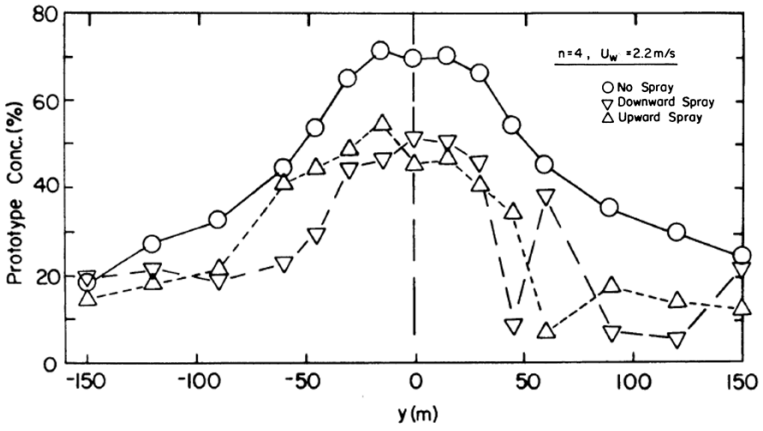

Fig. 17. Crosswind vapor concentrations near ground at x = 90 m (Heskestad et al., 1983)

A reduced-scale of wind tunnel experiment had been conducted to replicate the LNG vapor spill experiment of 60 m x 60 m. The CO_2 was used as LNG vapor simulant in 1:100 scale model set of 60 cm x 60 cm release. Fig. 17 shows the vapor concentration collected from the experiments. The concentration without the water spray application was recorded around 70%. The water spray application reduced the highest

concentration down to 50% for both upward and downward spray applications. The upward sprays performed well in diluting the LNG simulate. On the other hand, the downward sprays showed relatively less dilution effects, mainly due to insufficient mixing induced from the entrained air in downwind. It was concluded from the wind tunnel experiments that the upward sprays and downward-inclined sprays were the only two designs, which showed an effective dilution.

2.2.3 Forced Dispersion of LNG Vapors with Water Spray (MKOPSC)

The Mary Kay O'Connor Process Safety Center (MKOPSC) conducted outdoor LNG spill experiments at Brayton Fire Training Field to verify the dominant mechanisms and evaluate the effectiveness in dilution of the LNG vapor concentration (MKOPSC, 2010). A total of four experiments were conducted to investigate the effects of various types of commercial nozzles on controlling and dispersing LNG vapors (Rana, 2009). Rana et al. (2010) discuss one of the experimental setup that had been conducted in 2007 (Rana et al., 2010). Fig. 18 shows the schematic of the experimental setup used in November 2007 MKOPSC LNG spill experiment.

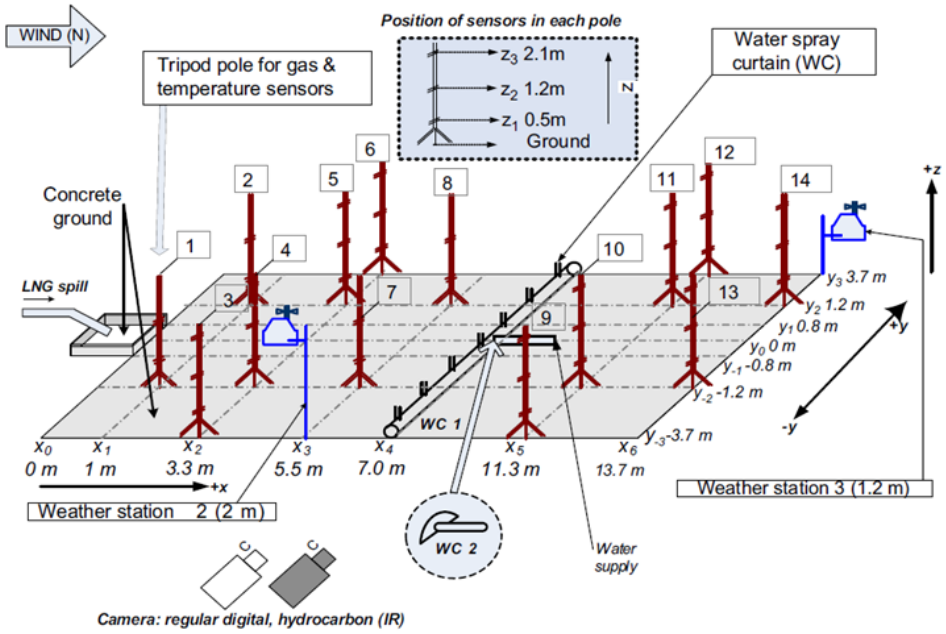

Fig. 18. Experimental setup of Nov 2007 MKOPSC LNG spill test (Rana et al., 2010)

An LNG pool was created by spilling LNG directly into a confinement on concrete and on water. The LNG vapors were generated from the confinement and dispersed in the prevailing downwind direction. The experimental variables, such as the water pressure and flow rate, LNG flow rate, atmospheric conditions were measured. The LNG vapor concentration was collected using the infrared hydrocarbon point gas detectors and thermocouples were installed to measure the temperature changes.

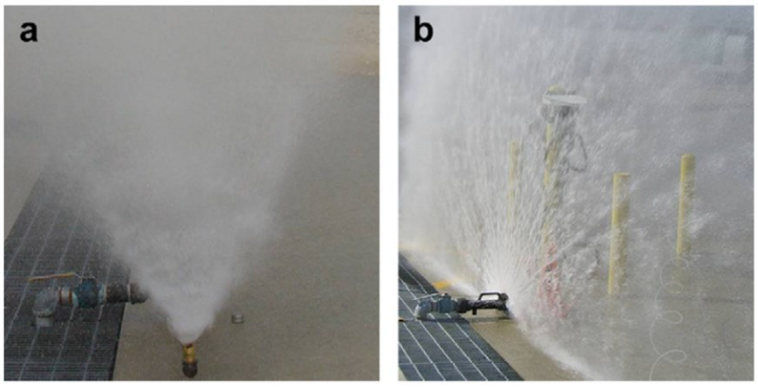

Fig. 19. Water spray nozzles used: (a) full cone nozzle,

and (b) flat fan nozzle (Rana et al., 2010)

The water spray was installed in the pathway of the LNG vapor clouds. Two different types of water spray nozzles were mainly compared as shown in Fig. 19: 60° full-cone spray nozzle and 180° flat-fan spray nozzle (Rana & Mannan, 2010). The full-cone type produces finer droplets, while the flat-fan type creates a thin barrier in the vicinity of nozzle and very course droplets as the bulk water travel and breaks into smaller droplets. The main mechanisms verified in the LNG forced dispersion were the mixing effects through entrained air and momentum effects.

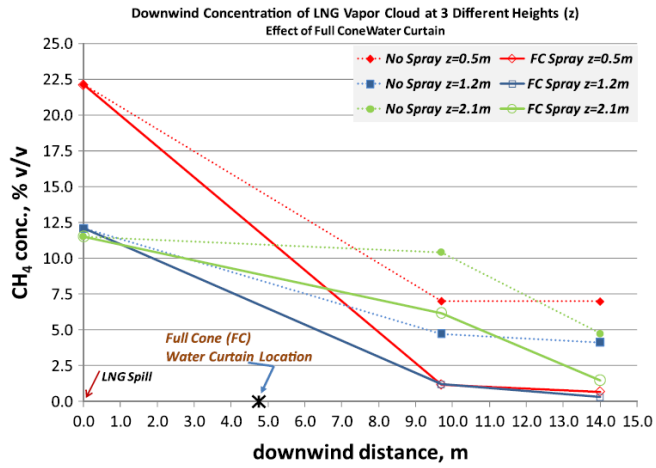

Fig. 20. Downwind concentration with full-cone application

(Rana & Mannan, 2010)

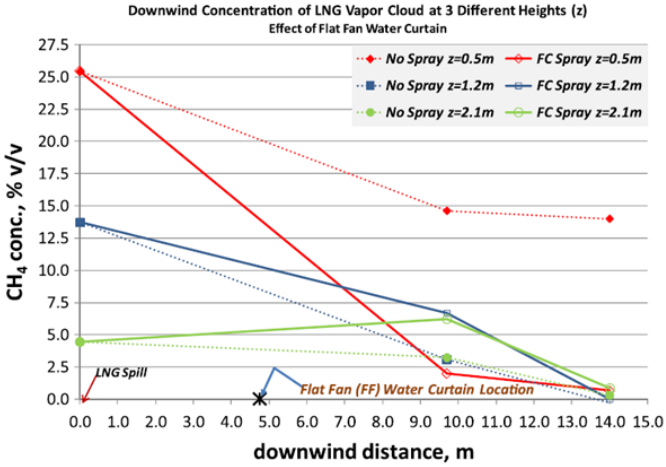

Fig. 21. Downwind concentration with flat-fan spray application

(Rana & Mannan, 2010)

Figs. 20 and 21 show the downwind concentration with the application of full cone type and flat-fan type spray nozzle. The full-cone spray type provides more

effective mixing with the air through high air entrainments. The flat-fan type, on the other hand, creates a physical barrier in the pathway of LNG vapors and provides high momentum from the droplets created from the water pressure. The vapor concentration decreased at all elevation for the full-cone type nozzle. This indicates that the mixing with air provided by the full cone resulted in an effective dilution of LNG vapors. For the flat-fan nozzle application, the vapor concentration decreases in the lower level, but increased at higher elevation. The LNG vapors were lifted from the ground level from the high momentum imparted from the droplets; however, the vapor concentration did not get diluted due to lack of mixing with air.

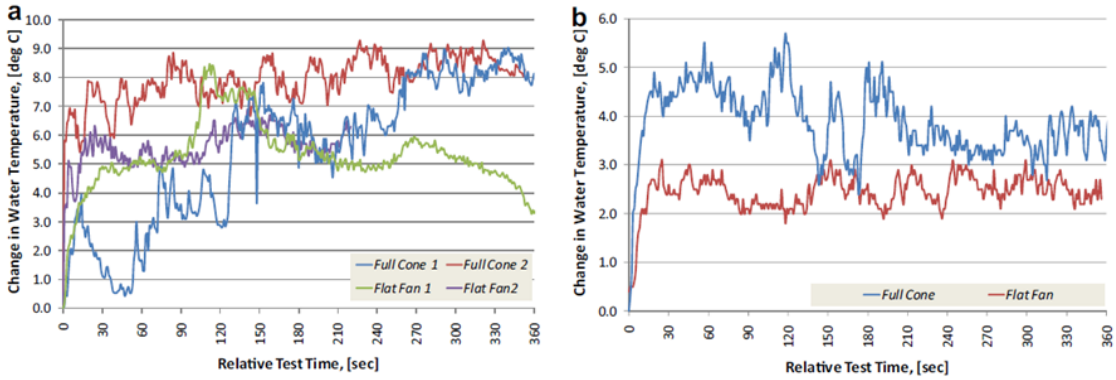

Fig. 22. Changes in water curtain temperature reading (a) 2007 and (b) 2009 tests (Rana & Mannan, 2010)

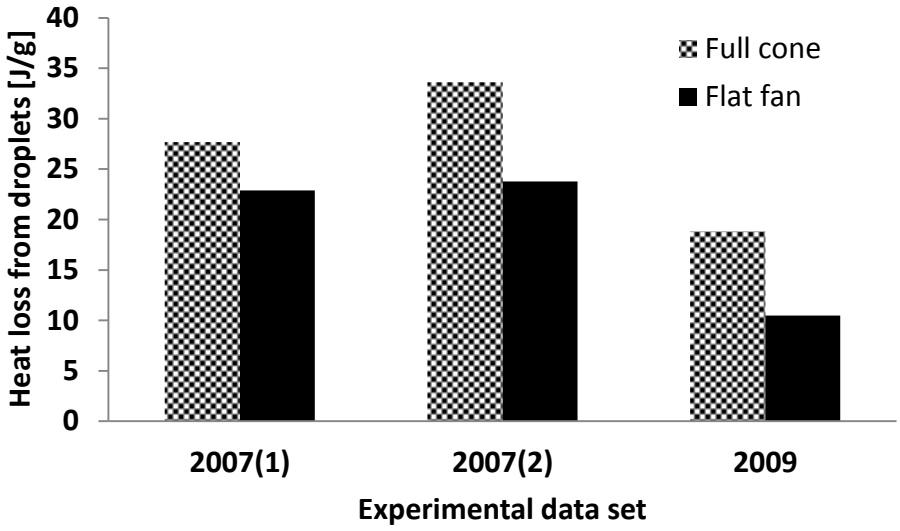

Fig. 23. Heat loss by water curtain [Adopted and modified from (Rana & Mannan, 2010)]

The temperature changes of the water droplets collected from the experiments and the heat loss evaluated by water curtain are shown in Figs. 22 and 23. The overall heat transfer evaluated from the experimental results showed that the droplets produced from the full-cone type nozzle provided more heat transfer to the LNG vapors than the flat-fan application. The full-cone type nozzle produces smaller droplets, which increases the surface area, where the heat transfer occurs. The LNG vapors traveled down to lower elevation with ineffective thermal effects of the droplets from the flat-fan type. It was concluded that the mixing effects through the entrained air promotes the LNG vapors. The heat transfer from the droplets ensures that the vapors are sufficiently warmed to become positively buoyant.

2.3 Modeling LNG Natural Dispersion and Forced Mitigation

During an LNG spill, LNG pool may form depending on the spill rate, surface properties and geometry of the confinement space. The LNG pool provides a source of flammable vapor clouds and determines the evaporation rate, which is an essential element in defining the source term in the LNG consequence modeling. The LNG vapors are heavier than air during the initial stage of evaporation as the methane is denser than air near the boiling point. During the initial dispersion from the LNG source, vapor clouds will behave like dense gas and travel near the ground level, until they are adequately warmed to become positively buoyant around –106 °C (–160 °F). It is essential for any consequence modeling to incorporate the dense gas behavior of LNG vapors, and the transition to lighter vapor mixtures as more heat transfers and mixing occur.

2.3.1 LNG Consequence Modeling

The integral-type models convert the complex conservation equations to set of coupled ordinary differential equations (Ermak, Chan, Morgan, & Morris, 1982; Spicer & Havens, 1987). Fig. 24 shows the simplified vapor movement produced from the box-model, which provides steady-state plume behavior. The details of vapor movement and concentration within the vapor fields are not specified, and instead, the vapor properties are averaged in bulk state. The vapor cloud is assumed homogenous within the specified gas fields and other properties are assumed constant over the gas volume. The mixing effect with air is implemented in the model through air entrainment rates.

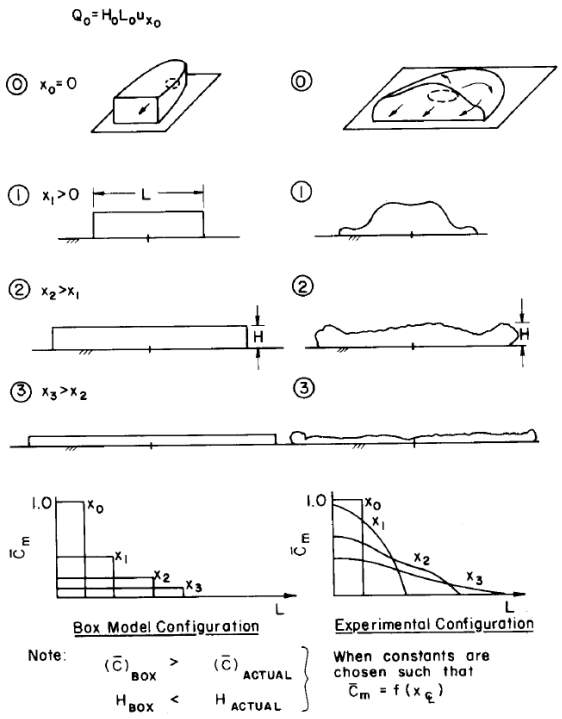

Fig. 24. Box-model plume behavior (Meroney & Neff, 1985)

The integral models do not implement any explicit temperature equations and the buoyancy of the vapor cloud is described through solving the Richardson number. It was found that the integral-type models were not capable of predicting the complex vapor behavior of the flows over the obstacles. Fig. 25 shows the prediction of LNG vapor dispersion in transient movement using the slab-model. The dispersion contour showed the LFL distance up to 300 m with the experimental setup from Burro No. 8 LNG spill condition.

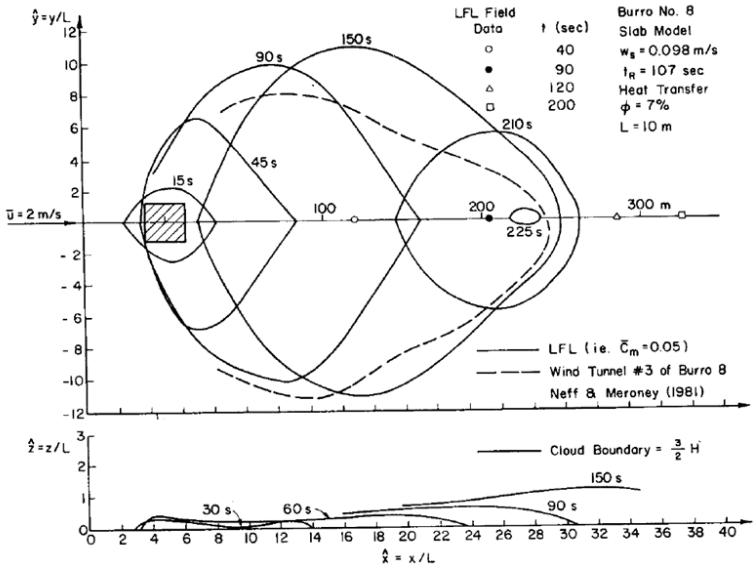

Fig. 25. Burro No. 8 LNG spill no spray conditions, plan view and vertical section (Meroney & Neff, 1985)

The computational fluid dynamics (CFD) modeling provides the complex behavior of fluid flow through solving the constitutive equations derived in three-dimensional space (Tu, Yeoh, & Liu, 2008). Applying the CFD codes in predicting the consequence of an LNG spill was recommended for the cases where the high impact of the public security and safety was involved (Hightower et al., 2004). When applying the CFD modeling, there are some uncertainties in the parameters used in describing the LNG vapor dispersion, which requires validation steps to ensure an accurate prediction (Ivings, Jagger, Lea, & Webber, 2007).

Luketa-Hanlin, Koopman, and Ermak (2007) presented a set of recommended guidance for setting up and running consequence assessment of LNG vapor dispersion using CFD codes (Luketa-Hanlin, Koopman, & Ermak, 2007). Turbulent mixing, heat

transfer from the atmosphere and details on defining the domain specifications are discussed. The authors concluded that the uncertainty in the LNG source terms and atmospheric setup may result in ± 20% differences in the LFL distances.

Cormier, Qi, Yun, Zhang, and Mannan (2009) conducted a series of parameter study and the effects on the LFL prediction (Cormier, Qi, Yun, Zhang, & Mannan, 2009). The ANSYS CFX, which is commercially available CFD code, was used to set up and calibrate the physical parameters using the experimental data obtained from MKOPSC LNG experiments. The turbulence effects, source term, and atmospheric setup were examined to verify the direct influence on the LNG behavior. The authors have identified that the parameters for defining the LNG source term, such as the release rate of LNG, pool area, gas phase velocity profile (LNG), and turbulence, influence the LFL prediction significantly. The heat flux from the surrounding, and wind velocity also have a significant impact on the results, while the atmospheric temperature, surface roughness and wind direction had relatively less impact on the results.

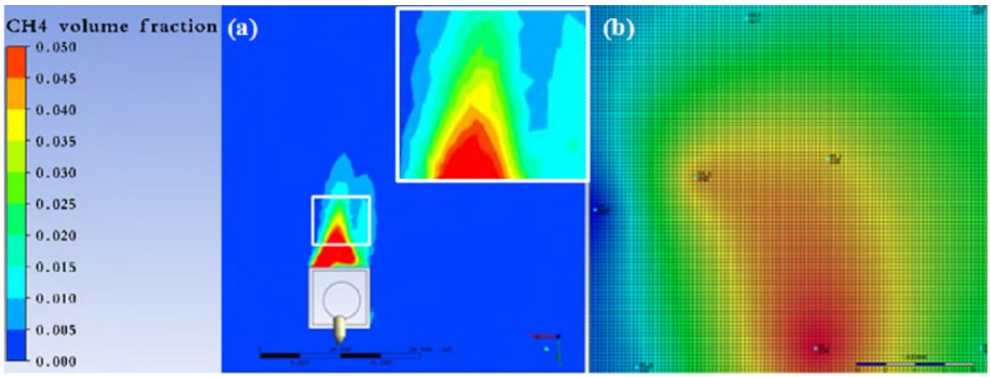

Fig. 26. Methane volume fraction contours at 0.3 m elevation (a) ANSYS CFX simulation and (b) test data (Qi, Ng, Cormier, & Mannan, 2010)

Qi, Ng, Cormier, and Mannan (2010) conducted a validation study using the ANSYS CFX and provided recommendations for improved prediction of the LNG vapor behavior (Qi, Ng, Cormier, & Mannan, 2010). Fig. 26 shows the comparison of the methane volume fraction of the CFD prediction and experimental results. The authors conducted the sensitivity analysis on the grid setup and turbulence intensity at the LNG source term. The mesh settings provided LFL distance that ranges up to 30% difference, while the turbulence intensity increased the LFL distance 300% more, when the intensity was increased from 1 to 10%. The authors demonstrated the importance of having a mesh-independent setup and proper source term model to ensure an accurate prediction.

Gavelli, Bullister, and Kytomaa (2008) simulated the Falcon series experiments and verified the effects of vapor barrier in reducing the LFL prediction (Gavelli, Bullister, & Kytomaa, 2008). The authors concluded that the ANSYS Fluent code was capable of providing the reproduction of Falcon test results reasonably well. Also, the importance of having a well-defined source term is further discussed (Gavelli, Chernovsky, Bullister, & Kytomaa, 2009). It was found that the turbulent mixing induced from the spill and vaporization of LNG at the source is more dominant than the turbulence induced from the atmospheric conditions. The turbulence induced from the wind was not sufficient enough to enhance the mixing within the LNG vapor clouds. Also, the recommended turbulence intensity (1–10%) only takes into account the fluid movement induced from the evaporation of LNG, and further consideration should be given to incorporate the high wave and boiling phenomenon at the LNG pool, which will improve the prediction of LFL distance.

2.3.2 LNG Forced Mitigation Modeling

The effectiveness of water spray application on LNG vapors had been investigated as a part of three phase research program conducted by Gas Research Institute (Zalosh, Alpert, & Heskestad, 1983). The vapor interaction with the droplets was evaluated using the 2-dimensional elliptic numerical code (SPRAY). The gas behavior of turbulent motion, and recirculation in 2-D field were evaluated by coupling the influence of the droplet spray to the gas flow by means of particle movement in the cell. The drag force, mass, energy momentum, and energy transfer from the droplets were considered. The LNG source term was simplified by assuming that the methane layer generated from the dike mixes with air, where it is assumed approximately 100% close to the layer. The interaction of droplet-LNG vapor is assumed adiabatic and the model provided the streamlines, isotherms, and isopleths of vapor movement. The model predicted that the effectiveness of dilution reduces from 65 to 18%, when the wind velocity increases from 1 to 4 m/s.

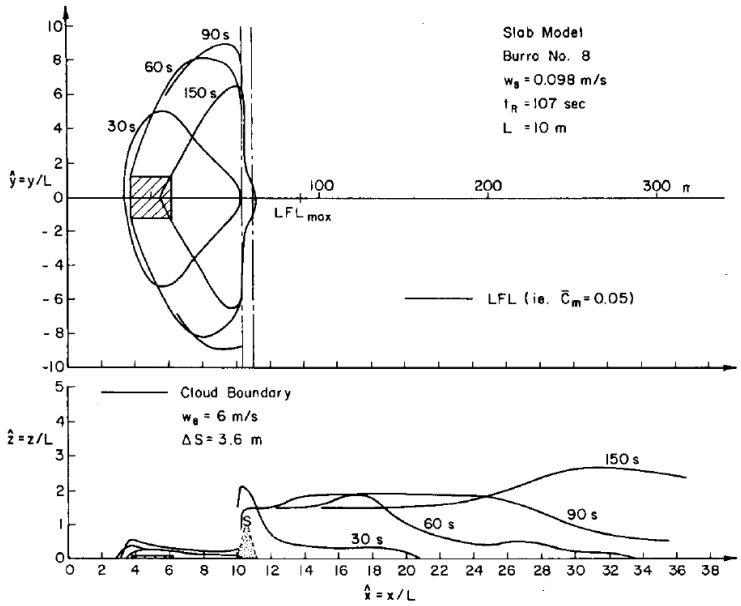

Fig. 11. Burro No. 8 LNG spill spray conditions, plan view and vertical section.

Fig. 27. Burro No. 8 LNG spill spray conditions, plan view and vertical section (Meroney & Neff, 1985)

Meroney and Neff (1985) developed a model that incorporates the numerical factors to both the box and slab model to predict the influence of the water spray dilution on the dense gas movement (Meroney & Neff, 1985). Fig. 27 shows the dilution effects evaluated from combining the slab model with the spray application. The semi-empirical factors are either added or multiplied to the entrainment velocity to provide detailed description of the dilution effects. The water spray setting that allows additional air entrainment of 6 m/s have shown 66% of the LFL distance reduction compared to the case without the mitigation effects. The models have shown that the height of the cloud increasing, which is the results of the vapor dilution. The numerical model predictions

were compared against the wind-tunnel experiments and the predictions showed reasonable agreements to the experimental data. This model was expanded later to also incorporate the effects of having vapor barriers around the source term (Meroney & Shin, 1992).

The integral-type modeling provided a quick prediction over the dense gas dispersion phenomena, and has shown reasonable prediction when compared to the small-scale experiments. However, the integral-models inherently present a fluid system, which limits the understanding of complex interaction and behavior of water droplets with the gas flow. The prediction results from the integral models are bounded by the simplified assumptions and correlations determined through semi-empirical parameters. Also, the integral-type model provided an under-prediction in certain scenarios, mainly because of the simplified assumption (Gavelli et al., 2008). These limited functions prevented from describing or predicting the complex dense gas behavior accurately when interacting within other geometries.

CHAPTER III

MODELING FORCED DISPERSION OF LNG VAPOR CLOUDS*

3.1 Introduction

In the present chapter, ANSYS Fluent was used to simulate the forced dispersion of an LNG vapor cloud using upward-oriented full-cone spray nozzles for which the results were validated against LNG spill experiments conducted at the Brayton Fire Training Field in March 2009. To simulate the gas (LNG vapors) and liquid (water droplets) phases properly, the CFD code was coupled with the Eulerian–Lagrangian spray model. The simulation setup was configured to include the dominant mechanisms of the water curtain, namely, momentum and heat transfer for dispersing the LNG vapor cloud upward, making it positively buoyant. Additional simulations were conducted with the atmospheric conditions from the Falcon-1 LNG spill test to consider a worst-case scenario of LNG releases and further determine the effectiveness of a water curtain in mitigating the vapor cloud. The sensitivity of the LNG vapor cloud reduction efficiency to the spray parameters was also investigated. The proposed work aims to provide guidance in setting up the assessment of the forced dispersion of an LNG vapor dispersion with a water curtain using the CFD code, which can be used for the design of an integrated, LNG-specific emergency response plan.

---

* Reprinted with permission from "Modeling of water spray application in the forced dispersion of LNG vapor cloud using a combined Eulerian-Lagrangian approach" by Kim, B. K., Ng, D., Mentzer, R. A., & Mannan, M. S. (2012). *Industrial & Engineering Chemistry Research*, 51, 13803-13814, Copyright 2012 American Chemical Society.

3.2 Numerical Simulation

The CFD code, which is based on the finite-volume method, was used to calculate the gas flow field. Subsequently, the Eulerian–Lagrangian spray model was integrated into the CFD code to simulate the interaction between water spray droplets (liquid/dispersed phase) and LNG vapors (gas/continuous phase). The liquid phase accounts for the movement of water droplets discharged from full-cone spray nozzles, whereas the gas phase describes the general airflow movement and methane gas emanating from the LNG pool.

3.2.1 Gas Flow Modeling

The simulation of the dispersion process of an LNG spill was performed using the finite-volume method to solve the basic equations governing the conservation of mass, momentum, and energy. The incompressible ideal-gas model was selected for the calculation of gas density, which is temperature-dependent and varies with the chemical composition. The governing equations can be summarized as follows:

The mass conservation equation is given by (Ranade, 2002)

$$\frac{\partial}{\partial t}(\rho m_k) + \nabla \cdot (\rho u m_k) = -\nabla \cdot (j_k) + S_k \qquad (3.1)$$

where ρ is the fluid density, m_k is the mass fraction of species k, u is the fluid velocity, j_k is the diffusive flux, and S_k is the mass production rate of species k from chemical reaction.

The momentum conservation equation:

$$\frac{\partial}{\partial t}(\rho u) + \nabla \cdot (\rho u u) = -\nabla \cdot \pi + \rho g + F_{ex} \qquad (3.2)$$

where

$$-\nabla \cdot \pi = -\nabla p + \nabla \cdot \tau \quad (3.3)$$

$$\tau_{ij} = \mu(\nabla u + \nabla u^{\mathrm{T}}) + (\kappa - \frac{2}{3}\mu)\delta_{ij}(\nabla \cdot u) \quad (3.4)$$

In these equations, π is the molecular flux of momentum, ρg is the gravitational body force, F_{ex} is the external body force, τ is the viscous stress tensor, δ_{ij} is the Kronecker delta (δ_{ij}= 1 if $i = j$ and δ_{ij}= 0 if $i \neq j$), μ is the coefficient of viscosity, and κ is the coefficient of bulk viscosity.

The energy conservation equation is given by

$$\frac{\partial}{\partial t}(\rho h) + \nabla \cdot (\rho u h) = -\nabla \cdot (q) + \frac{Dp}{Dt} - (\tau : \nabla u) - \nabla \cdot \left(\sum_k h_k j_k\right) + S_h \quad (3.5)$$

where

$$h = \sum_k m_k h_k \quad (3.6)$$

$$h_k = \int_{T_{\mathrm{ref}}}^{T} C_{\mathrm{p}k}\, dT \quad (3.7)$$

h is the enthalpy, T_{ref} is the reference temperature, $C_{\mathrm{p}k}$ is the specific heat of species k, q is the flux of enthalpy ($q = -k\nabla T$), and S_h is the volumetric source of enthalpy.

3.2.1.1 Atmospheric Boundary Condition

Details on setting up the atmospheric boundary conditions of the LNG spill in Fluent have been published elsewhere (Luketa-Hanlin et al., 2007). The Monin–Obukhov theory can be used to determine wind velocity, temperature, and turbulent profiles. Air flow in the atmospheric surface layer can be described as a transition from

shear-dominated to buoyancy-dominated turbulence that occurs at a particular elevation, known as the Monin–Obukhov length (Cormier et al., 2009).

In the case of limited data, an alternative approach introduced by Richards and Hoxey (1993) can be used (Richards & Hoxey, 1993). The measurements of wind velocity and turbulence are made at only one elevation assuming constant temperature along the elevation z.

$$U = \frac{u_*}{K} ln\left(\frac{z+z_0}{z_0}\right) \tag{3.8}$$

$$k = \frac{u_*^2}{\sqrt{C_\mu}} \tag{3.9}$$

$$\epsilon = \frac{u_*^3}{K(z+z_0)} \tag{3.10}$$

with,

$$u_* = \frac{KU_h}{ln\left(\frac{h_{ref}+z_0}{z_0}\right)} \tag{3.11}$$

where U is the wind velocity, u_* is the friction velocity, U_h is the specified velocity at the reference elevation h_{ref}, K is the von Karman constant (0.4), and z_0 is the surface roughness length.

The standard k-ϵ turbulence model was used to model the dense gas behavior of air-vapor mixture. This model has been shown to give relatively good predictions in modeling LNG vapor dispersion (Cormier et al., 2009; Luketa-Hanlin et al., 2007; Qi et al., 2010). The transport equations for turbulent kinetic energy (k) and its dissipation rate (ϵ) are given by (Ranade, 2002)

$$\frac{\partial(\rho k)}{\partial t} + \frac{\partial(\rho u_i k)}{\partial x_i} = \frac{\partial}{\partial x_i}\left(\frac{\mu_t}{\sigma_k}\frac{\partial k}{\partial x_i}\right) + G - \rho\varepsilon \tag{3.12}$$

and

$$\frac{\partial(\rho\epsilon)}{\partial t}+\frac{\partial(\rho u_i\epsilon)}{\partial x_i}=\frac{\partial}{\partial x_i}\left(\frac{\mu_t}{\sigma_\epsilon}\frac{\partial\epsilon}{\partial x_i}\right)+\frac{\epsilon}{k}(C_{1\epsilon}G-C_{2\epsilon}\rho\varepsilon) \quad (3.13)$$

where

$$G=\frac{1}{2}\mu_t\left[\nabla\bar{u}+(\nabla\bar{u})^T\right]^2 \quad (3.14)$$

In these equations, k is the turbulence kinetic energy, ϵ is the turbulence eddy dissipation rate, G is the turbulence generation term, and μ_t is the eddy viscosity. The default constant values for the standard k-ϵ turbulence model are C_μ = 0.09, $C_{1\epsilon}$ = 1.44, and $C_{2\epsilon}$ = 1.92. When simulating the atmospheric dispersion at < 100 m above the ground, one can consider using the constant values C_μ= 0.033, $C_{1\epsilon}$= 1.17, and $C_{2\epsilon}$= 1.92 to account for different thermal stratifications (Alinot & Masson, 2005).

3.2.1.2 Worst-Case Meteorological Conditions

Meteorological conditions, such as wind speed and direction, ambient air temperature, and amount of atmospheric turbulence, can have a significant role in determining the LNG release characteristics and vapor dispersion. The worst-case meteorology for LNG vapor dispersion is stable wind conditions, which can be represented with wind speeds of about 1–2 m/s and stability class F (NFPA, 2013). Under stable atmospheric conditions, there is very little turbulence; it is under such conditions that the release of LNG vapors poses the highest exposure potential. The stable case is characterized by limited mixing, providing little dilution of the released vapors. In this work, one of the atmospheric conditions from the 1987 LNG Vapor

Barrier Verification Field Trial conducted by the Lawrence Livermore National Laboratory was used as the worst-case dispersion conditions (T. C. Brown et al., 1990).

The LNG natural dispersion model was calibrated using the concentration data from experiments, and the physical parameters for LNG forced dispersion were obtained from the water spray setting used in the MKOPSC LNG spill experiments. The other parameters, such as the numbers of parcels, and the droplet velocity, were calibrated using the dilution factor. Using the LNG forced dispersion model, the atmospheric condition from the Falcon-1 experiment, which allows simulating an actual stable condition, was applied to show the worst-case dispersion condition. The worst-case scenarios show the largest credible concentration to be observed at the farthest location from the LNG source. The effectiveness of the water spray mitigation was represented by the momentum ratio and dilution factor (Hald, Buchlin, Dandrieux, & Dusserre, 2005).

3.2.2 Water Spray Modeling

To reduce the complexity associated with the mitigation process of LNG vapors with water sprays, several assumptions were made to simplify the problem. The water droplets were assumed to be spherical and to have a constant density, specific heat, and thermal conductivity. Instead of using the size distribution of the water droplets discharging from the spray nozzles, the simulated droplets were independently prescribed with an initial size, velocity, and position. In addition, the turbulence

generated within the spray and droplet breakup, collision, evaporation, and coalescence were not considered in this work.

In this work, a discrete phase model (DPM) was applied to simulate the water droplets using Lagrangian particle tracking. Because a large number of droplets can greatly increase the computation time, instead of tracking each individual droplet, the DPM optimizes the CPU efficiency by grouping the droplets into parcels to represent certain collections of droplets that share the same properties (Abraham, 1997; Dukowicz, 1980). Each parcel contains a comparable mass of water. In addition, the Lagrangian approach couples the solution of the disperse phase to the continuous phase, and as a result, the mass, momentum, and heat exchanges between the two phases can be computed.

The trajectory of the droplets is integrated in the Lagrangian reference frame using the force balance, which is expressed as (ANSYS, 2009)

$$\frac{du_p}{dt} = F_D\left(u - u_p\right) + \frac{g_x(\rho_p - \rho)}{\rho_p} + F_x \tag{3.15}$$

$$F_D = \frac{18\mu_f}{\rho_p d_p^2}\frac{C_D Re}{24} \tag{3.16}$$

$$\mathrm{Re} \equiv \frac{\rho d_p |u_p - u|}{\mu} \tag{3.17}$$

$$C_D = a_1 + \frac{a_2}{\mathrm{Re}} + \frac{a_3}{\mathrm{Re}^2} \tag{3.18}$$

$$F_x = \frac{1}{2}\frac{\rho}{\rho_p}\frac{d}{dt}\left(u - u_p\right) + \left(\frac{\rho}{\rho_p}\right)u_{p_i}\frac{\partial u}{\partial x_i} \tag{3.19}$$

where F_D is the drag force per unit mass; u_p, u and ρ_p, ρ are velocities and densities, respectively, of the droplets and of the gas phases; g_x is the gravitational vector; and F_x

is the sum of virtual mass force and pressure gradient; μ_f is the fluid viscosity; C_D is the drag coefficient, with constants a_1, a_2, and a_3 determined by the Reynolds number range (assuming a spherical droplet shape (Morsi & Alexander, 1972)); d_p is the droplet diameter; and Re is the Reynolds number. The virtual mass force arises from the displacement of the fluid by the droplets, acting in the opposite sense of the drag force, and the pressure gradient force is the force acting on the air from the spatial variations of the pressure (Barry & Chorley, 2003; Crowe, 2006). It was assumed that the water droplets interact only with the mean gas flow, and thus, the effects of turbulence on droplet dispersion were not considered.

The change in the droplet temperature, T_p from heating or cooling effects was calculated using the expression

$$m_p c_{p_{\mathrm{p}}} \frac{dT_p}{dt} = h_\infty A_p\left(T_\infty - T_p\right) + \epsilon_p A_p \sigma(\theta_R^4 - T_p^4) \qquad (3.20)$$

where m_p, $c_{p_{\mathrm{p}}}$, and A_p are the mass, heat capacity, and surface area, respectively, of the droplets; T_∞ is the temperature of the gas phase; h_∞ is the convective heat transfer coefficient; ϵ_p is the droplet emissivity, σ is the Stefan-Boltzmann constant, θ_R is the radiation temperature [$\left(\frac{G}{4\sigma}\right)^{1/4}$, where G is the incident radiation]. The radiation term in the heat transfer equation is considered only when the contribution of radiation heat transfer is significant; however, this phenomenon is very unlikely and is not applicable in this work.

As the droplets disperse in the continuous phase, the momentum transfer in each control volume from the droplets is calculated as

$$F = \sum \left(\frac{18\mu C_D Re}{\rho_p d_p^2 24} (u_p - u) + F_{other} \right) \dot{m}_p \Delta t \tag{3.21}$$

where F_{other} represents the other interaction forces, such as the virtual mass force and pressure gradient force; $\dot{m}_p$ is the mass flow rate of the droplets; and Δt is the time step.

The heat transfer to the gas phase from the droplets is also calculated when the droplets disperse through each control volume. The heat transfer equation in the absence of chemical reaction is given by

$$\mathrm{Q} = \frac{\dot{m}_{p,0}}{m_{p,0}} \left[-m_{p\mathrm{out}} \int_{T_{ref}}^{T_{p\mathrm{out}}} c_{p_\mathrm{p}} dT + m_{p\mathrm{in}} \int_{T_{ref}}^{T_{p\mathrm{in}}} c_{p_\mathrm{p}} dT \right] \tag{3.22}$$

where $m_{p,0}$, $\dot{m}_{p,0}$ are the initial mass and initial mass flow rate, respectively, of the droplet injection; $m_{p\mathrm{in}}$ and $m_{p\mathrm{out}}$ are the masses of the droplets upon cell entry and cell exit, respectively; c_{p_p} is the heat capacity of the droplets; H_{pyrol} is the heat of pyrolysis as volatiles are evolved; $T_{p\mathrm{in}}$ and $T_{p\mathrm{out}}$ are the temperatures of the droplets upon cell entry, and cell exit, respectively; T_{ref} is the reference temperature for enthalpy; and $H_{lat\mathrm{ref}}$ is the latent heat at the reference conditions.

Because of the low solubility of natural gas (mostly consisting of methane) in water, the effect of mass transfer was neglected. Moreover, the inert type particle was applied from DPM, where only the momentum and heat transfer equations in the continuous phase were calculated. The effects of the heat of pyrolysis and latent heat are not involved for the inert type particle, as combustion and evaporation effects were not considered.

3.3 Experimental Setup

Fig. 28 shows the experimental setup of LNG-water curtain outdoor experiment at the Brayton Fire Training Field in March 2009. A total of eight conical nozzles (1-in. TF 48 NN BETE fog nozzle) were installed in a 2-in.-o.d. OD carbon pipe. Two sets of four nozzles were installed consecutively on a two 8-ft-long carbon pipes in V-shaped pipe sections. The conical spray used in this experimental work produced a 60° full cone, spiral pattern.

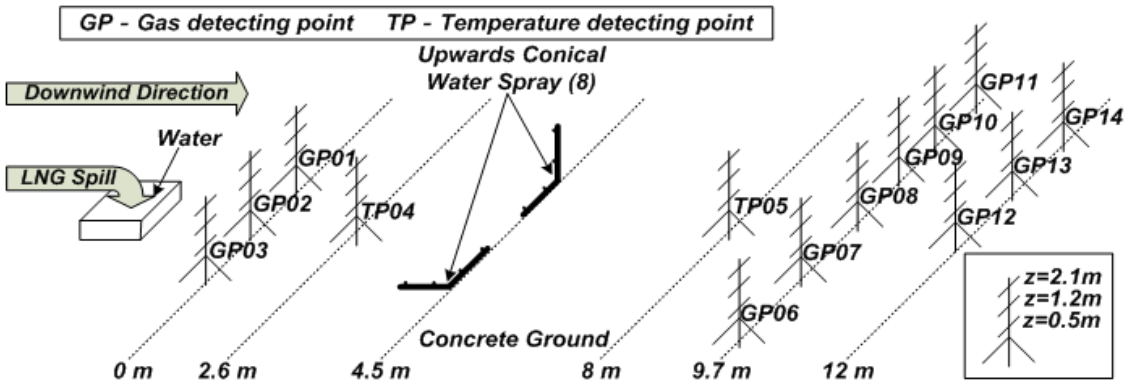

Fig. 28. MKOPSC March 2009 LNG outdoor experimental setup

Table 1 summarizes the water spray settings used in the forced dispersion of LNG vapors experiment in the March 2009 test (Rana, 2009). Fig. 29 shows the conical water curtain used in the experimental work when fully activated.

Table 1. March 2009 MKOPSC LNG outdoor experiment test-1

water nozzle information

Type	Upward Conical Type
Number of nozzle	8
Water pressure [kPa]	327.4±17
Total water flow rate [m^3/s]	36.5×10^{-3}
Water flow rate per nozzle [m^3/s]	4.6×10^{-3}
Time of activation [s]	400
Water total [m^3]	14.6
SMD [mm]	0.89 - 0.98
Avg. water curtain elevation [m]	4.60

Fig. 29. Upward conical water sprays from March 2009 MKOPSC LNG experiment

Fig. 30. LNG pool setup from March 2009 MKOPSC LNG experiment

The LNG was spilled onto a confined area of 1.52 m × 1.52 m × 0.31 m. A total of 40 m^3 of LNG was spilled on the water using an L-shaped discharge pipe with a flow rate of 0.30–0.34 m^3/s. The LNG pit setup is shown in Fig. 30. The point gas detectors and type-K thermocouples were placed at different downwind distances from the LNG pool to collect concentration and temperature data. Thermocouples were also installed above the LNG pool at different elevations to measure the changes in temperature, which is an important parameter for estimating the evaporation rate. The average mass flux used in this work was 0.2 kg/(m^2 s) (Rana, 2009). To ensure consistency in collecting the dispersion data, the design of the experiment was carefully reviewed by considering the local weather forecast. The locations of the gas detectors and thermocouples were determined using wind information collected from the weather

station at the experimental site. Data on LNG natural dispersion were collected for 600 s and the conical water spray was applied for 400 s. The experiment was designed to allow the data to be collected throughout the duration of LNG dispersion to ensure that the data represented the effectiveness of LNG forced dispersion with a certain level of confidence. The concentration data collected from the LNG forced mitigation was averaged over time to acquire a mean value of the concentration to determine the effectiveness of the water spray application.

3.4 Simulation Specifications

3.4.1 LNG Vapor Dispersion

The computation domain was created in ANSYS platform with the downwind direction set in x-direction. The y and z directions were set perpendicular and vertical, respectively, with respect to the downwind direction. The simulation of natural dispersion of LNG spills was set for 600 s and that of forced dispersion of LNG vapors with water spray was applied for 400 s. These scenarios are based on the experimental work from the March 2009 test. The inlet boundary condition was applied for the LNG vapors flowing into the domain with an average mass flux rate of 0.2 kg/(m^2 s), which was calculated from March 2009 data (MKOPSC, 2010; Rana, 2009). For simplicity, it can be assumed that the physical properties of LNG are the same as those of pure methane at 111 K. This assumption is reasonable because, during the release of LNG, methane vaporizes rapidly as compared to other heavier hydrocarbons (Cormier et al., 2009). The meteorological conditions used for inlet profiles for validating the model

were obtained from the experimental work by Rana and Mannan (2010), and the Falcon-1 meteorological data were used for simulating the worst-case release scenario (T. C. Brown et al., 1990; Rana & Mannan, 2010). The pressure outlet boundary condition was set at the downwind boundary. A symmetry condition was applied to the two sides and upper boundaries, such that the normal velocity and gradients of all variables were equal to zero. The ground was considered as a wall boundary condition with an appropriate roughness inferred from the wind profile. Because the water droplets were treated as discrete particles in the discrete boundary condition, the ground was set as a trap condition to terminate the droplet trajectories as they contacted the ground.

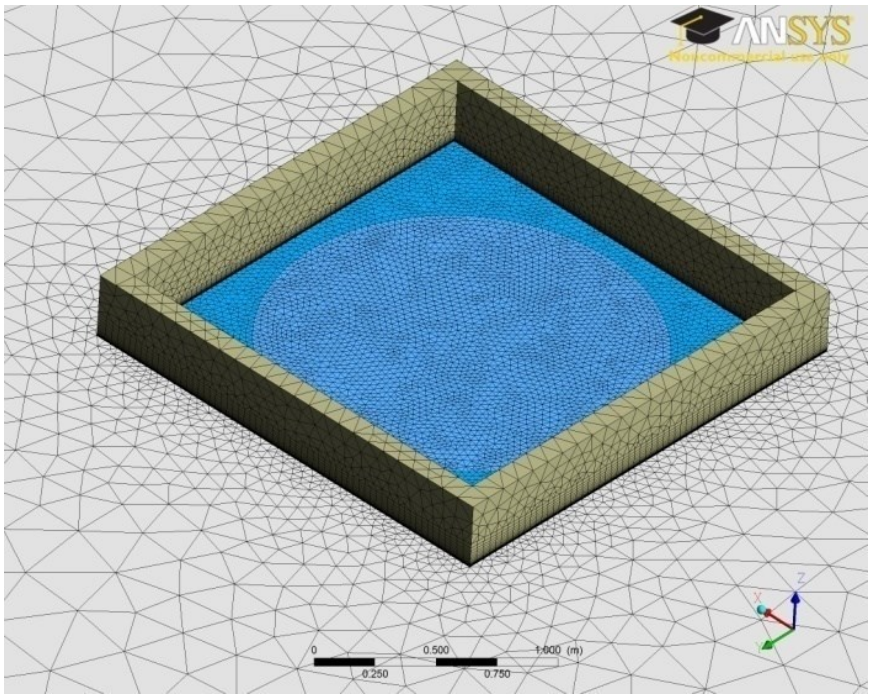

Fig. 31. Geometry construction and meshing details around LNG source

The atmospheric conditions were set with the weather data, and the size of the grid was reduced until no significant difference was observed from the steady state solution of the wind profile. The difference in the velocity profile was within the range of 2%, which was 0.07 m/s in magnitude along the z coordinate when fully developed. With the grid-independent setting, a total of approximately 985,000 elements were created. The mesh at the source term was refined up to 0.024 m to achieve better resolution (Fig. 31). A finer grid was set with inflation layers from the ground level to improve the solution where LNG vapors propagated initially until sufficiently warmed to become positively buoyant and disperse into the atmosphere.

A simplified approach to predicting the turbulence within the source term was proposed by Luketa-Hanlin et al. (2007). This turbulence model, which assumes that the pool is round and has an inlet velocity, is expressed by the following equations (Luketa-Hanlin et al., 2007)

$$k = \frac{3}{2}\left(v_g T_i\right)^2 \tag{3.23}$$

$$\varepsilon = C_\mu^{3/4} \frac{k^{3/2}}{0.07D} \tag{3.24}$$

where

$$v_g = \frac{(\rho v)_{\text{liq}}}{\rho_{\text{g}}} \tag{3.25}$$

In these equations, v_g is the inlet pool velocity for the LNG source, $(\rho v)_{\text{liq}}$ is the mass flux of LNG, ρ_{g} is the methane density (1.76 kg/m^3 at 111 K), T_i is the turbulence intensity (1-10 %), and D is the pool diameter. The recommended range for the turbulence intensity at the source term is between 1 and 10 % (Cormier et al., 2009).

This setting considers only the evaporation effect of an LNG vapor from the source term. The actual intensity can be greater than 10% when the effects of fluctuations in the flow rate of discharged LNG and water movement under the LNG are considered (Gavelli et al., 2009).

3.4.2 Water Spray

The CFD simulation of the forced dispersion of LNG vapor clouds by a water curtain was performed using the experimental settings listed in Table 1. Table 2 summarizes the details of the settings applied in simulating the forced dispersion for the water curtain simulation.

Table 2. Simulation setting for the forced dispersion

Injection type	Solid-cone
Radius (nozzle size) [m]	1.27×10^{-3}
Cone angle (half-angle of cone) [degree]	30^0
Particle type	Inert
Material	Water
Droplet diameter [mm]	0.935
Temperature [K]	300
Mass flow rate ($\dot{m}_p$) [kg/s]	4.6
Drag law	Spherical
Heat transfer	Two-way coupling

The dilution factor was evaluated to find the effectiveness of forced dispersion modeling with the experimental data. The dilution factor in this work was defined as the ratio of the average concentrations at 0 and 9.7 m downwind, as measured from the same elevation. The downwind direction was assumed to have a constant speed throughout the propagation of the vapor cloud. In addition, the meteorological conditions from the Falcon-1 test were employed in the simulation setup to evaluate the efficiency of the forced dispersion of LNG vapors by a water curtain. To evaluate the influence of the spray's momentum transfer on the LNG vapor dispersion, two parameters, namely the initial droplet velocity and the water flow rate, were adjusted to evaluate different scenarios with various momentum ratios under the same atmospheric conditions. The momentum ratio is defined as the ratio between the momentum of the water droplet and the air-vapor mixture (Hald et al., 2005). In addition, the heat transfer effects from various water droplet temperatures were evaluated by altering the droplet temperature from 283 to 313 K while keeping the rest of the parameters constant.

The simulation time was set to 200 s for each scenario based on the results of the previous simulations, in which the concentration data reached steady state within the first 100 s in all cases. The natural dispersion modeling of the LNG vapor cloud was set up with the same settings applied in the model calibration. The domain created from the calibration step was applied with different forced dispersion settings to accommodate the momentum ratio for each scenario. Each scenario consisted of 200 s of natural dispersion without the water barrier and another 200 s of forced dispersion with the water barrier.

3.4.3 Model Validation

The volumetric concentration and temperature data collected from the March 2009 test were used to calibrate the physical parameters for modeling the natural dispersion of LNG vapor clouds. Prior to injecting the LNG vapor clouds into the computation domain, the steady state solution was achieved with the wind profile, and the transient mode initiated with time set at t = 0 s. At t = 0 s, the LNG vapor was introduced at the constant mass flow rate, with all other conditions, such as the atmospheric conditions and mesh setting, left unchanged until the simulation was terminated at 600 s. This step provided the whole domain with the fully developed wind profile and minimized any numerical errors that might have occurred when the LNG vapor cloud was initially introduced into the domain.

The turbulence intensity at the LNG source was calibrated in the range of 1 to 10%. As the turbulence intensity was increased from 1 to 10%, no significant difference was observed in the concentration data. This is mainly due to the size of the LNG spill, which was rather small as compared to other reported LNG spill experiments in the literature. In this work, a turbulence intensity of 10% is assumed at the LNG source, which considers only the vaporization effect of the LNG. This simplified turbulence intensity is often applied in modeling LNG vapor dispersion because phase transitions are complicated phenomena that are computationally expensive to simulate.

The grid size at the ground was refined to calibrate the volumetric concentration data more thoroughly. The overall concentration in the downwind region was controlled by properly modifying the grid size at the ground; the ground mesh was directly related

to the number of grid points generated in the spatial region above. The size was refined to one-half the size of the grid applied at atmospheric level to calibrate the simulation results to the experimental data. The overall calibration focused on achieving a more conservative prediction that overpredicted the concentration data, resulting in a greater safety distance.

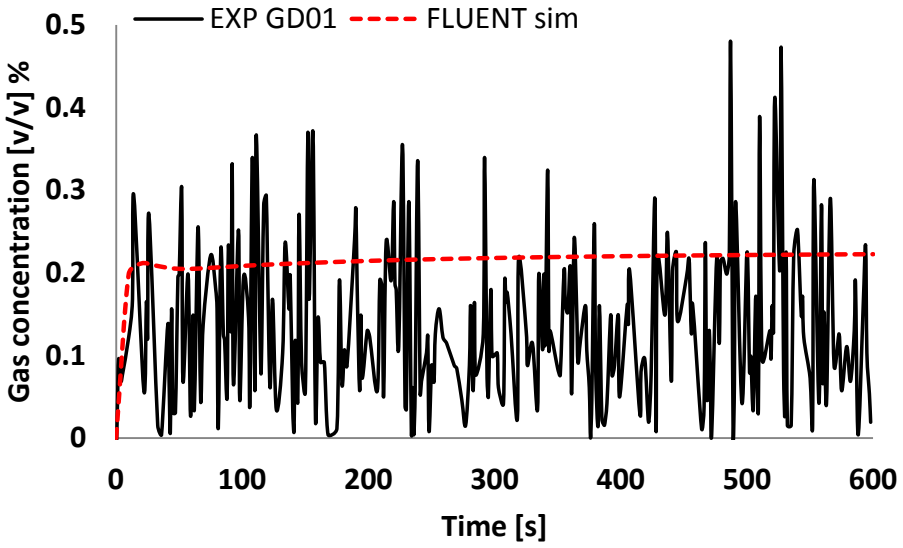

Fig. 32. Comparison of volumetric gas concentration in simulation result with experimental data at 0 m downwind distance (z = 0.5 m)

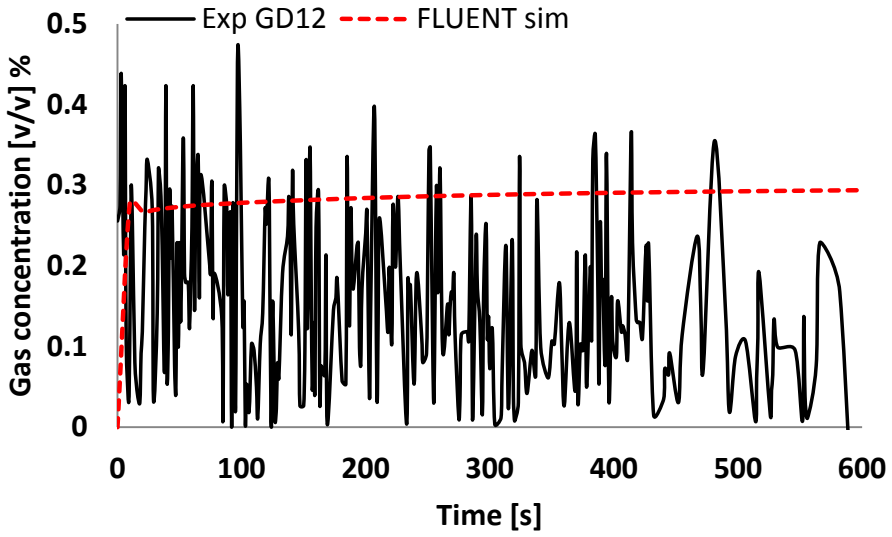

Fig. 33. Comparison of volumetric gas concentration in simulation result with experimental data at 0 m downwind distance (z = 1.2 m)

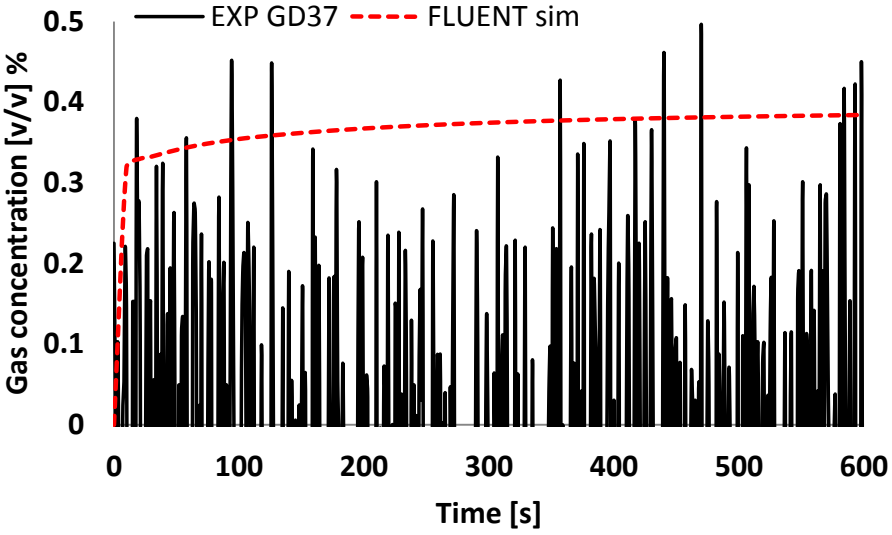

Fig. 34. Comparison of volumetric gas concentration in simulation result with experimental data at 9.7 m downwind distance (z = 0.5 m)

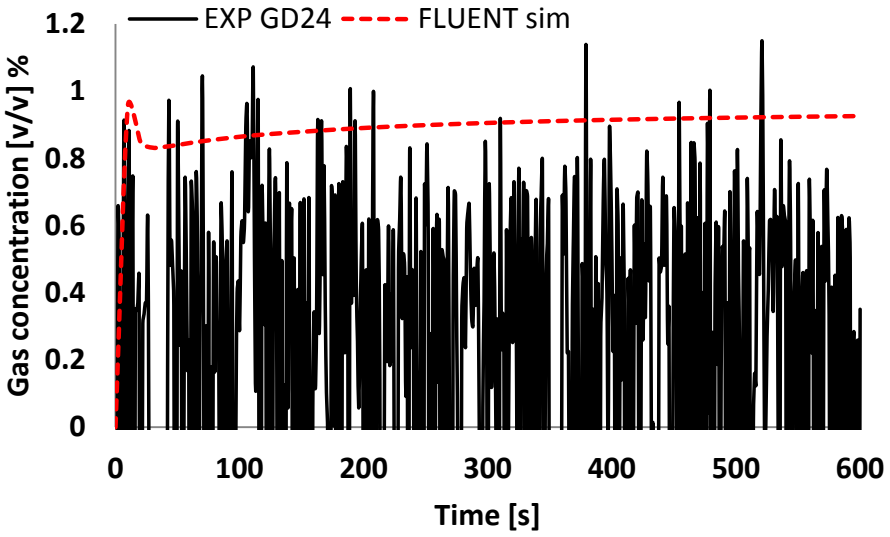

Fig. 35. Comparison of volumetric gas concentration in simulation result with experimental data at 9.7 m downwind distance (z = 1.2 m)

Figs. 32–35 show the measured gas concentrations from the experimental work and simulation predictions at two downwind distances (0 and 9.7 m). The fluctuations in the experimental data were caused by wind gusts and turbulence induced from the small confinement around the spill area. It can be seen that all of the simulation results overpredicted the experimental data, which is a desirable outcome in determining the LNG vapor cloud exclusion zone. When the LNG was released into the small confinement, it began to vaporize rapidly to form a cold, dense gas cloud and drift downwind. The increase in downwind gas concentrations in the event of an LNG release is shown here through CFD simulations. As seen in Figs 34 and 35, the simulated profile at 9.7 m downwind showed higher concentration levels at both ground level and 1.2 m elevation compared to the predicted profile near the spill location (0 m). This implies

that the CFD simulation is capable of depicting the change in cloud buoyancy. The underprediction of some peak concentrations in Fig. 32 might be caused by the incomplete description of heat transfer at the source term in the simulation setup. To obtain an accurate result, heat transfer from the ground and solar radiation should be included in the simulation setup.

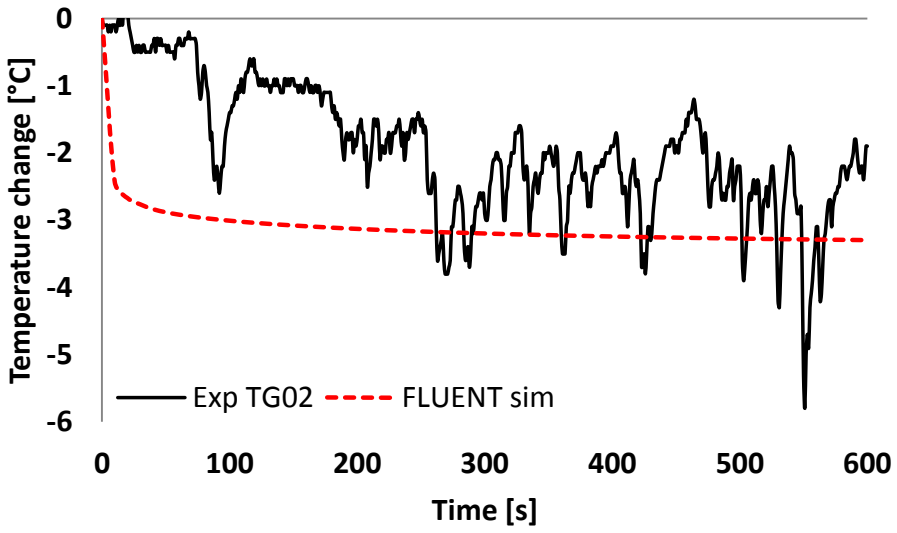

Fig. 36. Temperature change profile of air-vapor mixture at 2.6 m downwind distance (z = 1.2 m)

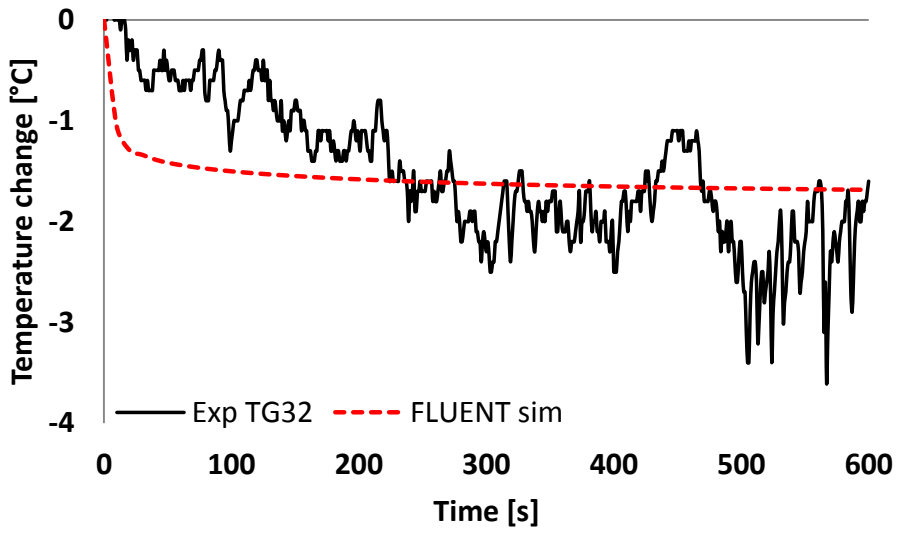

Fig. 37. Temperature change profile of air-vapor mixture at 8 m downwind distance (z = 1.2 m)

As stated above, the cloud buoyancy is affected by different heat transfers to the LNG vapors, which can be depicted through the change in downwind air-vapor mixture temperatures, as shown in Figs. 36 and 37. At 1.2 m elevation, the simulated results in Figs. 36 and 37 fall within the range of measured values. It can be concluded that the temperature change from the simulation work shows an overall agreement with the results of the natural dispersion experiment.

Forced dispersion modeling was applied using the discrete particle model (DPM). Sensitivity analyses were conducted with different numbers of parcels to obtain the optimum number of parcels to be injected at every time step. The number of parcels introduced per time step was increased until no further change in the simulation output was observed. For this simulation, 100 parcels were injected from each nozzle per time

step. The time step was set at 0.5 s. Sensitivity analyses were also conducted with various droplet velocities to determine the appropriate range of initial droplet velocity because of the unavailability of this information from the experiments. The water flow velocity was calculated from the flow rate, and the droplet velocity was estimated from the calculated velocity value, assuming that the droplets accelerated from the pressure gradient as the bulk liquid traveled across the water nozzle. The droplet velocity was used to simulate the water spray to compare the height of the spray generated with the water spray height observed from the MKOPSC LNG spill experiments to ensure the validity of the estimated droplet velocity. The dilution factor from the experimental setup was averaged over the whole period of time (400 s). The average value of the dilution factor from the experiment was 10.43. The physical parameters, such as the parcel produced per time step and initial velocity, were calibrated. The dilution factor value from the simulation results was 10.46, which is in close agreement with the 10.43 value derived from the experimental data.

Using the validated CFD baseline model and the Eulerian-Lagrangian approach to account for the water spray mechanisms, additional simulations were performed to evaluate the different effects of the dominant mechanisms in diluting the LNG vapors: the momentum and heat transfer.

3.4.4 Effects of Momentum on LNG Vapor Clouds

Fig. 38 shows the correlation between the momentum ratio and dilution factor of water sprays for 17 different scenarios simulated. The 17 different momentum ratios were calibrated by alternating the water flow rate and the initial droplet velocity.

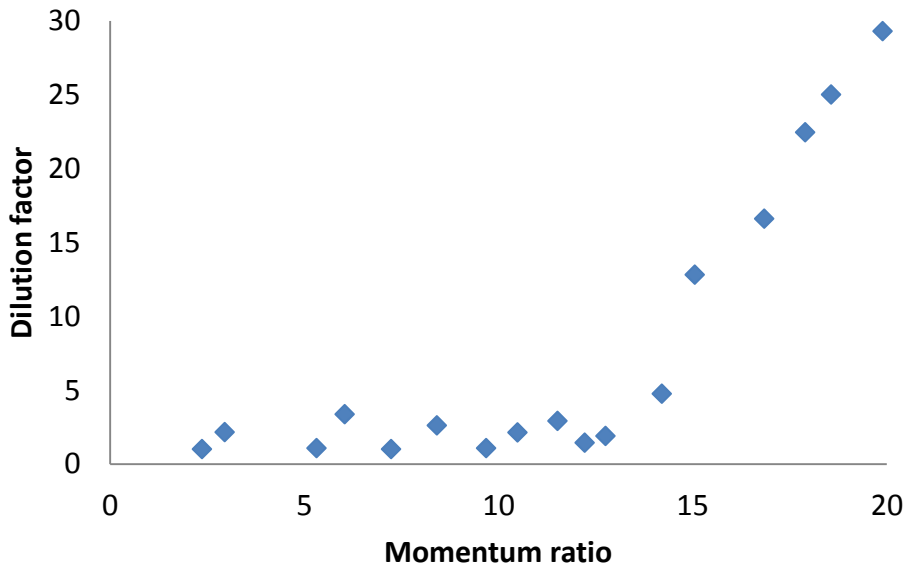

Fig. 38. Correlation between momentum ratio and dilution factor

The momentum ratio increased from the lowest scenario (R_M = 2.36) to the highest scenario (R_M = 19.90) owing to an increase in the droplet velocity and water flow rate. These two parameters play an important role in determining the momentum transfer from the water droplets to the LNG vapors. The effectiveness of the forced dispersion of vapor clouds by a water curtain becomes more apparent when the momentum ratios increase. This holds true because low momentum sprays create

insufficient air entrainment in the vapor cloud, resulting in less dilution of LNG vapors, whereas the use of a high momentum spray can rapidly dilute the cloud below its lower flammability limit.

3.4.5 Vapor Behavior of LNG Natural/Forced Dispersion

Figs. 39–42 show the predicted simulation results at the downwind concentrations from the natural dispersion and forced dispersion tests at four different elevations (z = 0, 0.5, 1.2, and 2.1 m) above ground level. The simulated gas concentration profiles from the forced dispersion tests are shown with two different momentum ratios (R_M = 5.32 and 12.76).

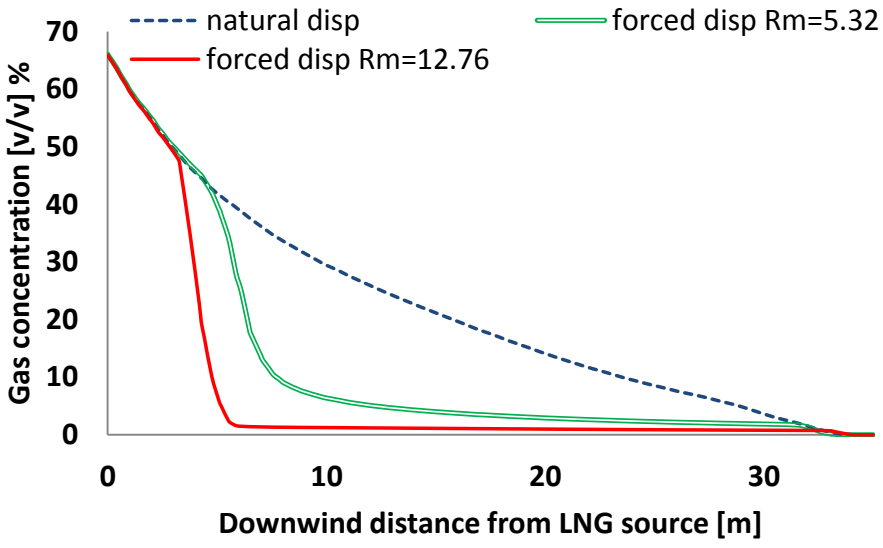

Fig. 39. Volumetric concentration along the downwind direction at z=0m for natural/forced (RM=5.32)/forced (RM=12.76) dispersion

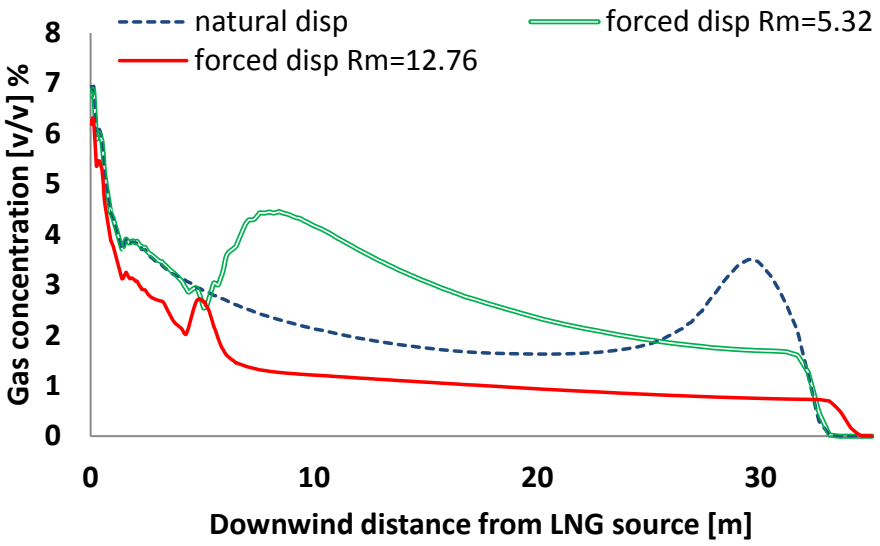

Fig. 40. Volumetric concentration along the downwind direction at z=0.5m for natural/forced (RM=5.32)/forced (RM=12.76) dispersion

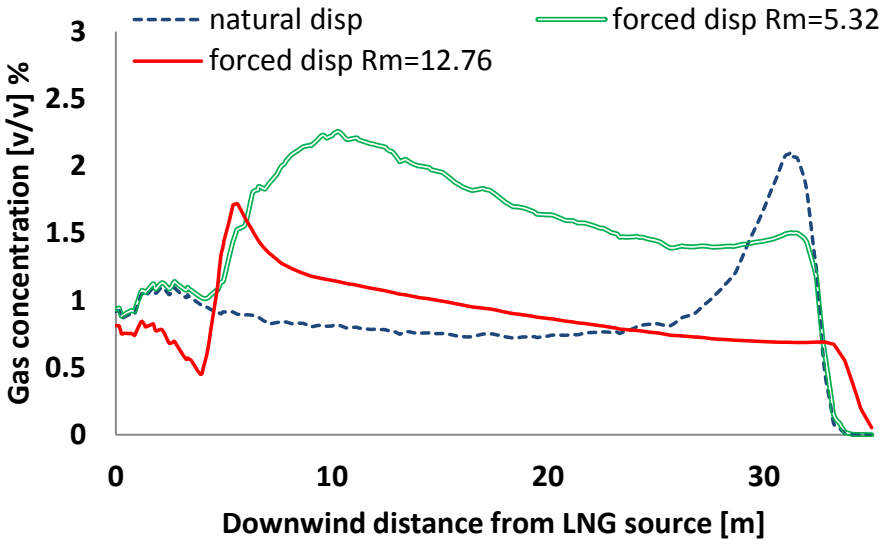

Fig. 41. Volumetric concentration along the downwind direction at z=1.2m for natural/forced (RM=5.32)/forced (RM=12.76) dispersion

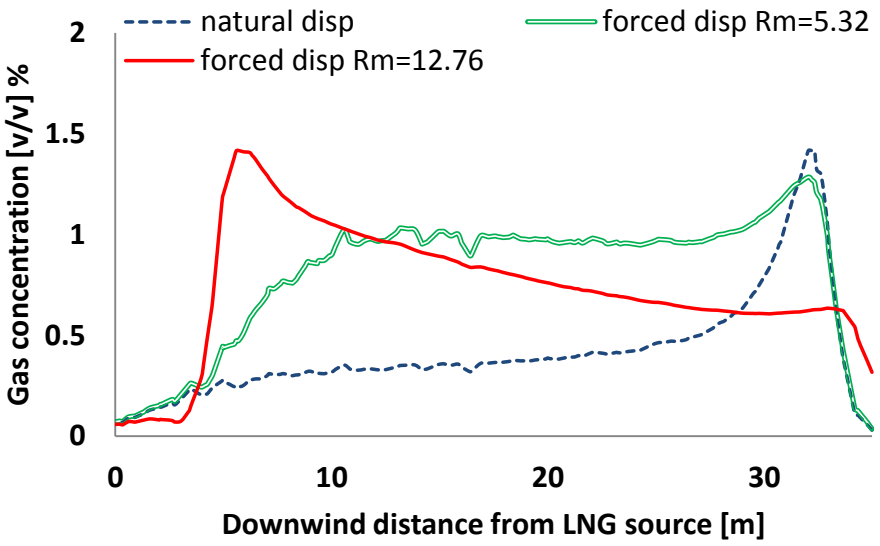

Fig. 42. Volumetric concentration along the downwind direction at z=2.1m for natural/forced (RM=5.32)/forced (RM=12.76) dispersion

As shown in Fig. 39, the decrease in the downwind concentrations after the water curtain activation is most apparent at the ground level, particularly for the profile with a momentum ratio of 12.76. As seen from the natural dispersion profile, the vapor cloud exclusion zone, that is, the distance to the 50% lower flammable limits (2.5% v/v) as measured from the downwind vertical centerline plane, is 31 m from the LNG source. With water spray activation, the exclusion distance further decreases to 23 and 5.5 m (25.8% and 82.3% reductions in the safety distance) for the momentum ratios of 5.32 and 12.76, respectively. This result is in agreement with the correlation between the momentum ratio and dilution factor depicted in Fig. 38, where a high momentum ratio is effective in changing the course of vapor dispersion and promoting dilution through air entrainment, thereby reducing the vapor exclusion zone.

As seen in Figs. 40 and 41, in the absence of water sprays, the gas concentration continues to decrease downwind because of mixing with the surrounding air and starts to rise at approximately 30 m, with a significant amount of buoyant vapors present at higher elevation. As more mixing occurs, more buoyant vapors are detected at higher elevations, as shown by the gradual increase of gas concentration in Fig. 40. This trend is in agreement with the concentration data from Figs. 32–35, where the vapor concentration increased at both elevations (z = 0.5 and 1.2 m) as the vapor traveled in the downwind region for the LNG natural dispersion. The postspray concentration profiles also show an overall reduction in concentration along the downwind distance; the sudden rise in concentration after passing the spray envelope might be caused by the turbulence induced by the air velocities within the spray. For the momentum ratio of 5.32, the concentration increased at all elevations above ground level. However, the vapor concentration did not drop to zero, but rather followed behavior similar to that for natural dispersion around 30 m from the LNG pool in the downwind direction. This is due to the fact that the forced dispersion with a momentum ratio of 5.32 did not provide sufficient spray momentum to push the vapor cloud upward and disperse it into the atmosphere. The vapor cloud at the ground level was only pushed to the upper detection levels, leading to an increase in concentration at higher levels. This implies that forced dispersion with a momentum ratio of 5.32 is not an effective mitigation measure.

On the other hand, the graph at 0.5 m elevation shows a rapid decrease in concentration when the momentum ratio is 12.76. This implies that the vapor clouds were sufficiently pushed by the water sprays to disperse in the atmosphere and that the

vapors did not accumulate below the 0.5 m range detection level after passing through the water curtain. The concentration data at 1.2 m and 2.1 m elevations for the momentum ratio of 12.76 also show an increasing trend, similar to that of the momentum ratio in the 5.32 case. However, for the data at 2.1 m elevation, the concentration rapidly increased after passing through the spray envelope, implying that the momentum ratio of 12.76 was more efficient in pushing the gas upward than the 5.32 case, in which the trend of concentration drop due to dispersing in the atmosphere 30 m in the downwind direction was no different from that for natural dispersion. The postspray concentration profile with a momentum ratio of 12.76 was more effective in vapor mitigation, as depicted by the gradual drop in concentration over downwind distance.

In summary, whereas the concentration data above ground level showed a higher trend for a momentum ratio of 5.32 than 12.76, the concentration at ground level indicated more reduction for the momentum ratio of 12.76. The lower vapor concentration observed at 0.5 and 1.2 m for the momentum ratio of 12.76 is due to the vapors being pushed beyond the detection level and dispersing into the atmosphere after passing through the spray envelope region. The momentum ratio of 12.76 showed more favorable results, where the vapors were sufficiently dispersed and there was no accumulation of the vapor cloud at the lower level.

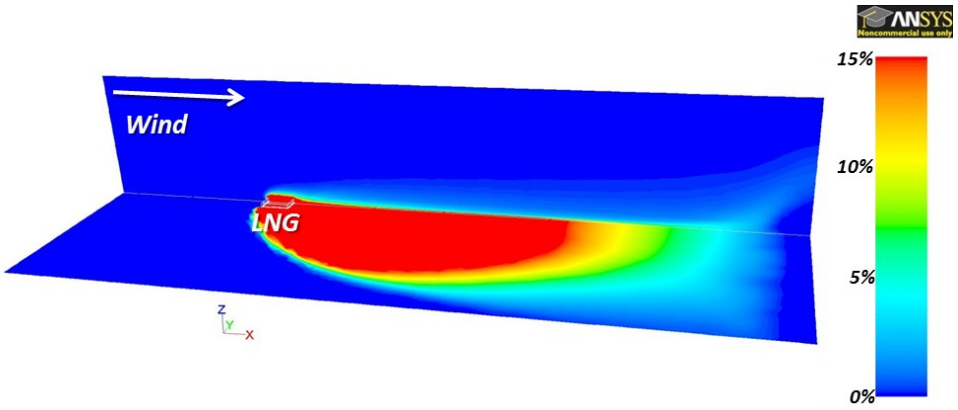

Fig. 43. Volume fraction contour of natural dispersion of vapor cloud at t = 200

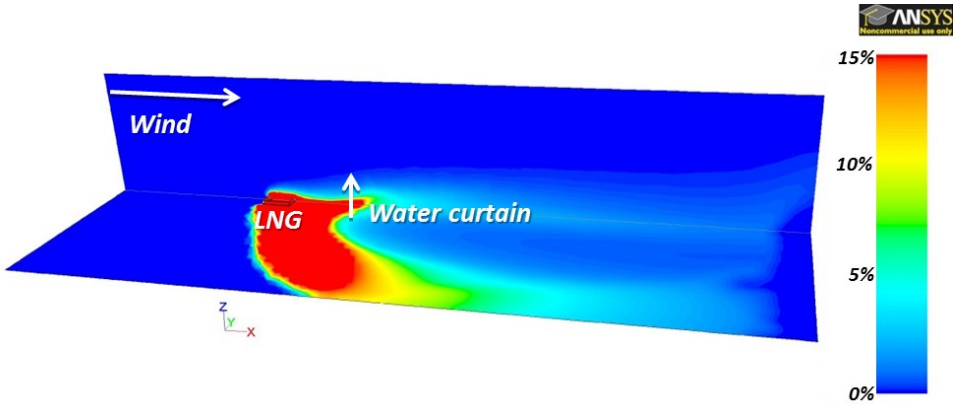

Fig. 44. Volume fraction contour of forced dispersion of vapor cloud at Rm=5.32

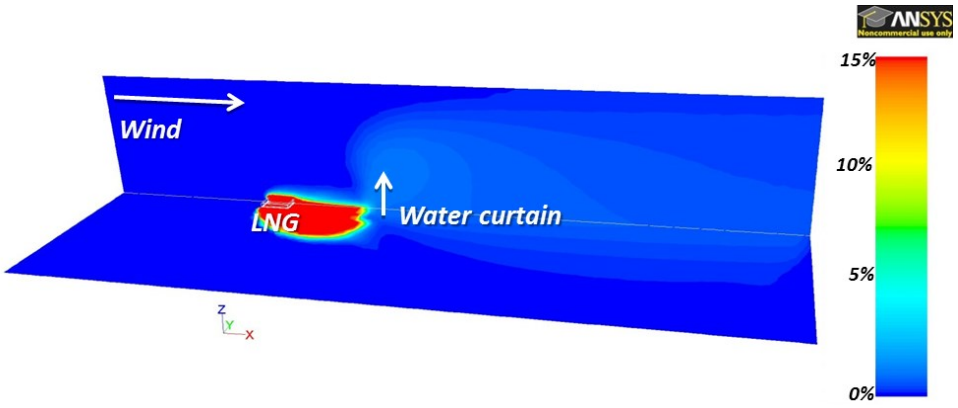

Fig. 45. Volume fraction contour of forced dispersion of vapor cloud at Rm=12.76

Fig. 43 shows the LNG volume fraction contour from the natural dispersion simulation after 200 s. As seen in Fig. 43, the cold vapor cloud drifted in the downwind direction and behaved like a passive Gaussian cloud before it started lifting into the atmosphere. The contour result also does not show any significant wind driven mixing in the cloud dispersion, mostly because of the stable atmospheric condition applied from the Falcon-1 test. To observe the effects of forced mitigation by water sprays, simulations on natural and forced dispersion were repeated with the same settings applied from March 2009 experiments as shown in Fig. 28. The water spray activation was set up 4 m from the LNG source. Figs. 44 and 45 show the volume fraction contours of the forced dispersion of LNG vapors applied at two different momentum ratios: R_M = 5.32 and R_M = 12.76. In both cases, dilution was enhanced when the air and vapors were being drawn in radially to the center of the spray envelope and then redirected upward by the upwind force created by the spray momentum. As seen in Fig. 44 (R_M = 5.32), the momentum imparted by the water sprays was not sufficient to form spray barriers, thus

causing a significant portion of the vapors to flow to the sides of spray envelope. The resulting vapor cloud movement followed the flow pattern of natural dispersion. On the contrary, Fig. 45 (R_M = 12.76) clearly shows that the water curtain changed the course of vapor propagation by deflecting the vapor cloud vertically upward and redirecting the flow downward due to the formation of a recirculation zone in the immediate wake of the water sprays, which enhanced dilution with entrained air. As a result, a significant dilution effect was observed behind the spray envelope for the test scenario with a momentum ratio of 12.76.

3.4.6 Heat Transfer on LNG Vapor Dispersion

The evaluation of the heat transfer effect on the forced dispersion of LNG vapors by water spray was conducted with various water temperatures. While other parameters for the water curtain simulation were fixed to constant values, the temperature of the droplets was varied (283, 293, 303, and 313 K).

To observe the extent of heat transfer contribution to vapor mitigation, further simulations of natural and forced dispersion were performed with the same conditions as before, with the exception of water temperatures, which were varied to examine the effects of heat transfer. The LNG vapors were introduced into the domain for 200 s and the water spray was activated at 200 s.

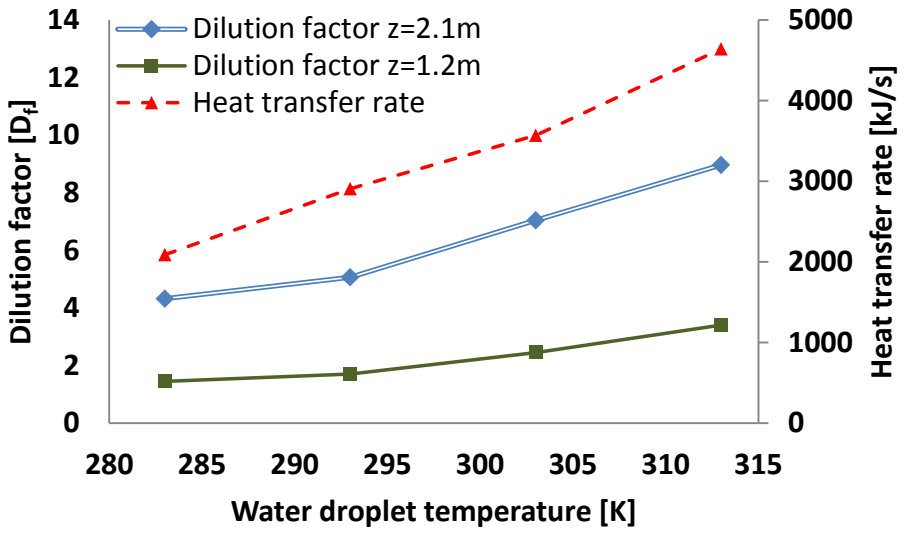

Fig. 46. Heat transfer rate and dilution factor at different water droplet temperatures

Fig. 46 shows the correlation between the temperatures of the water spray with the heat transfer rate and the dilution factor at two different heights (z = 1.2 and 2.1 m). The data from the mass flow and heat transfer rate at the outlet boundary were collected. These data were collected when the vaporized LNG/air mixture exited the domain through the outlet boundary, which is located at highest x coordinate in the downwind direction. The energy of air-vapor mixture exiting the domain without the water spray was used as the reference when evaluating the heat transfer rate of various water spray settings. The dilution factor was evaluated using the concentration data at 8 m from the LNG source in the downwind direction at two different heights. The mass flow rate exiting the domain through the outlet boundary remained constant for the corresponding temperatures; however, the heat transfer rate changed rapidly with increasing water droplet temperature. This confirms that the water temperature plays an important role in

the dilution and heating of the vapor. Future experimental work should be conducted to observe the optimal time needed to produce positively buoyant vapors and the reduction in vapor travel distance for different water temperatures.

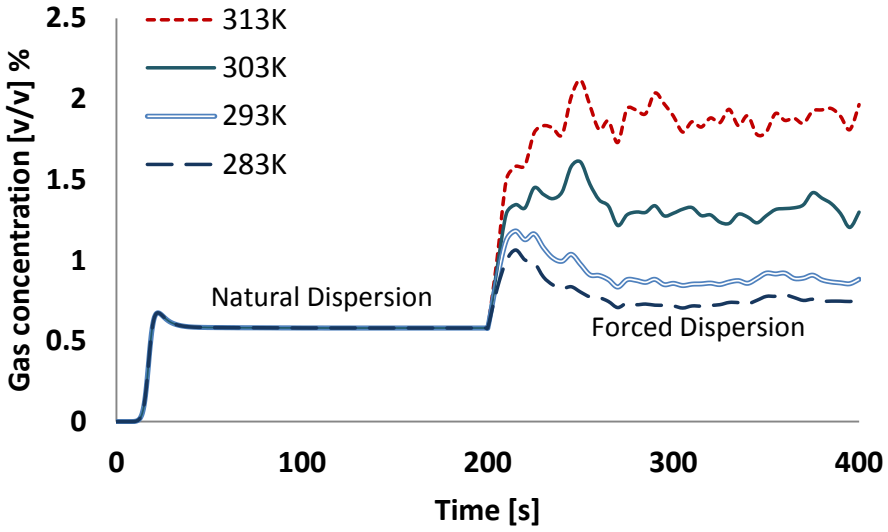

Fig. 47. Volumetric concentration data at 8 m downwind distance (z = 1.2 m)

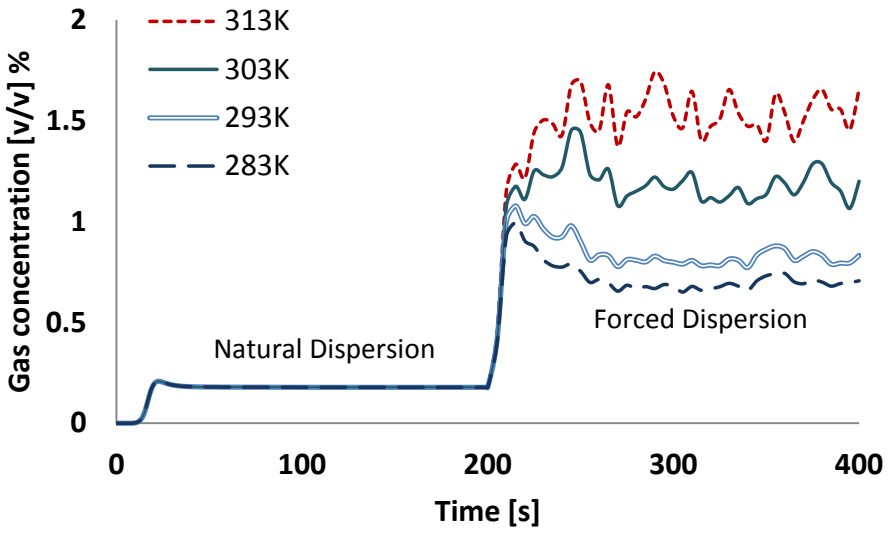

Fig. 48. Volumetric concentration data at 8 m downwind distance (z = 2.1 m)

Figs. 47 and 48 show the profiles of predicted gas concentration at two different elevations, 1.2 and 2.1 m, as measured 8 m downwind (behind the spray envelope). As mentioned previously, the vaporized/LNG air mixture received higher heat energy transfer from the water spray with higher temperatures. The concentration profiles from Figs. 47 and 48 indicate that the vapor cloud gained more positive buoyancy from the water temperature at 313 K, causing the concentration of the buoyant vapors to increase at higher elevations.

As seen in Figs. 47 and 48, the concentration of the vapors with the higher heat transfer from the water droplet showed more fluctuating behavior of the air-vapor mixture. This was more obvious for higher water droplet temperatures: 303 and 313 K. This implies that the heat transfer from the water droplets at temperatures of 303 and 313 K, have induced distinctive air-vapor mixture behavior from the other cases with lower

water droplet temperatures: 283 and 293 K. The unique vapor behavior might be caused by the natural circulation within the air-vapor mixture caused by the uneven temperature distribution resulting from higher heat transfer. The circulation within the air-vapor mixture enhances the mixing effect, hence providing a favorable effect in diluting the flammable vapor. These data can be used to determine the optimal water droplet temperature, which could induce sufficient heat transfer to induce positive buoyancy of LNG vapors.

3.5 Conclusions

The CFD code was used in this section to setup forced dispersion modeling of LNG vapor clouds using the water curtain. The modeling has been validated against the experimental data from the MKOPSC outdoor LNG experiment of March 2009. Physical parameters and setup variables for the dispersion modeling were discussed, such as the grid setting and turbulence intensity at the source of release. The dilution factor from the experimental data was used to calibrate the physical parameters for forced dispersion modeling using the Eulerian-Lagrangian reference frame. The parameters, such as the parcels produced from the nozzle as well as the initial velocity for the particles, were calibrated.

The effectiveness of the forced dispersion model was evaluated from the correlation of the dilution factor and momentum ratio. A total of 17 scenarios with different momentum ratios were simulated. The results showed that the dilution factor is proportional to the momentum ratio. The dilution factor increased in the scenario where

forced dispersion was more dominant. Although no additional experimental work was carried out to verify the results from this simulation, the trend of these results agrees with the wind tunnel and field experiments reported by Hald et al. (2005). In addition, the postspray concentration profiles showed that a high momentum ratio is more effective in changing the course of vapor dispersion and promoting dilution through air entrainment, thereby reducing the vapor exclusion zone. Additional analysis showed that the heat transfer from the water spray heated the LNG vapors. Subsequently, the post-spray concentration profiles showed that the vapor cloud gains more positive buoyancy with a high water temperature, as indicated by an increase of buoyant vapor concentrations at higher elevations.

CHAPTER IV

ANALYTICAL STUDY ON PHYSICAL MECHANISMS OF LNG FORCED DISPERSION

4.1 Introduction

LNG forced dispersion is when additional forces influence the behavior of the LNG vapor mixtures, enhancing the dispersion effects to mitigate the consequence of an LNG spill (Rana, 2009). Water droplets dispersed from the nozzle induce various physical effects in the vicinity of the spray region, which play an essential role in reducing the vapor exclusion zone. The droplets are created from the relative velocity between the bulk liquid and surrounding air, which is induced from the discharged pressure (Lane, 1951). The bulk liquid breaks into smaller droplets as the inertia force exerted exceeds the surface tension. The droplets induce the mechanical effects from the momentum imparted to the vapor clouds, dispersing in the downwind direction (CCPS, 1997). The thermal exchange can warm up the gas, if initially released at a low temperature, and the entrained air enhances the mixing effects with the surrounding air.

This section applies computational fluid dynamics (CFD) to simulate the forced dispersion of LNG vapor clouds to investigate the different physical mechanisms associated with enhancing vapor dispersion using the upward-oriented full cone spray application. The dominant mechanisms behind the physical interaction between the droplets and vapor dispersion are discussed. A sensitivity analysis was carried out for various operating parameters to investigate the turbulence effects on the vapor behavior.

4.2.1 Mechanical Actions from Water Droplets

The water curtain system generates a physical barrier in the vicinity of the spray system. As LNG vapor clouds approach near the spray region, the entrained air envelops the air-vapor mixture and the droplets force it in the direction of the spray application. Fig. 49 provides a schematic of naturally dispersing LNG and forced dispersion with water spray application.

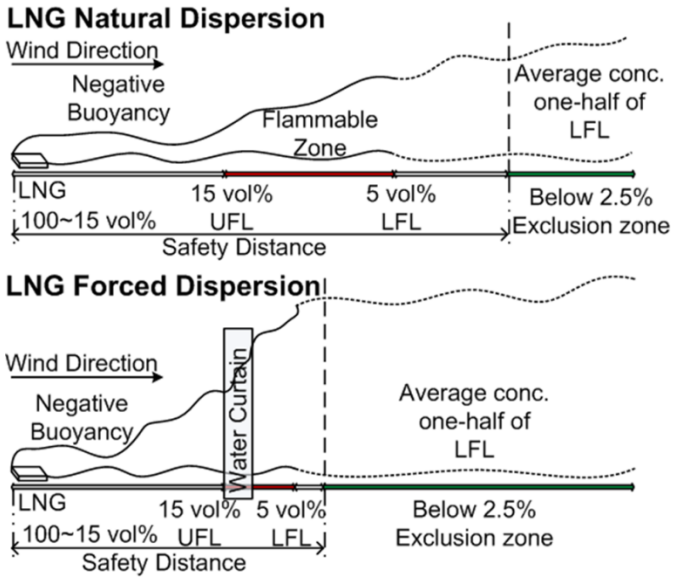

Fig. 49. Schematic of LNG natural/forced dispersion

The momentum effects enhance LNG vapor cloud dispersion and reduce the vapor cloud exclusion zone by displacing the LNG vapors away from the ground level (Rana & Mannan, 2010). The small-scale experimental works conducted by the US Coast Guard in the 1970s have identified that the mechanical effects enhance LNG vapor

dispersion (L. Brown et al., 1976). Rana and Mannan (2010) have verified that the upward-oriented nozzle imparting high momentum can push vapors upwards, increasing the concentration at higher elevations, which is in agreement with the conclusion from the experimental work conducted by Moore and Rees (1981) (Moore & Rees, 1981; Rana & Mannan, 2010). Hald et al. (2005) conducted experimental work and theoretical modeling for dense gas mitigation using the water spray system and the results indicated that the dilution effects became more apparent as the momentum imparted from the water spray increased (Hald et al., 2005). An Eulerian-Lagrangian spray model was coupled with the vapor flow using the CFD modeling to investigate the LNG forced dispersion (Kim, Ng, Mentzer, & Mannan, 2012). The effectiveness of the dilution phenomena of LNG vapors dramatically improved as the momentum imparted from the water droplets increased, which is in agreement with the correlations provided by the additional study conducted by Hald et al. (2005).

The momentum imparted from the water droplets is quantified using the momentum ratio (R_{M}) as follows (Hald et al., 2005):

$$R_{\mathrm{M}} = \frac{\dot{m}_{1,\mathrm{u}} U_{\mathrm{d0}}}{\rho V^2 H_{\mathrm{wc}}} \tag{4.1}$$

where, $\dot{m}_{1,\mathrm{u}}$ is the liquid-flow rate per unit length [kg/m-s], U_{d0} is the initial droplet velocity at the nozzle orifice [m/s], ρ is the cloud density [kg/m^3], V is the wind speed [m/s], and H_{wc} is the height of the water curtain [m]. Currently, there is a lack understanding on the influence of each operational parameter of the water spray application, such as the water flow rate or droplet velocity. Most of previous modeling work has focused on applying the entrained air theory or focused on the overall dilution

effects for pre-designated operating conditions (McQuaid & Fitzpatrick, 1983; Meroney & Neff, 1985).

The influence of the water flow rate and droplet velocity had been investigated by modifying the prescribed operating conditions of the water spray application. The dilution effect was evaluated using the dilution factor (D_{F}), which is the ratio between the concentrations of natural dispersion to forced dispersion. The flow pressure at the water source controls the two main variables: the mass flow rate and droplet velocity. In this work, the droplet velocities and water flow rates are assumed independent parameters. This assumption is reasonable because, although the water pressure mainly determines the water flow rate and droplet velocity for a nozzle, the droplet velocity can also be controlled independently by the nozzle design specifications.

The water spray must be installed a certain distance away from the LNG pit to avoid rapid phase transition (RPT) hazards, which may occur if water comes in contact with the LNG pool (Rana, 2009). An alternative configuration, where the nozzles are tilted to introduce the droplets in different degrees, has also been investigated. The turbulence promoted from modified designs and the overall effectiveness of vapor dilution has been discussed.

4.2.2 Thermal Effects of Droplet-Vapor Interaction

The thermal effects from the water droplets to the vapor cloud, particularly for cold gas releases, can enhance the dissipation of the vapor clouds by warming to gain positive buoyancy (CCPS, 1997). A simple theoretical heat transfer model developed by

St.-Georges and Buchlin (1994) considered the heating effects of conduction and convection between the two phases (gas/vapor) at the boundary layers (St-Georges & Buchlin, 1994). This model has shown that the heat transfer rate increased as the droplet size decreased, which is in agreement with the experimental results by Rana and Mannan (2010). Rana and Mannan (2010) estimated the thermal effects from the droplets to the LNG vapor clouds by evaluating the temperature changes of the water droplets (Rana & Mannan, 2010). The sprays that produced larger droplet sizes were not effective in warming the LNG vapor, and the dilution effect was limited as the vapor cloud traveled back to lower levels. The heat transfer rate evaluated from the LNG forced dispersion study using the CFD modeling have shown that smaller droplet sizes provided more heat transfer to the air-vapor mixture, which enhances the dilution effects in the downwind region (Kim et al., 2012). The water droplets with higher temperature promoted more fluctuating movement of the LNG vapors, which may have been induced from the turbulence promoted by the uneven temperature distribution.

The thermal effects from the droplets play a significant role in promoting buoyant LNG vapor (Rana, 2009). Relatively few studies have been carried out on the turbulence effects involved in LNG forced dispersion from the heat transfer. Different water droplet temperatures had been applied to induce various thermal effects to investigate the influence on the turbulence effects and overall dilution of the LNG vapors. The water droplet temperatures were varied to estimate the turbulence effects induced from the different levels of heat transfer, while keeping the other operating elements constant. The turbulent flows induced from different water droplet

temperatures were compared and the concentration data of the LNG vapors at different elevations were analyzed to investigate the influence from various levels of thermal effects of the water droplets.

4.2.3 Air Entrainment Effects

The air entrainment rate is determined by various spray elements; droplet sizes, droplet velocity, spray location, and configuration (CCPS, 1997). The entrained air dilutes and decreases the vapor concentration as the water droplets enhance mixing effects with enveloped air (Rana, 2009). A numerical calculation had been conducted by the Gas Research Institute (GRI) to evaluate quantitatively the interaction between the spray and LNG vapor mixture (Zalosh et al., 1983). The model was based on the air entrainment rate from the nozzles and had verified the wind effects on the dilution and thermal transfer. Rana and Mannan (2010) compared the experimental data of different types of commercial nozzles and concluded that the nozzles that induce more mixing effects with entrained air can effectively disperse LNG vapor clouds (Rana & Mannan, 2010).

Heskestad, Kung, and Todtenkopf (1981) presented a semi-empirical approach in developing an air entrainment model by integrating the momentum exchange between the liquid droplets and entrained air (Heskestad, Kung, & Todtenkopf, 1981). The model calculates the momentum mechanics of liquid spray into the gas phase in one-dimension. The water droplet velocity (U_p) and the air velocity (U) in the spray can be estimated using following equations:

$$\frac{dU_p}{dx} = \left(\frac{g}{U_p}\right) - \frac{3}{4} B \frac{v^{0.5}}{d^{1.5}} \left(\frac{\rho}{\rho_w}\right) \frac{(U_p - U)^{1.5}}{U_p} \tag{4.2}$$

$$\frac{dU}{dx} = -\frac{1}{2}\frac{U}{A}\left(\frac{dA}{dx}\right) + \frac{3}{8} Q_w B \frac{v^{0.5}}{d^{1.5}} \frac{(U_p - U)^{1.5}}{U_p UA} \tag{4.3}$$

where, u_p is the water droplet velocity, u is the air velocity in the spray, x is the axial location in the spray, g is the gravitational acceleration, B is the numerical constant (12.6), v is the air kinematic viscosity, d is the droplet diameter, ρ is the air density, ρ_p is the water droplet density, A is the cross-sectional area of spray, and Q_w is the volumetric discharge rate of water from spray. It was shown that the theoretical modeling exhibited good agreement with the experimental flows. The entrained air rate into the spray increased significantly as the nozzle angle increased, while the operating pressure has a less significant effect on the air entrainment rates (Rana, 2009). In this work, the water sprays with different rates of air entrainment had been applied in the pathway of LNG vapors to evaluate the physical interactions involved. The dilution effects from different air entrainment rates were evaluated using various nozzle angle sizes: 30°, 45°, 60°, and 75°.

The theoretical air entrainment model by Heskestad et al. (1981) has been solved numerically to evaluate the estimated entrainment rates for the different sizes of nozzle angles. A non-dimensional analysis was undertaken to estimate the air velocity in the spray and entrainment air rate for nozzle angle sizes of 30°, 45°, 60°, and 75°. The governing equations were solved with the initial conditions estimated from the experimental work conducted by MKOPSC. The numerical equations were solved using the Runge-Kutta-Fehlberg methods (RKF45), which is widely recommended for its

flexibility by varying the time scales for the estimation (Forsythe, Malcolm, & Moler, 1977).

4.3 Results and Discussions

4.3.1 Mass Flow Rates and Droplet Velocities

The dilution effects were evaluated with wide ranges of the mass flow rate (1 – 5 kg/s) and droplet velocity (3 – 30 m/s), to investigate the effects of the main operating elements of the water spray application. Fig. 50 shows the dilution factor evaluated from each scenario.

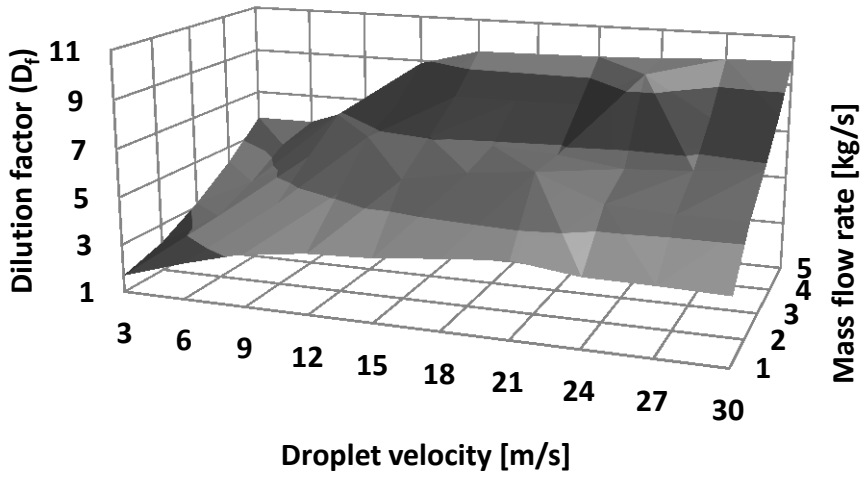

Fig. 50. Dilution effects from different mass flow rate [kg/s] and droplet velocity [m/s]

The dilution effects improved as the mass flow rate and droplet velocity increased. The dilution factor showed a significant increase above the mass flow rate of

3 kg/s. A similar trend is observed for the droplet velocity cases, where the dilution factor increased more significantly as the mass flow increased with the droplet velocity set above the range of 9 – 12 m/s. The 3-d surface plot shows only effective dilution when both the mass flow rate and droplet velocity were set to provide an adequate momentum.

The overall momentum discharged from the water spray system is mainly determined from the water flow rate and droplet velocity as indicated in Equation 4.1. The results in Fig. 50 indicate that the design of the nozzle and operating conditions must provide above certain mass flow rate and droplet velocity simultaneously to ensure the effective forced mitigation. This finding implies that relying solely on the momentum ratio evaluated from Equation 4.1 when designing the operating variables may misguide towards implementing an under-sized water spray system. A proper study must be carried out to evaluate the minimum operating ranges for defining an effective water spray system for a specific facility.

The vapor contours have been compared to investigate the influences of the water flow rate and droplet velocity on the vapor behavior in the post-spray region. Fig. 51 shows the vapor concentration contour ([v/v] %) for LNG forced dispersion with the water spray applied at the flow rate of 1 and 5 kg/s, and droplet velocities of 3 and 30 m/s. The LNG vapor concentration is illustrated to 15 [v/v] %, which is the upper flammable limit (UFL) of LNG vapor.

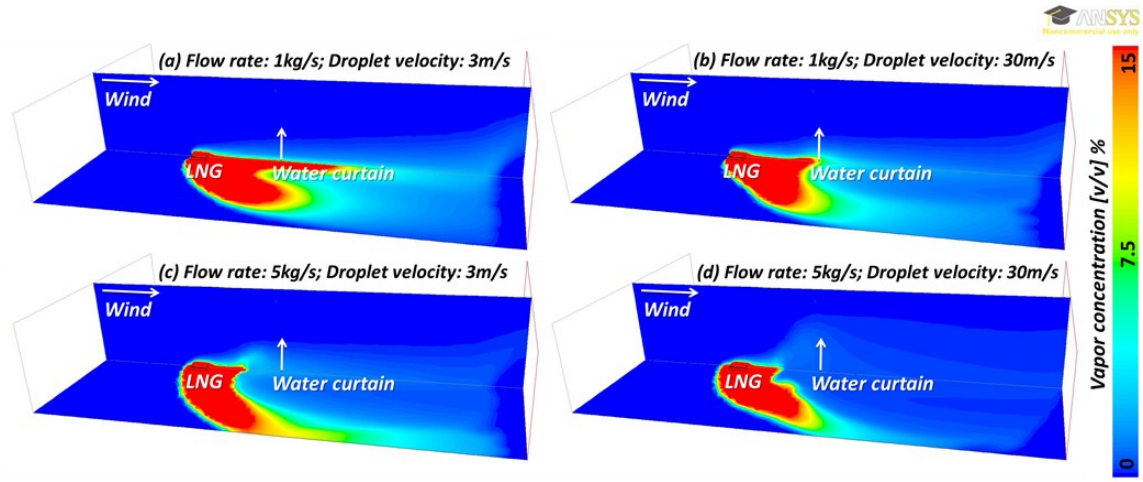

Fig. 51. Vapor concentration contour ([v/v] %) for various water spray applications

The vapor contours of the LNG forced dispersion with the water spray settings at the low mass flow rate (1 kg/s) show no signs of any significant forced mitigation effects as shown in Fig. 51 (a) and (b). With the low mass flow rate of 1 kg/s, the vapor dispersion rather shows similar behavior to natural dispersion of a vapor field in the post spray region. The LNG vapors are only lifted away from the ground in the vicinity of the water spray and most of the vapors travel through the existing gap in the centerline between the water sprays installed or around the water sprays with the low droplet velocity of 3 m/s, as illustrated in Fig. 51 (a). This result implies that at the flow rate of 1 kg/s and droplet velocity of 3 m/s, the water droplets discharged from the nozzles do not provide significant momentum to the vapors to be diluted or dispersed to the atmosphere. The vapors are more evenly distributed in the post-spray region, but still show rather limited dilution effects as the vapors mainly propagate at the lower level when the droplet velocity was increased to 30 m/s as shown in Fig. 51 (b). The higher

droplet velocity promoted mixing effects, which forced the vapors to propagate more evenly. However, the vapors still stay close to the ground as insufficient water flow is provided. With the mass flow rate increased to 5 kg/s, more vapors are directed away from the centerline, as the water droplets impose a physical barrier in the pathway of the vapor clouds as shown in Fig. 51 (c) and (d). The higher flow rate introduced a sufficient amount of water droplets from the nozzle to interact and lift the vapors from the ground level more effectively regardless of the low droplet velocity of 3 m/s as shown in Fig. 51 (c). More vapors are lifted from the ground, however, the LNG vapors start pushing the relatively lighter air and start propagating around the water spray from the physical barrier imposed by the large amount of droplets. The case with the highest flow rate of 5 kg/s and droplet velocity of 30 m/s is shown in Fig. 51 (d). Less LNG vapors are traveling at the ground level as the water spray effectively envelops the vapors in the vicinity of the nozzle, while the high droplet velocity setting helps the vapors to be dispersed to the atmosphere.

The vapor behaviors from different spray applications had been investigated using the vapor contours. The integral-type or traditional consequence assessment relies heavily on the point data source or the concentration reduction in the centerline from the LNG source. This information may provide limited information on the vapor behavior induced from the different water curtain applications. The results presented in Fig. 51 show a promising methodology to evaluate the overall LNG spill hazards by taking into account the changes in the LNG vapor behaviors. The unforeseen hazards where the LNG vapors propagate sideways can be determined by applying certain spray

specifications, which can ultimately assist in designing a site-specific water spray system.

4.3.2 Nozzle Configurations

The nozzles were tilted at 30°, 45°, and 60° in the downwind direction to study the different vapor behaviors induced from the droplets applied at various angles. A vertical installation case (90°) was also used as a reference to compare the influence of the tilted angle design with the commonly used vertical application. The water spray applications were set at 2 m away from the LNG source, which is half the distance away from other simulation works to compare with the previous water spray applications. The turbulence kinetic energy (TKE) generated in the downwind region with the forced dispersion using the modified nozzle design is shown in Fig. 52.

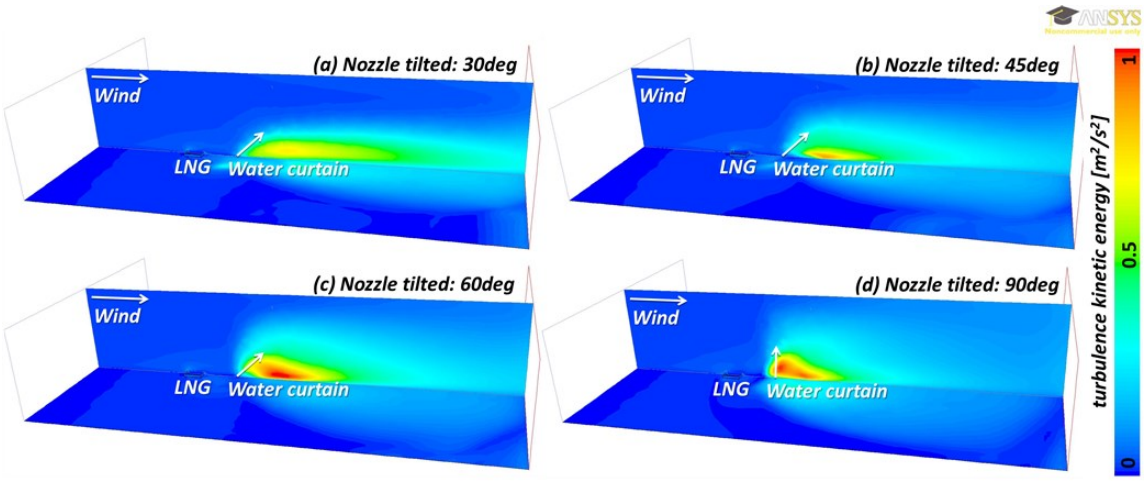

Fig. 52. Turbulence kinetic energy (TKE) contour for tilted installation designs

Only a slight wake of turbulence is observable in the post-spray region for 30° and 45° cases, as illustrated in Fig. 52 (a) and (b). This is because there are no significant forces being imposed in the pathway of the LNG vapors as the water droplets are mainly discharged in the direction of the prevailing wind. The nozzle tilted at 60° shows a higher turbulence induced in the post-spray region and uniformly distributed in the downwind region. This implies that the nozzle tilted at 60° discharges the droplets in the direction where the momentum could effectively promote an overall turbulent flow of LNG vapors. A similar turbulence trend was observed from the vertical nozzle application (90°), where the turbulent flow was generated locally in the post-spray region and increased in the downwind region uniformly.

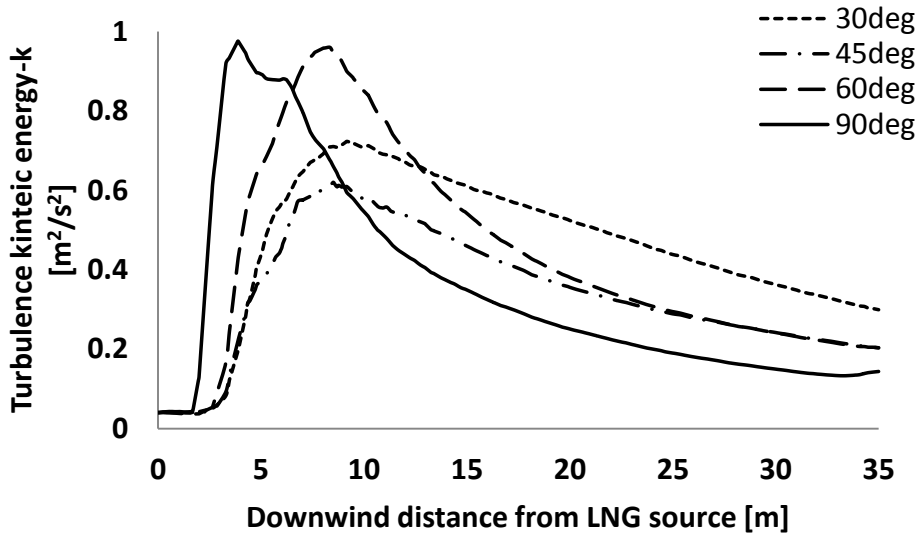

Fig. 53. Turbulence kinetic energy (TKE) for tilted installation designs at ground level

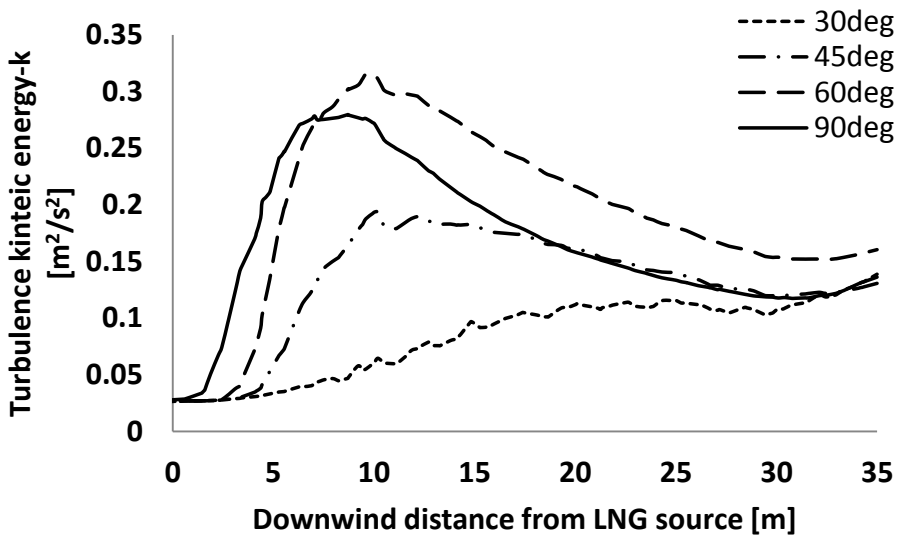

Fig. 54. Turbulence kinetic energy (TKE) for tilted installation designs at 8 m elevation

The turbulence effects induced from the nozzles tilted in different configurations are plotted in Figs. 53 and 54. The turbulence kinetic energy exceeded the rest of applications approximately 13 m away from the LNG source for the nozzle tilted at 30° at the ground level, whereas at 8 m elevation, the nozzle shows the lowest turbulence being induced. This indicates that the nozzle tilted at 30° is not capable of pushing the LNG vapors effectively into higher elevation, hence, shows higher turbulence at the ground level, where the vapors mainly travel in the downwind region. A similar trend is observed from the nozzle tilted at 45°, with slightly higher turbulence at 8 m elevation. The vertical application (90°) shows the highest turbulence being induced in the vicinity of the water spray region, at the closest distance away from the LNG source, as shown in Fig. 53. The nozzle tilted at 60° shows a similar level of turbulence being promoted approximately 5 m behind the highest point observed from the vertical application (90°).

The turbulence at 8 m elevation indicates that the nozzles tilted at 60° showed approximately 11% more turbulence than the 90° application. The vapor concentration ([v/v] %) resulting from applying various tilted designs of nozzles were plotted for two elevations, at the ground level and 8 m elevation, in Fig. 55 and 56.

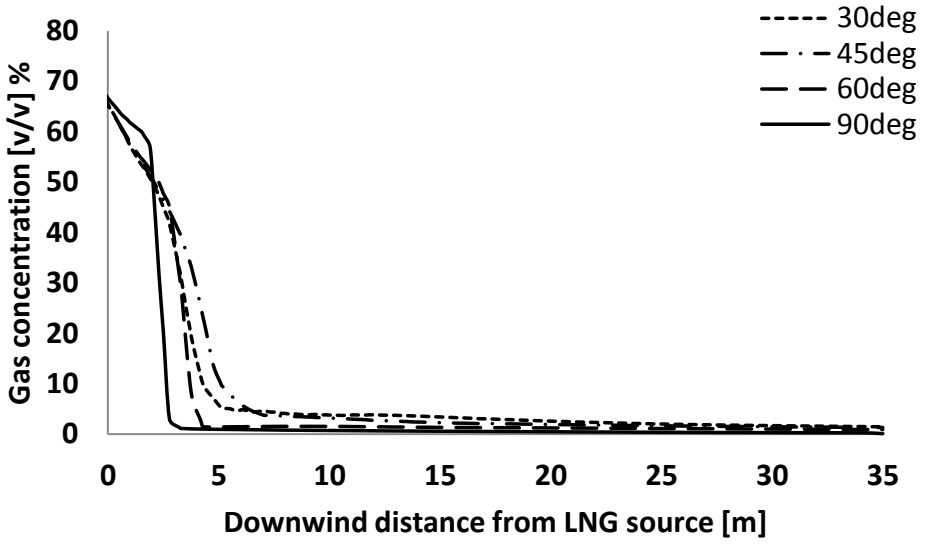

Fig. 55. Vapor concentration ([v/v] %) for tilted installation designs at ground level

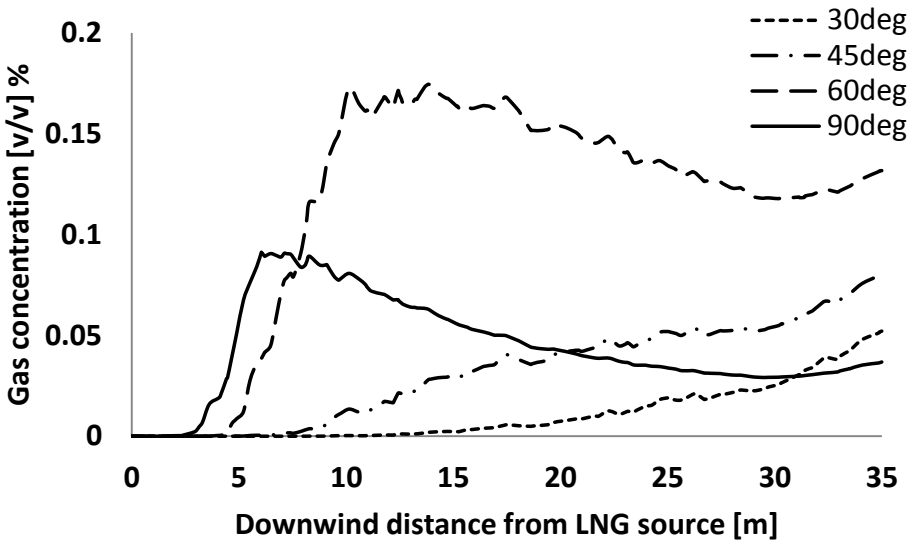

Fig. 56. Vapor concentration ([v/v] %) for tilted installation designs at 8 m elevation

A significant concentration reduction is shown for the vertical design (90°) at the closest distance from the water curtain region as shown in Fig. 55. The other angles show no significant differences in the vapor concentration reduction at the ground level. By contrast, the nozzles tilted at 60° showed approximately 89% more vapor at 8 m elevation compared to the vertical nozzle application (90°), where only 11% of turbulent difference was observed in Fig. 54. The nozzles tilted at 60° showed the most favorable design, where the spray induced the most buoyant vapors to disperse to the atmosphere. The droplets tilted at 60° may promote turbulence in the downwind region within the vapor field, which encourages the vapors to mix and disperse more effectively. With the nozzles configured to discharge the water droplets in the downwind direction, the water curtain system may safely be moved closer to the LNG pit, which enhances the overall dilution effects.

4.3.3 Droplet Temperatures

The water droplet temperature was set at 283 K, 293 K, 303 K, and 313 K to evaluate different turbulence effects promoted from the various levels of thermal transfer from the droplets to air-vapor mixtures. The turbulence kinetic energy induced in the post-spray and downwind region is illustrated ranging up to 1 m^2/s^2 in Fig. 57.

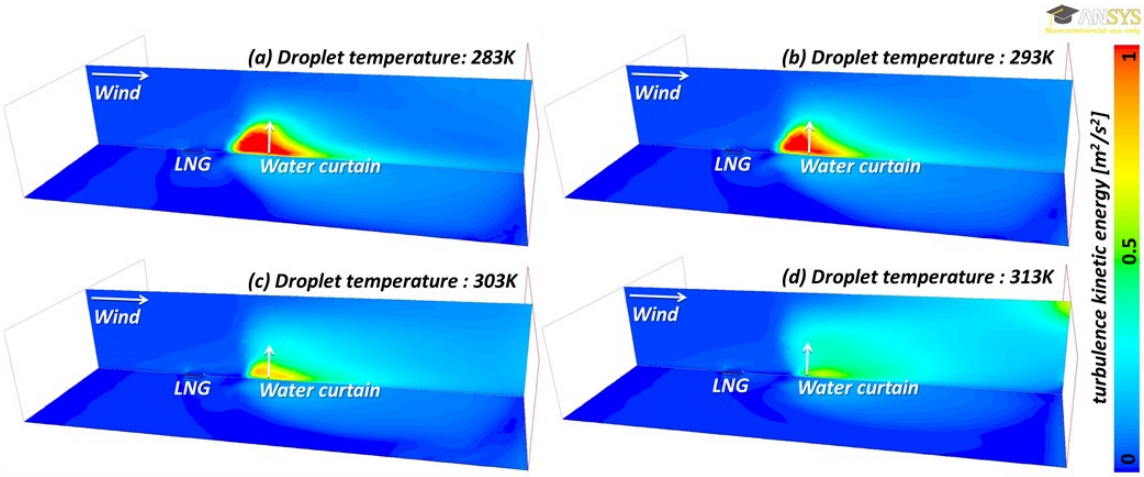

Fig. 57. Turbulence kinetic energy (TKE) contour for different droplet temperature applications

With the lower droplet temperature applications, at 283 and 293 K, higher turbulence kinetic energy was induced in the vicinity of the water spray. The high turbulence kinetic energy values around the water spray might be due to insufficient thermal effects. The LNG vapors are not warmed up effectively to dissipate to the atmosphere and get held up around the water spray area by the physical barrier the water spray imposes. This phenomenon is not observed for the higher water droplet

temperature applications of 303 and 313 K, where the turbulence kinetic energy was reduced significantly around the water spray and was evenly promoted in the downwind region. The water droplets with higher temperature applications provide adequate thermal effects to the air-vapor mixture to promote dispersion of the vapors to higher elevations. A unique turbulent flow is observed at the highest elevation at the outlet boundary for the 313 K application. This might be due to the vapor circulation zone induced from the high thermal effects, which may have induced lower pressures at certain regions. This may have led certain amounts of air-vapor to flow back into the domain from the outlet boundary at higher elevations. The TKE were plotted for two different elevations at the centerline from the LNG source in Figs. 58 and 59.

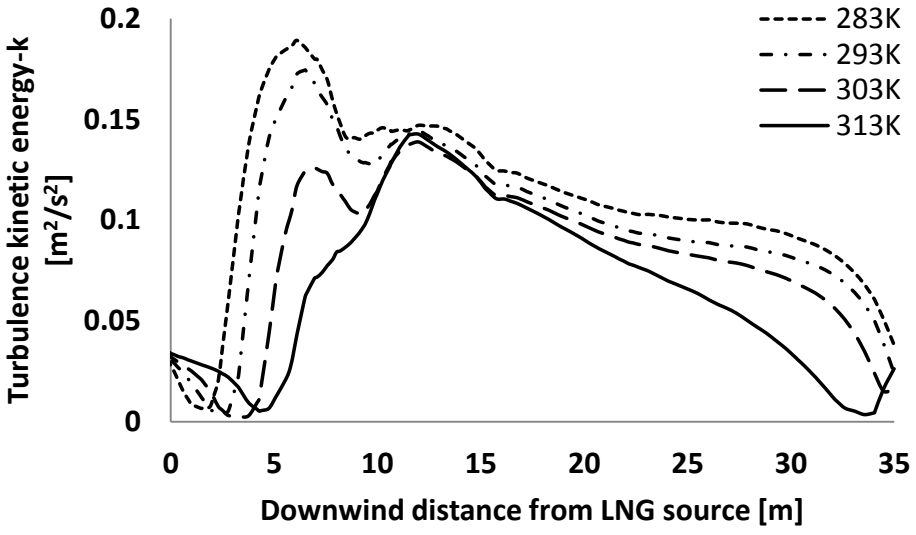

Fig. 58. Turbulence kinetic energy (TKE) for different droplet temperature applications at ground level

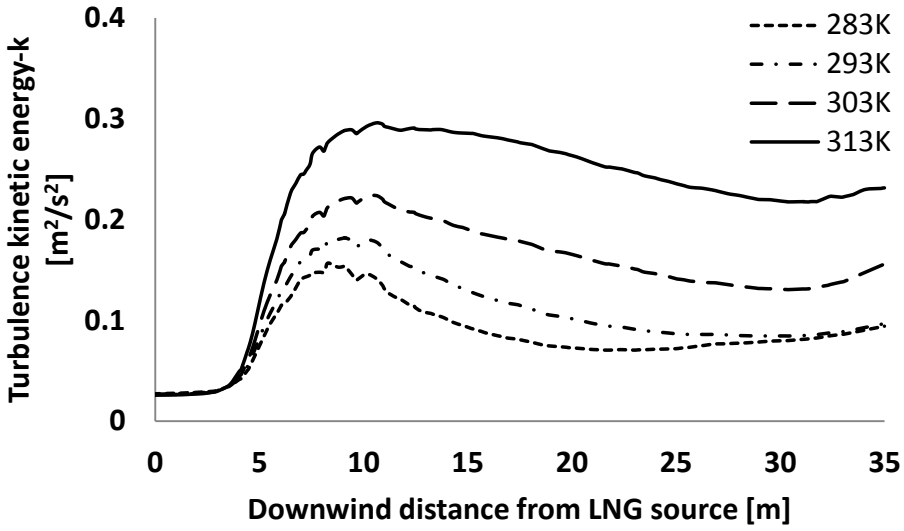

Fig. 59. Turbulence kinetic energy (TKE) for

different droplet temperature applications at 8 m elevation

As illustrated in Fig. 57, with the absence of adequate thermal effects from the droplets, the spray barrier hinders the cold gas movement around the nozzle installation. The 283 and 293 K cases showed the highest turbulence kinetic energy induced in the vicinity of the water spray, as the vapors were being held around the spray region at the ground level, as shown in Fig. 58. The highest TKE was induced from the lowest water droplet temperature application (283 K) at the ground level and decreased as the higher droplet temperatures were applied. This is because of the insufficient thermal effects from the lower droplet temperatures, which cause the cold vapors to travel dominantly at ground level. Beyond the 12 m region, the droplet temperature of 313 K showed further decrease of turbulence kinetic energy approximately to zero, as more buoyant vapors promoted less substantial turbulence at the ground level. There is a clear disparity

compared to the TKE induced at 8 m elevation, where the highest TKE was induced from the water droplet with 313 K as shown in Fig. 59. The higher thermal effects from the water droplets at 313 K showed more than double the turbulence kinetic energy compared to the lower droplet temperatures (283 and 293 K), as the vapors travel in the downwind region. The vapors with the higher heat transfer will contribute to various distinctive vapor behaviors, such as natural circulation, which encourages mixing with the air. The LNG vapors will gain buoyancy faster and have adequate time to disperse and increase turbulence evenly within the vapor cloud fields.

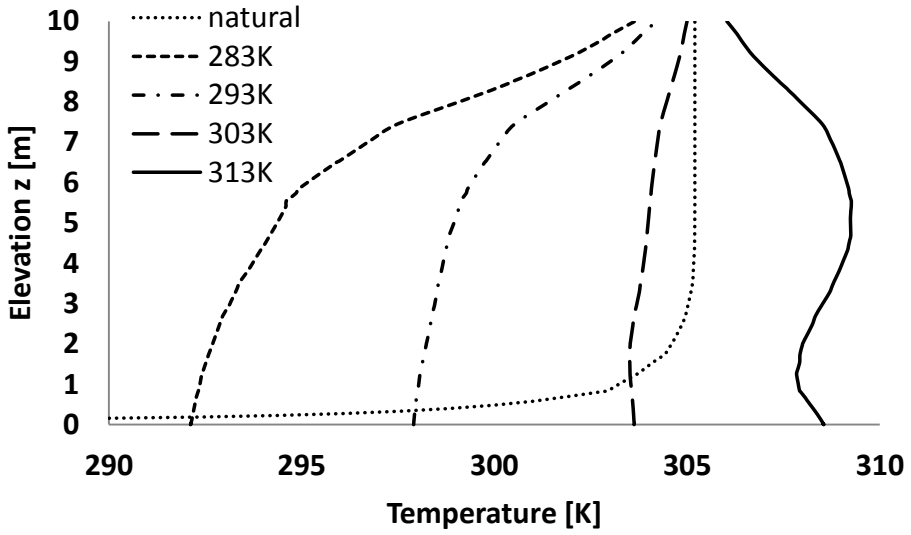

Fig. 60. Temperature profiles for different droplet temperature applications at 8 m away from LNG source

The temperature profiles were compared after applying forced mitigation with different droplet temperatures to investigate atmospheric stratification in Fig. 60. When

LNG disperses without any water spray application, a very stable stratification was formed, where the cold vapors decreased the atmospheric temperature up to 3 m elevation. The temperature gradient also shows very stable atmospheric stratification for droplet temperatures of 283 and 293 K, where the temperatures are lower at ground level and increase vertically. The droplet temperature of 313 K induced the temperature profile of a typical unstable atmospheric stratification. There are two zones, where the temperature profile decreases vertically, from ground level to 1 m elevation, and 6 to 10 m elevation. These zones could promote natural convention within the vapor cloud fields, enhancing the turbulence effects at higher elevation as observed in Figs. 57 and 59.

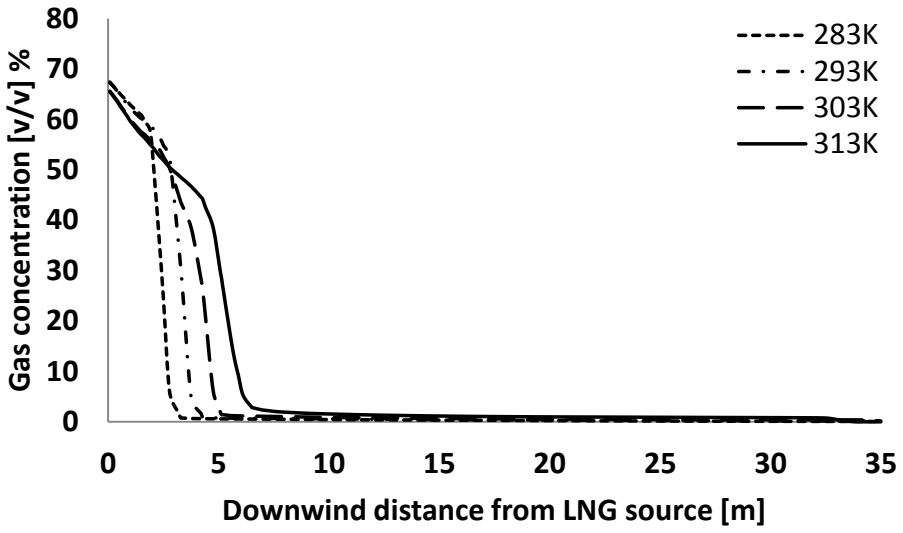

Fig. 61. Vapor concentration ([v/v] %) for different droplet temperature applications at ground level

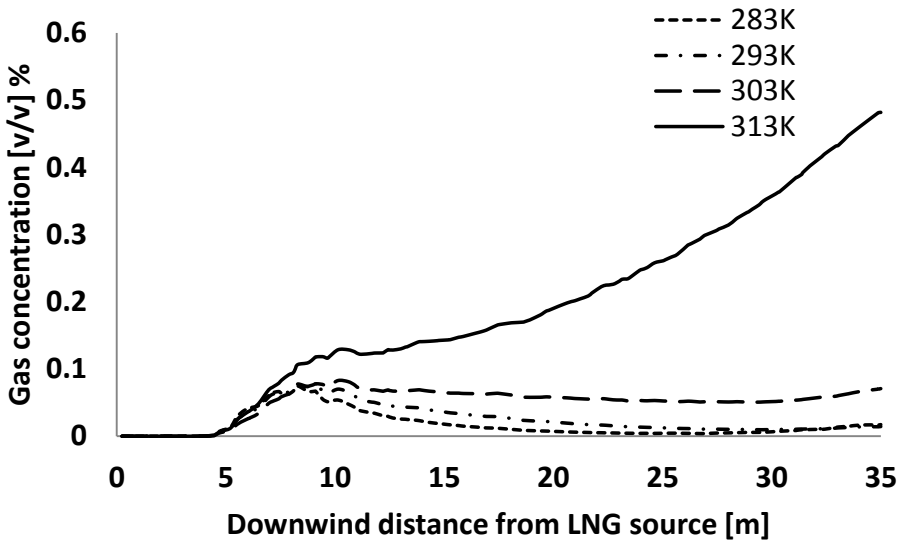

Fig. 62. Vapor concentration ([v/v] %) for different droplet temperature applications at 8 m elevation

The vapor concentration ([v/v] %) resulting from different water droplet temperatures are plotted in Figs. 61 and 62. At the ground level, the lowest droplet temperature (283 K) showed the concentration reduction closest to the LNG source as shown in Fig. 61. This is due to the LNG vapors being pushed around the water spray region. As the water droplets dispersed in the pathway of the LNG vapors fail to provide adequate heat transfer, the momentum imparted from the droplets exceeds the force pushing the vapor clouds from the prevailing wind. The cold vapors are held back around the water spray area, and a large portion of vapor clouds start to push the relatively lighter air around the water spray. This is typical behavior of LNG vapors when insufficient mitigation effects are involved. On the contrary, this vapor behavior is not observed for the droplet temperature of 313 K at 8m elevation, where the LNG

vapors travel through the water spray region and the vapor concentration reduces behind the water spray region. This allows more effective vapor-droplet interaction, and subsequently, increases the vapor concentration at 8 m elevation from delivering more buoyant vapors to the atmosphere as shown in Fig. 62. This prediction is also in agreement with the turbulence induced at 8 m elevation in Figs. 57 and 59, where the water spray with higher heat transfer promoted more turbulence by dispersing more vapors from the ground level.

The CFD predictions indicate that the thermal effects promoted more turbulence within the vapor fields and enhanced the dilution of LNG vapors. The results presented in Fig. 61 show the limitation of assessing the forced dispersion effects by analyzing the concentration reduction, which had been the main resources obtainable from the integral-type model. Whereas the overall results suggest that the water droplet temperature must provide adequate thermal effects to the LNG vapors, the vapor concentration reduction in Fig. 61 indicate the opposite. With the additional information available from applying CFD modeling, it is possible to provide comprehensive solutions to the droplet-vapor interaction and complex LNG vapor behavior evaluated from the constitutive equations of fluid flow.

4.3.4 Nozzle Angle Sizes

A total of four different angle sizes (30°, 45°, 60°, and 75°) were simulated to investigate the influence of different levels of air entrainment on the vapor dispersion.

The turbulence kinetic energy induced from each nozzle setting is illustrated, ranging from 0 to 1 m^2/s^2 in Fig. 63.

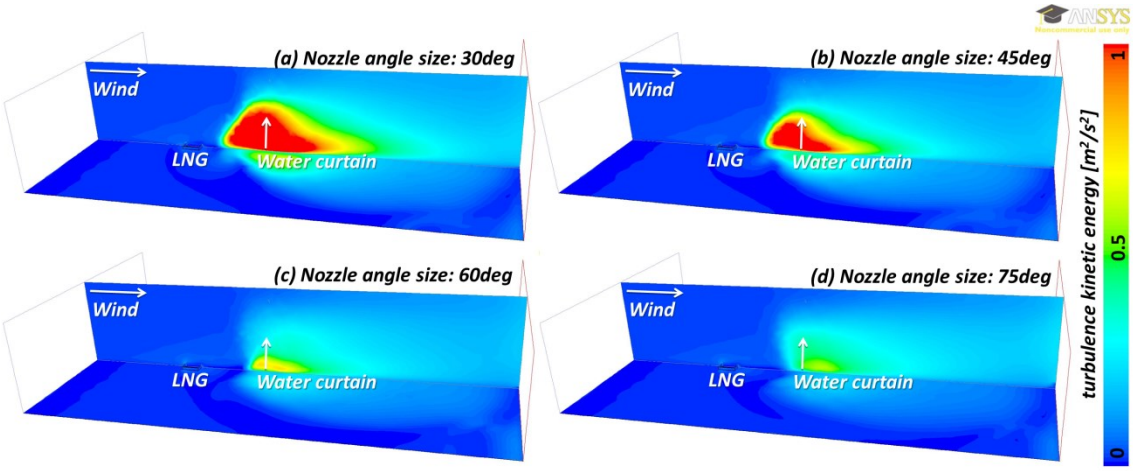

Fig. 63. Turbulence kinetic energy (TKE) contour for different nozzle angle sizes

The nozzles with smaller angles, 30° and 45°, showed higher turbulence kinetic energy induced in the vicinity of the water spray. The turbulence around the water spray region was reduced and the turbulence effects were observed uniformly in the downwind region for larger angle applications of 60° and 75°. It is highly probable that the spray angle serves as the dominant factor in inducing different turbulence effects in Fig. 63, as the other operating parameters were set constant.

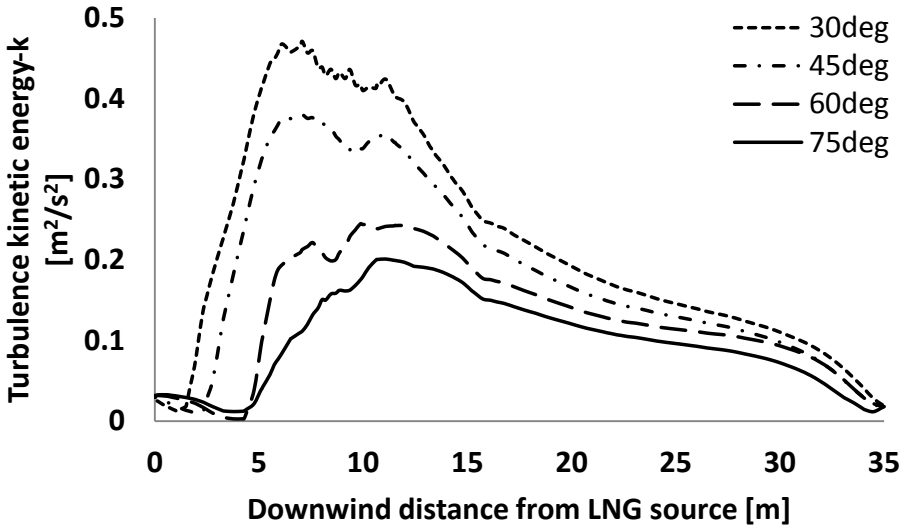

Fig. 64. Turbulence kinetic energy (TKE) for different nozzle angle sizes at ground level

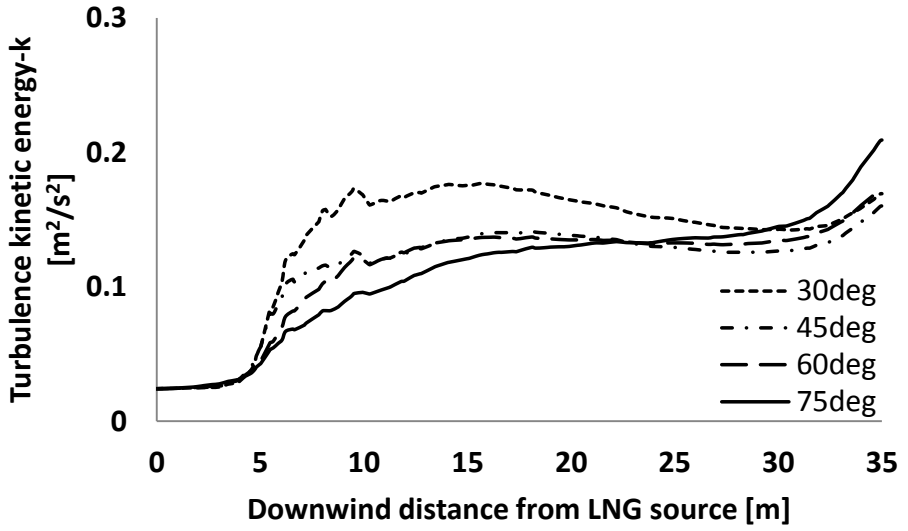

Fig. 65. Turbulence kinetic energy (TKE) for different nozzle angle sizes

at 8 m elevation

Figs. 64 and 65 show the turbulent flow induced at two different elevations, ground level and 8 m elevation. The spray with the smallest angle (30°) induced the highest turbulence at the ground level and the overall turbulence kinetic energy decreased as the size of the nozzle angle increased as shown in Fig. 64. The turbulent flow presents consistent trends at 8 m elevation compared to the ground level with perhaps half the TKE. The turbulence induced from the nozzle size at 75° started to exceed the rest of the applications at approximately the 20 m region as shown in Fig. 65. It appears likely that the nozzles with the smaller angle size promote turbulence more effectively at both ground and 8 m elevation after droplet-vapor interaction. The smaller size of angle focuses the water droplets within smaller regions compared to the nozzles with a larger angle application, where the water droplets are dispersed covering a broader area.

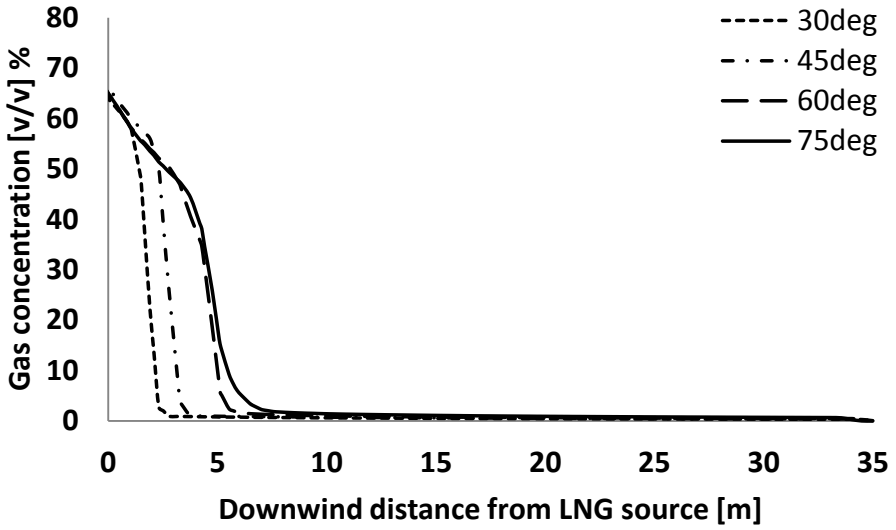

Fig. 66. Vapor concentration ([v/v] %) for different nozzle angle sizes at ground level

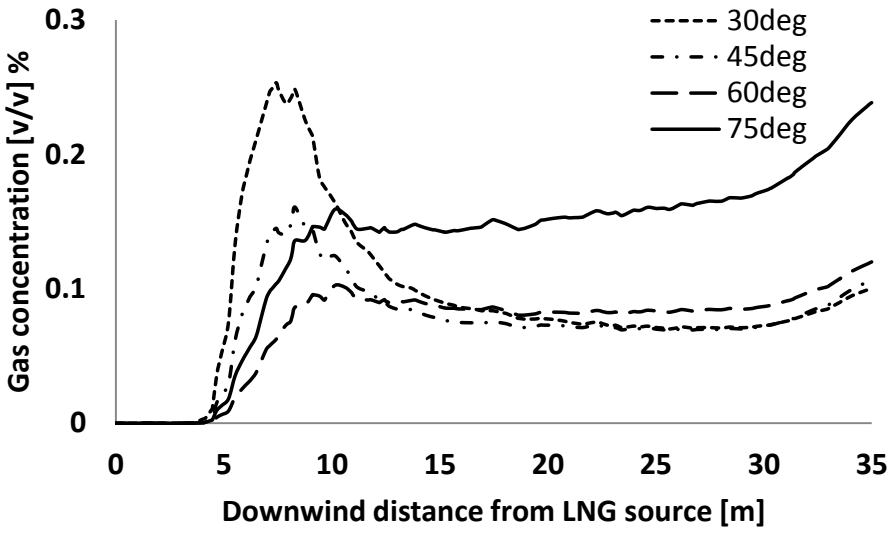

Fig. 67. Vapor concentration ([v/v] %) for different nozzle angle sizes at 8 m elevation

The vapor concentrations obtained from applying various entrained air rates on the LNG vapors are compared in Figs. 66 and 67. Despite the trend indicating a significant similarity to the vapor prediction from various levels of heat transfer shown in Fig. 61, there is clear distinction between the means of concentration reduction observed by the applications of different droplet temperature and air entrainment rates at the ground level as shown in Fig. 66. While the droplet with lowest temperature indicated rather limited dilution effects from the LNG vapors being pushed sideways by the water spray, the nozzle with the smallest angle actually enhanced the LNG dispersion to atmosphere, increasing the vapor concentration dramatically at 8 m elevation as shown in Fig. 67.

At 8 m elevation, the nozzle angle at 75° showed a steady increase of vapor concentration, reaching about twice that of LNG vapors being dispersed, with no signs

of a high concentration spike in the vicinity of water spray as observed in the other applications. As the 75° nozzle applied the water droplets covering a broader area, it entrains more air into the spray, enhancing the LNG vapor dispersion gradually in the downwind region.

In contrast to the role turbulence played in the heat transfer effects, the entrained air from the water spray application showed less significant influence on the vapor dilution. High thermal effects from the water droplets induced turbulent flow within the gas field, which promotes buoyant vapors to disperse more effectively, as discussed in the previous section. The effectiveness of the vapor dispersion for different angle sizes indicates that the nozzle, which induces the highest turbulent flow showed the minimal effectiveness in dispersing vapors to the atmosphere. The entrained air velocities and rates were estimated using the air entrainment model and nozzle specification parameters discussed in Section 4.2.3.

The wind effects from the spray developments for the 30°, 45°, 60°, and 75° nozzles are plotted in Figs. 68 and 69.

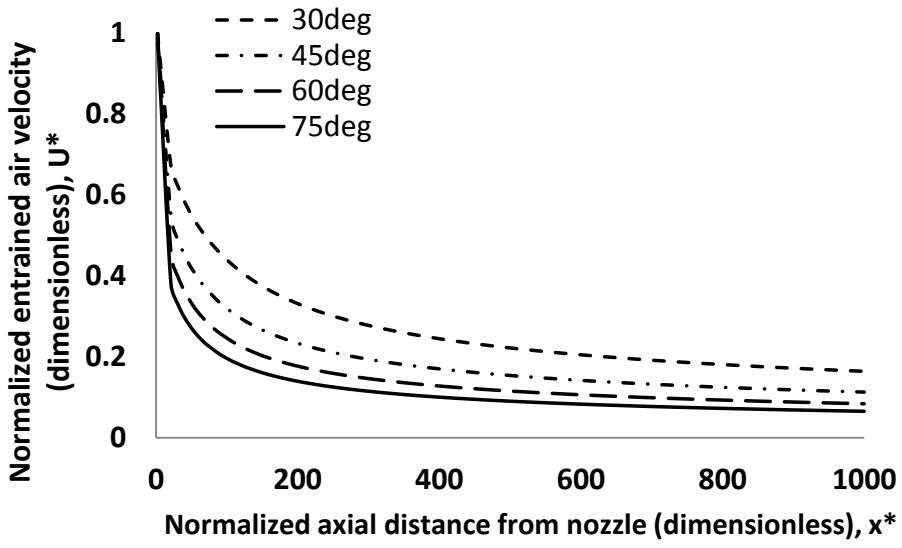

Fig. 68. Normalized entrained air velocity for different air entrainment applications

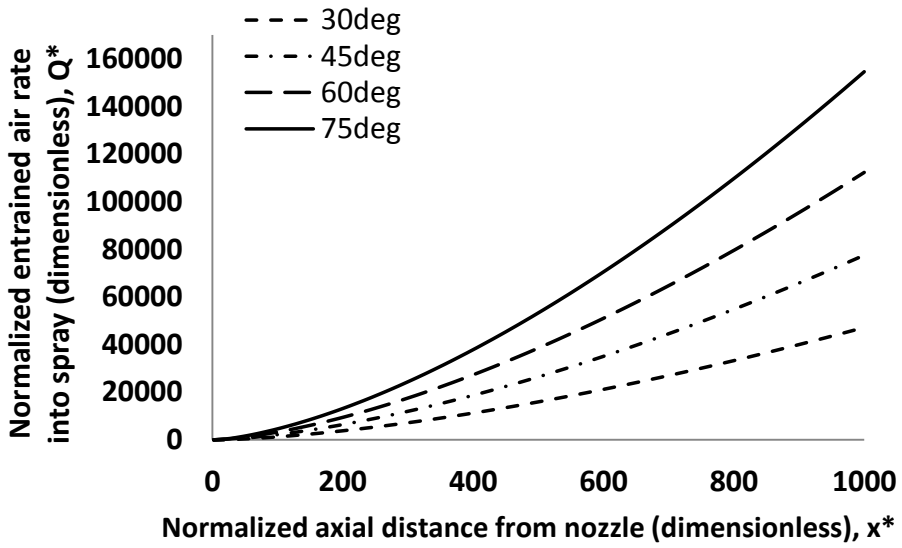

Fig. 69. Normalized entrained air rate for different air entrainment applications

The estimated entrained air velocity showed that the air movement within the water spray development decreased significantly as the droplets travel further away from the nozzle point, as shown in Fig. 68. The smallest angle nozzle (30°) promoted the fastest air velocity and decreased as the size of the nozzle angle increased. Smaller angle nozzles direct the water droplets in the smaller region in the vicinity of the water spray region, enhancing the local turbulence effects around the water spray region, as observed in Figs. 63 to 65. The high-entrained air velocity simultaneously lifted the LNG vapors from the ground level, which resulted in an effective concentration reduction at the ground level and concentration peak around the water spray at 8 m elevation for the smaller angle nozzle, as shown in Figs. 66 and 67.

The total volumetric airflow over a cross section of the water spray, where Q^* is the normalized entrained flow rate of Q/Q_w (Q: total air entrainment flow, Q_w: volumetric flow rate of water from spray), is plotted in Fig. 69. Approximately four times more entrained air was induced into the spray with the nozzle angle size of 75° compared with the 30° application. The nozzles with larger angle sizes enhance the mixing effects with a large amount of entrained air, which promotes the vapors to disperse effectively to the atmosphere, as observed in Fig. 67. In short, the forced dispersion from air entrainments mainly influences the mixing effects with a large portion of entrained air, and turbulence plays a less significant part in the overall effectiveness.

4.4 Conclusions

Various physical mechanisms involved in the forced dispersion of LNG vapors were investigated. Understanding the dominant mechanisms influencing the vapor dispersion is essential in developing engineering guidelines for designing an effective forced mitigation system for LNG facilities. The influences of various operational elements on inducing the turbulent flow within the vapor field have been verified. The fluid turbulences and vapor behaviors had not been available through the integral-type model, which had been bounded by the semi-empirical correlations. The CFD codes provide detailed flow movement and can serve as critical information in designing a site-specified mitigation system, where high turbulent flow may exaggerate the consequences of a LNG spill.

CHAPTER V

KEY PARAMETRIC ANALYSIS ON DESIGN VARIABLES OF WATER SRPAY APPLICATION*

5.1 Introduction

The water curtain system has been recognized as one of the most effective and economic mitigation systems in the chemical and petrochemical industries (Uzanski & Buchlin, 1998). Applying the water curtain directly to LNG vapors has been proven to enhance the dispersion and reduce the safety distance to a lower flammability limit (LFL) range (Martinsen et al., 1977; Rana & Mannan, 2010). However, there has been minimal research in drawing definitive solution to establishing engineering design criteria for water curtain applications in LNG facilities (Atallah et al., 1988). Research on understanding the complex interaction between the water droplets and LNG vapors is still in its early stage, as there is still a significant gap in the experimental works. This work applies computational fluid dynamics (CFD) in attempt to explore the Eulerian–Lagrangian spray model coupled with LNG vapor dispersion to evaluate the global key parameters for designing an effective forced mitigation system. This paper aims to demonstrate CFD code as an assessment tool in analyzing the direct influence of droplet characteristics on the forced dispersion of LNG vapors.

---

* Reprinted with permission from "Key parametric analysis on designing an effective forced mitigation system for LNG spill emergency" by Kim, B. K., Ng, D., Mentzer, R. A., & Mannan, M. S. (2013). *Journal of Loss Prevention in the Process Industries*, doi: http://dx.doi.org/10.1016/j.jlp.2013.01.007. In Press, Corrected Proof. Copyright 2013 Elsevier.

The LNG spill experiments had verified that the full cone spray provides effective mixing with air through the turbulence induced (Rana, 2009). A 1” TF 48 NN BETE Fog Nozzle is a conical full type water nozzle, which had been used during the Mary Kay O’Connor Process Safety Center (MKOPSC) outdoor LNG spill experiments. A total of eight conical nozzles were installed on two separate 2” OD carbon steel pipelines. Fig. 70 shows the fully activated upward-oriented water spray system that was used in the experimental work. Four nozzles were installed on each pipeline in a V-shape, which produces a 60º full cone, spiral pattern.

Fig. 70. Upward-oriented full conical water spray system

The natural dispersion results obtained from the March 2009 work showed good agreement with the prediction from LNG forced dispersion modeling work (Kim et al., 2012). The upwards-conical application has been coupled with the LNG vapor dispersion using the Eulerian-Lagrangian approach to simulate the interaction between

the air-vapor mixture and the water droplets. The release scenarios are based on the assumption of the LNG spill in a predetermined location, which was adopted from the experimental setup of MKOPSC March 2009 test. To evaluate the influence of the global key parameters on LNG vapor behavior, the operating variables of the spray application had been adjusted to simulate different scenarios with various dispersion conditions under the same atmospheric condition. The atmospheric conditions from the Falcon-1 experiment were applied to simulate an actual stable condition (Brown et al., 1990), where the largest concentration is observed at the furthest location from the LNG source.

5.2 Design Parameters

Water curtains apply the water droplets created from the breakup of bulk liquid from the nozzles (Jiang, Siamas, Jagus, & Karayiannis, 2010). Important global parameters for designing effective water curtain systems include droplet sizes, droplet temperature, installation distance, and nozzle configuration (CCPS, 1997).

5.2.1 Droplet Characteristics

The momentum and heat transfer effects are the dominant physical mechanisms of LNG forced mitigation (Rana & Mannan, 2010). The momentum transfer plays an important role in lifting the LNG vapors from the ground, reducing the vapor concentration in the post-spray region. Subsequently, the heat transfer effect contributes to further reduction of the vapor concentration by warming up the LNG vapors to be

positively buoyant. The water droplets that induce higher thermal effects enhanced the effectiveness of the forced mitigation significantly. It was observed from the experimental work that the LNG vapors traveled down to ground level with the absence of sufficient heat transfer, after interacting with the water droplets.

Water nozzles produce droplets from the pressure difference across the nozzle inlet and the atmosphere. The water pressure and nozzle design determine the droplet size, which is an intrinsic characteristic for a specific nozzle design (CCPS, 1997). The droplet size used in this work is characterized using the Sauter mean diameter (SMD), which represents the droplet size by the surface and volume of the droplets. Smaller droplets entrain more air into the water spray, but provide less momentum to the air-vapor mixture and the heat transfer effect is also heavily influenced by the droplet size.

Table 3. Selected case study scenarios (1" TF 48 NN BETE Fog Nozzle)

		S01	**S02**	**S03**	**S04**	**S05**	**S06**	**S07**	**S08**	**S09**
Mass flow rate	**Kg/s**	2.11	2.99	4.23	5.18	5.98	6.69	7.33	8.46	9.46
Droplet size	**mm**	1.43	1.16	0.94	0.83	0.76	0.71	0.68	0.62	0.58

A total of 9 different scenarios were developed for evaluating the heat transfer effects between the droplets and LNG vapors as summarized in Table 3. These conditions were estimated using the direct flow pressure correlation of 1" TF 48 NN BETE Fog Nozzle, provided by the nozzle vendor (BETE, 2007). The size of water droplets produced from the nozzle is inversely proportional to the water pressure increase. Higher water pressure introduces more inertial force to the bulk water, which

increases the pressure gradient across the nozzle breaking up the droplets into finer sizes (Crowe, Sommerfeld, & Tsuji, 1998).

5.2.2 Installation Distances

The location of the water spray application from the potential LNG source is one of the important factors in determining the effectiveness, as dilution effects can be dramatically influenced from how far the mitigation measures are installed (CCPS, 1997). Water curtains must be placed so that the droplets can effectively interact with the vapor clouds, while it cannot be placed close to the LNG source as the water droplets may enter the LNG pit (Rana, 2009). When water droplets contact the LNG, a physical explosion known as a rapid phase transition (RPT) may occur (BP, 2007).

Relatively few studies have attempted to analyze the influence of the installation distance and how the effectiveness changes as the nozzles are moved closer to the LNG source. The dilution effects were evaluated for various installation distances (0 m, 2 m, 6 m, 10 m, 14 m, 18 m, 22 m, 26 m, and 30 m). The safe distance evaluated from the LNG forced dispersion simulation of the MKOPSC outdoor LNG spill experiment was approximately 31 m away from the LNG source. The safe distance is the range of the exclusion zone, where the concentration becomes one half of the LFL, which is at 2.5 [v/v] % for the LNG vapor dispersion. The effectiveness of dilution from each scenario was compared by analyzing the reduction of the safe distance.

5.2.3 Nozzle Configurations

The water spray installation has only been limited to vertical applications in the previous experimental works (L. Brown et al., 1976; Heskestad et al., 1983; Rana & Mannan, 2010). The nozzles tilted in the downwind direction may allow the water curtain system to be placed closer to the LNG source, as the trajectory of the water droplets will face the opposite direction of the potential LNG spill location.

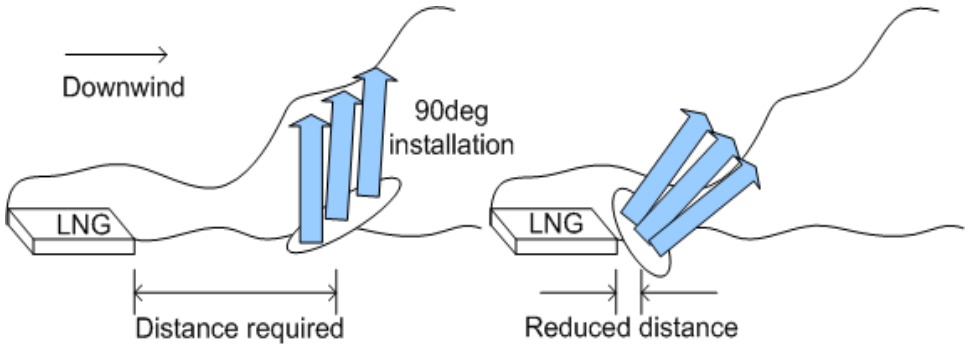

Fig. 71. Tilted configuration of water spray application

In this work, the nozzles were tilted at the angles of 30°, 45°, and 60°, and the effects on the behavior of LNG vapors for each scenario have been investigated. Fig. 71 shows a schematic of the water spray application tilted in the downwind direction, which had been applied in this modeling work. The water nozzles tilted in various angles discharge the droplets to different extents where the horizontal and vertical momentum forces from the water droplets will vary for each case. The vertical design (90°) was also considered to compare the vapor behavior with the water curtain application used in the previous experimental works. These configurations, in a real application, will allow the

water curtain system to be installed closer to the potential LNG spill without the risk of the water droplets entering the LNG pit.

5.2.4 Air Entrainment Rates

The air entrainment is one of the dominant physical mechanisms involved during the water spray applications, which promotes the mixing effects and enhances the vapor dispersion in the downwind region (CCPS, 1997). The air entrainment rate into the spray is mainly determined by the angle of the nozzle and a larger angle induces more air into the water spray (Rana, 2009). Nozzles with a small angle can provide higher entrained air velocity, while larger angle applications induce a higher entrained air rate. The flow pressure at the water source affects only the vertical coverage of the water spray and does not affect the air entrainment rate significantly.

The effects of different air entrainments on diluting the LNG vapors are evaluated for the upwards-oriented conical type water nozzle applications. The nozzle cone angles (30°, 45°, 60°, and 75°) were modified to apply various rates of air entrainment on the gas flow. The water droplets are dispersed from the nozzle within the prescribed angle assigned for each water spray application. The other operating parameters were set constant, and the vapor behavior and concentration changes in different elevations were compared.

5.3.1 Droplet Sizes

Figs. 72 and 73 show the predicted gas concentration results ([v/v] %) at ground level and 2.1 m elevation for the scenarios summarized in Table 3.

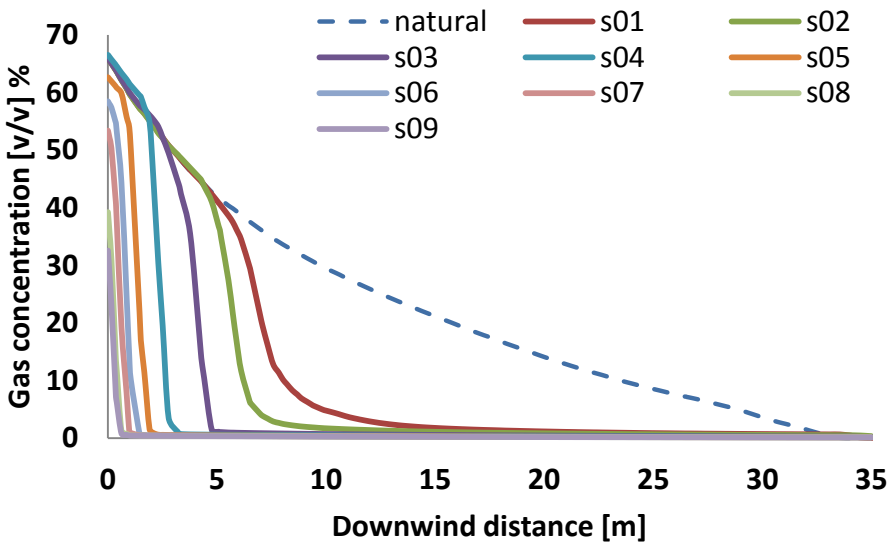

Fig. 72. LNG vapor concentration ([v/v] %) in downwind distances at ground level (z=0m) for various droplet applications

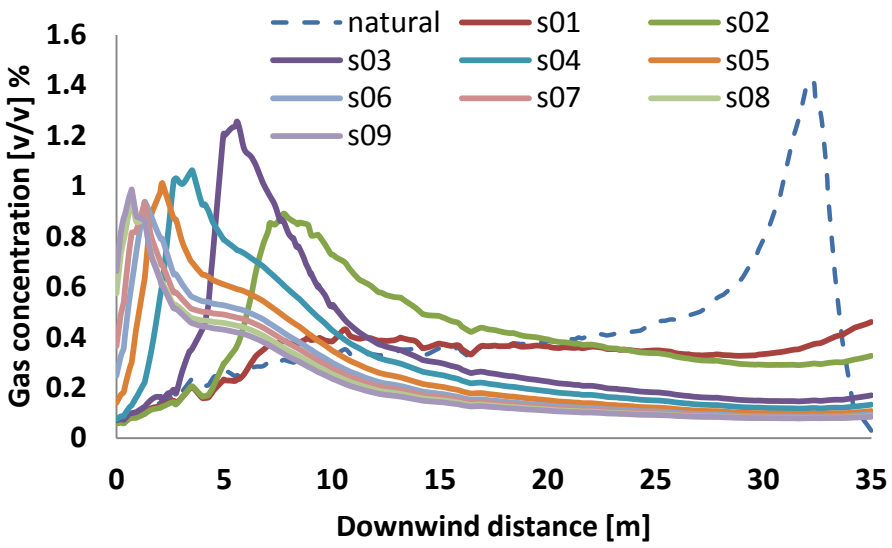

Fig. 73. LNG vapor concentration ([v/v] %) in downwind distances at z=2.1m elevation for various droplet applications

The LNG natural dispersion case (dotted line) shows that the concentration decreases as the vapors warm up sufficiently to disperse to atmosphere at the ground level. On the other hand, the vapor concentration increases gradually as the more buoyant vapors travel towards higher elevations at 2.1 m elevation. The vapor concentration drops to zero at approximately 31 m away from the LNG source as more buoyant vapors are present in this region. The vapor concentration for the forced mitigation cases in Fig. 68indicate that the mitigation effects become more apparent for the scenarios with finer droplet sizes (s09, 0.58 mm) compared to the larger droplets (s01, 1.43 mm). The smaller droplets are produced from the higher water pressure, which also increased the water flow rate. The momentum imposed from the water droplets is larger due to the higher flow rate, therefore, showed better concentration

reduction at the ground level. Most of the water curtain applications at 2.1 m elevation showed consistent dispersion effects, where the vapor concentration prediction ranged from 0.8 to1.0 [v/v] % as shown in Fig. 69. The scenario with 0.94 mm (s03) droplet size indicated higher concentration, showing approximately a 20 % increase of vapor concentration.

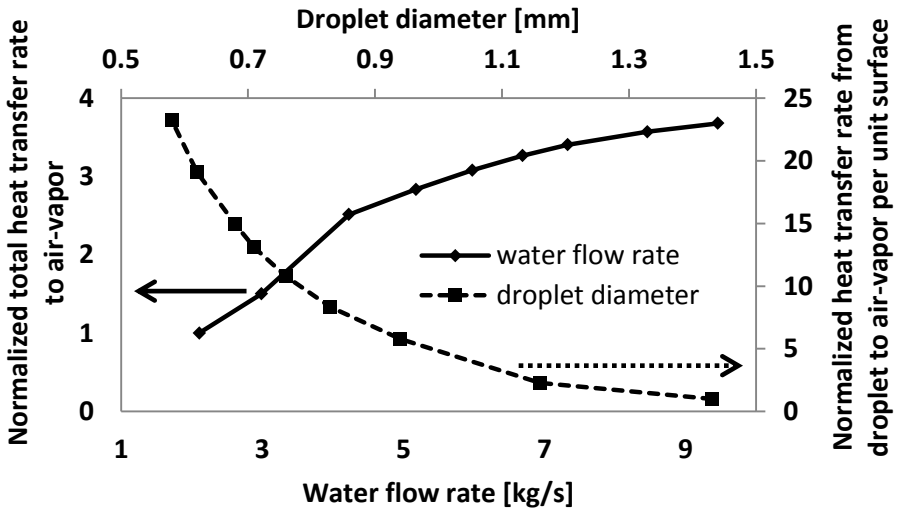

Fig. 74. Heat transfer rate from droplets and droplet surface to air-vapor mixture

To investigate the contribution of the heat effects from various droplet sizes, the overall amount of energy transferred from the water droplets dispersed in the gas phase was analyzed. Fig. 74 shows the total heat transfer rate from the droplets and droplet surface to air-vapor mixture. The heat transfer rate was normalized by the amount of the air-vapor mixture exiting the domain and the total amount of water droplets involved in the forced dispersion. The results clearly indicate that the total amount of heat

transferred from the water droplets to the air-vapor mixture increased proportionally as the water flow rate increased. More water droplets discharged from the nozzle introduced a sufficient heat source for greater thermal effects. The heat transfer from the surface of the water droplets was also evaluated using the droplet surface sizes applied in each scenario. The total amount of heat transferred from the droplet surface to air-vapor mixture decreased significantly as the droplet size increased. The amounts of the heat transfer provided from the finest droplet size (0.58 mm) showed more than 20 times of heat transfer involved from the droplet surface compared to the largest droplet (1.43 mm) applied. Smaller droplets provide larger surface areas per mass flow, where the convection heat transfer between the vapor and liquid phases mainly takes place.

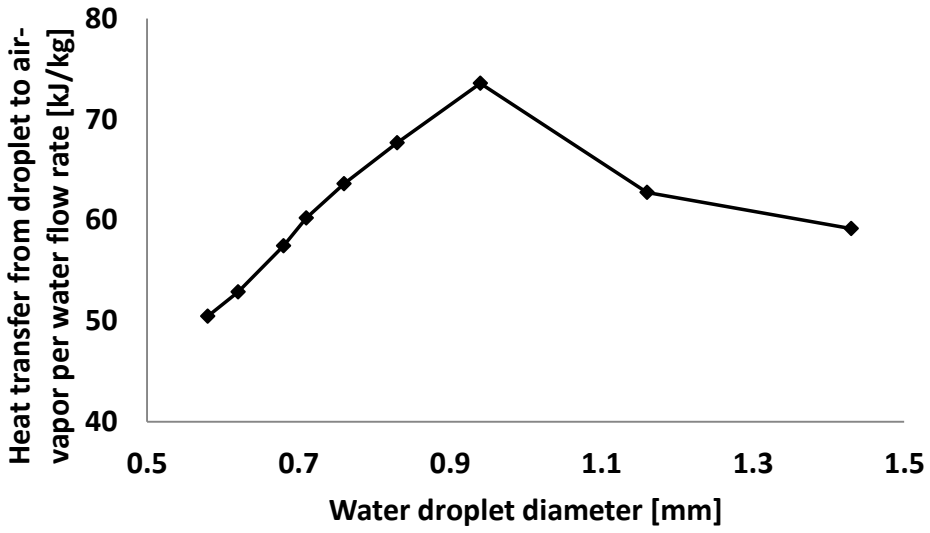

Fig. 75. Heat transfer rate per water flow rate

The total amount of heat transfer from each scenario was normalized using the water flow rate applied. The overall heat transfer effects induced from each droplet size are summarized in Fig. 75. The water droplet with 0.94 mm diameter showed the highest heat transfer rate from the water droplets per flow rate. This result is in agreement with the highest concentration observed for the droplet size of 0.94 mm (s03) at 2.1 m elevation in Fig. 73.

The operational condition of the water spray application, which induces the most effective thermal effects, can be identified as optimal setting. This setting allows the LNG vapors to disperse most effectively with adequate heat transfer. The Eulerian-Lagrangian spray model coupled with the gas flow model showed a rigorous approach in investigating the influence of the detailed characteristics of water droplets on the LNG forced dispersion. The optimal droplet size evaluated in this work corresponds to nozzle specified in Section 5.2.1 and could flexibility be applied for any types of nozzles given that the detail spray specifications are available.

5.3.2 Droplet Temperatures

The vapor behaviors induced from various levels of thermal effects were investigated by applying various water temperatures. The droplet temperatures were varied (283 K, 293 K, 303 K, and 313 K) while the other variables, such as the water droplet size and flow rate, were set constant. The water spray was applied using different droplet temperatures, until no further changes in the vapor behavior was observed.

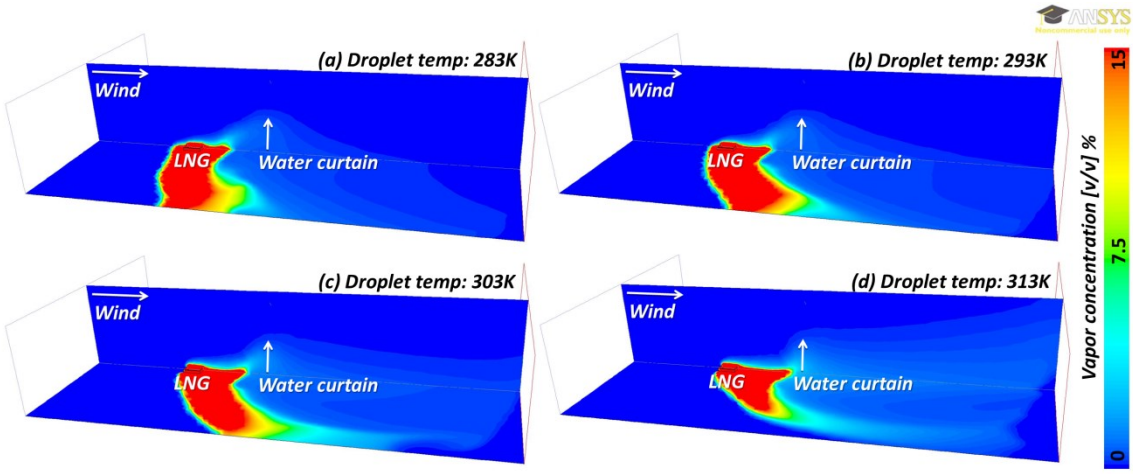

Fig. 76. LNG vapor contour ([v/v] %) of forced dispersion with various droplet temperatures; 283K, 293K, 303K, and 313K

Fig. 76 shows the vapor concentration contours ([v/v] %) of LNG forced dispersion with different water droplet temperature applications. The concentration of the air-vapor mixture is illustrated from 0 to 15 [v/v] %, which is the upper flammability limit (UFL) of LNG vapors. At the droplet temperature of 283 and 293 K, the LNG vapors travel back to the ground after interacting with the water droplets. This implies that the LNG vapors are not sufficiently warmed up to disperse at higher elevation. As the heavy LNG vapors stagger in the vicinity of the water spray, the air-vapor mixture is pushed to the side of the water spray, where there is relatively less dense air. The LNG vapors start propagating in the crosswind direction, traveling around the water spray region and significant amounts of the air-vapor mixture exit the domain through the side boundaries at the ground level. For the droplet temperature of 303 K, the amount of the air-vapor mixture exiting the domain through the side boundaries is reduced and more

vapors are lifted from the ground. The droplet temperature of 313 K shows the LNG vapors being sufficiently warmed up becoming buoyant vapors after the droplet-vapor interaction. The LNG vapors traveling in the crosswind direction at the ground and exiting the domain through the side boundaries are not observed.

The vapor contours indicate that droplets must provide adequate thermal transfer to promote the LNG vapors to be positively buoyant; otherwise, the effectiveness of dispersion can be rather limited. Some of the cases at lower droplet temperatures show potential hazards of having an under-designed mitigation system. The vapors started to travel around the water curtain region when the LNG vapors were insufficiently warmed up to gain buoyancy. This type of vapor behavior might create additional hazards during an LNG spill as the LNG vapor movement becomes less predictable. The study of various thermal effects from the water droplet can be used to determine the temperature criteria for designing an effective water spray system.

5.3.3 Installment Configurations

The locations of the water spray installation were set at 0 m, 2 m, 6 m, 10 m, 14 m, 18 m, 22 m, 26 m, and 30 m away from the LNG source. The configurations and operating conditions of the water spray system were set constant for all the scenarios.

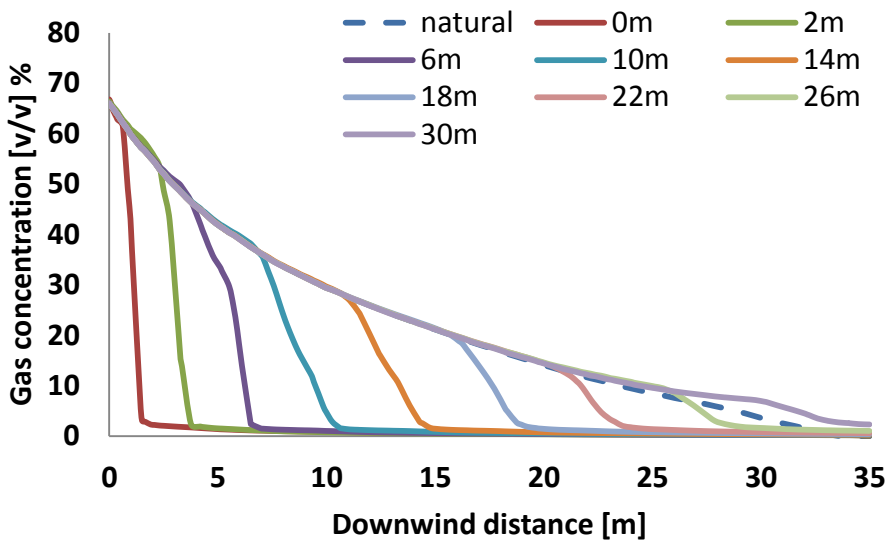

Fig. 77. LNG vapor concentration ([v/v] %) in downwind distances at ground level (z=0m) for different installation distances

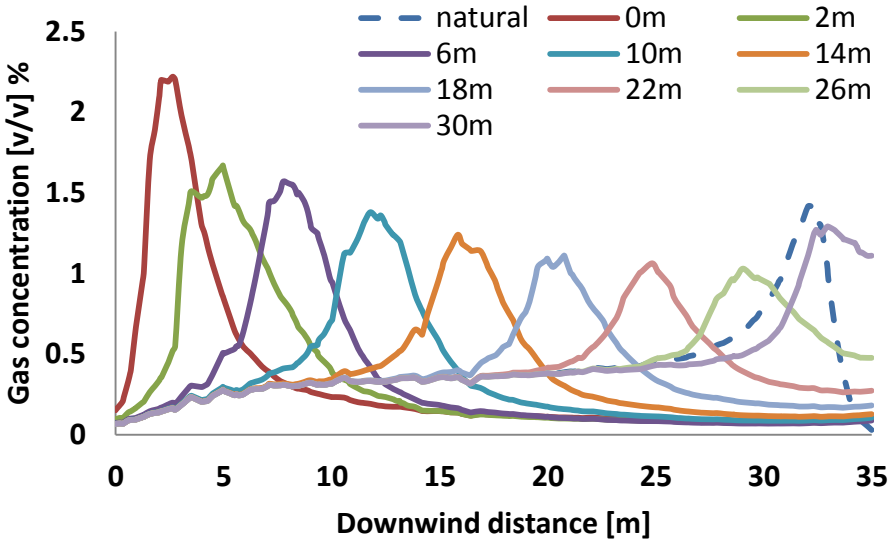

Fig. 78. LNG vapor concentration ([v/v] %) in downwind distances at ground level (z=2.1m) for different installation distances

Figs. 77 and 78 show the vapor concentrations ([v/v] %) at ground level and 2.1 m elevation. The vapor concentration decreased significantly in the vicinity of each water spray application at the ground level. The water curtain applied at 26 m and 30 m away from the LNG source showed no significant influence of the spray, but rather followed the LNG natural dispersion trend. The vapor concentration is the highest around the water spray at 2.1 m elevation and decreases as depicted in Fig. 78. The concentration decrease indicates that the vapors are dispersed in the atmosphere, as the concentration at the ground level shows no sign of accumulations as seen in Fig. 77. The water spray applied closest to the LNG source shows the highest vapor concentration approximately 2.5 [v/v] % at 2.1 m elevation, and the vapor concentration decreases as the location of the water spray application gets further away from the LNG source. This indicates that the water spray applied closer from the LNG source provides sufficient time to mix with air and disperse more effectively after interacting with water droplets.

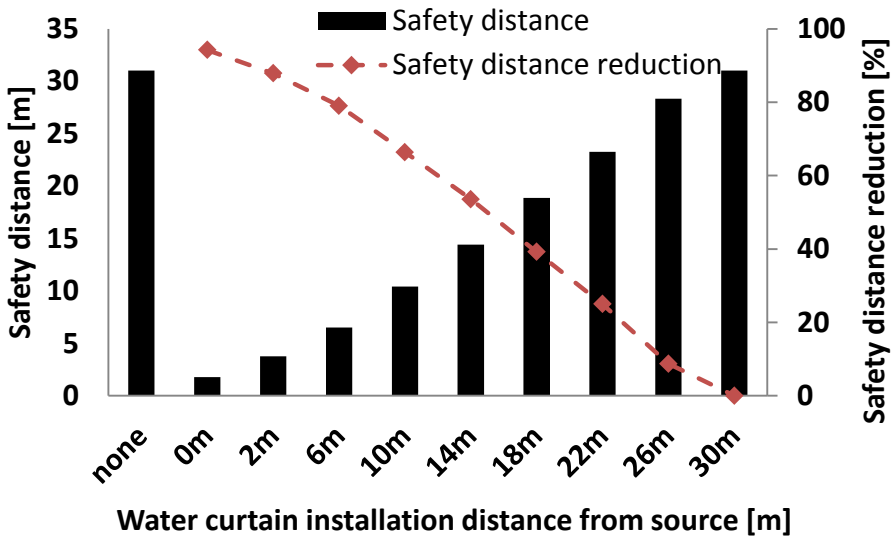

Fig. 79. Safety distance and distance reduction from various installation distances

Fig. 79 summarizes the safe distance and distance reduction evaluated from different locations of the water curtain applications. The safe distance, defined as where the LFL is decreased by 50 % (2.5 [v/v] %), reduced dramatically as the water curtain was installed closer to the LNG source. The water spray applied closest to the LNG source showed the maximum reduction of LNG vapor concentration at the ground level. The mitigation effects became less significant for the water spray installed further away from the LNG source, and for 26 m and 30 m cases, the reduction became below 10 %. The installation distance influences the concentration reduction at the ground level, as well as the buoyancy of the vapors in the post-spray region, as seen from higher elevations in Fig. 74. The results can be applied to develop a correlation of the mitigation effects to determine the distance factor when designing a water spray system.

5.3.4 Tilted Installations

The vapor concentration contours ([v/v] %) for the water nozzles tilted in various degrees are depicted in Fig. 80. The water spray system was set up at 2 m away from the LNG pit, which is approximately 2 m closer than the MKOPSC outdoor LNG spill experimental design.

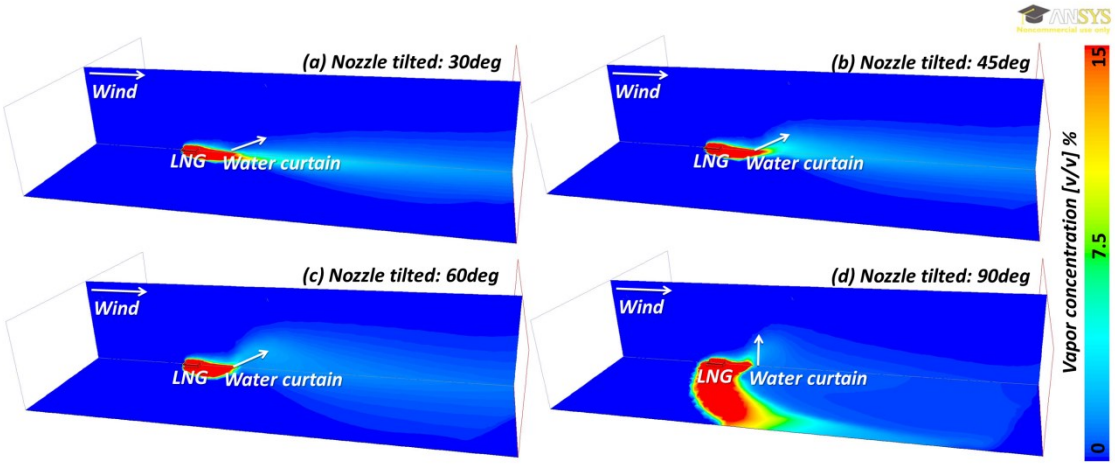

Fig. 80. Vapor concentration contour ([v/v] %) of LNG forced dispersion with modified nozzle installation (tilted); 30°, 45°, 60°, and 90°

The nozzles tilted at 30° and 45° showed the LNG vapors being guided in the direction of the water nozzle configuration. Significant amounts of LNG vapors traveling at the ground level were removed for the 30° and 45° cases. As the droplets are dispersed in the direction of the prevailing wind, the water spray does not impose any significant forces from the physical barrier created in the pathway of the LNG vapors. The nozzle tilted at 60° also shows a similar trend, where the LNG vapors are lifted from

the ground level and dispersed in the atmosphere. Whereas more vapors are observed traveling at the ground level for the 60° application, LNG vapors are also being encompassed in the spray region and are lifted to the atmosphere more effectively. This implies that the 60° application discharges the water droplets in the direction that envelopes the LNG vapors most effectively, while applying certain level of momentum in the pathway of the LNG vapors. The physical barrier imposed forces that enhance the LNG dispersion in the direction of prevailing wind. While the vapors are partially being pushed into the atmosphere for the vertical application (90°), a large portion of LNG vapors traveled around the water spray region as physical barriers are formed directly in the pathway of the LNG vapors. This tendency of LNG vapors traveling around the water spray is observed when ineffective mitigations are involved in dispersing the vapor clouds.

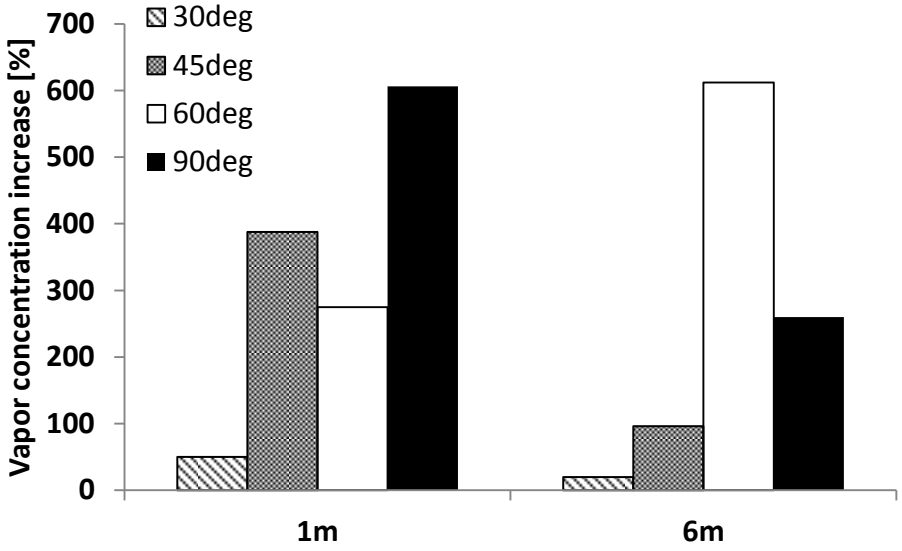

Fig. 81. Vapor concentration increase (%) at 1m and 6m with different nozzle installations (tilted); 30°, 45°, 60°, and 90°

Fig. 81 shows the vapor concentration increase (%) of the tilted nozzle applications at two different heights (1 m and 6 m). The vapor concentrations of LNG dispersion in the absence of water spray were used as a reference when evaluating the concentration increase at each elevation. For the water spray tilted 30° in the downwind direction, the concentration increased at both elevations, however, the concentration increase at 6 m elevation (20 %) decreased from the increase observed at 1 m elevation (50 %). The concentration at 1 m elevation for 45° tilted installation shows approximately a 390 % increase of concentration, which dropped to 100 % increase at the 6 m elevation. The water curtain applied vertically (90°) shows the highest concentration increase of approximately 600 % at 1 m elevation. This indicates that the water curtain applied vertically is the most effective in forcing the LNG vapors to

disperse into the atmosphere at the lower elevation, pushing approximately 6 times more LNG vapors. The concentration at 6 m elevation shows approximately a 260 % concentration increase, which is still a large increase compared to the 30° and 45° applications. The water curtain tilted at 60° showed a 280 % increase at lower elevation (z = 1 m) and shows approximately a 600 % increase of vapor concentration at 6 m elevation. The nozzle tilted at 60° is the only case where the concentration increase at 6 m elevation is higher than 1 m elevation, increasing from 280 % to 600 %. This implies that the water spray tilted at 60° is most effective in dispersing the LNG vapors into higher elevation and continuously promoting the vapors to disperse to the atmosphere. For the vertically installed water spray application (90°), although the vapors were pushed effectively in the vicinity of the water spray, most of the vapors traveled in the crosswind direction or propagated at the lower level around the water spray region as shown in Fig. 80.

The LNG forced dispersion becomes more effective as the water spray lifts the vapors away from the ground level. However, the results from applying various configurations imply that the systematic criteria for the forced mitigation must ensure that the LNG vapors are removed from the ground level and allowed to constantly disperse to the atmosphere. The results of water curtains tilted at 30°, 45°, and 90° indicate that these cases show limited mitigation effects. Whereas the vapor concentration increased both at 1 m and 6 m elevation, the concentration increase reduces to below one half at 6 m elevation for 30°, 45°, and 90° cases. The 60° application shows the ideal forced dispersion scenario, where the vapor concentration

increases more at higher elevation. This might be due to the nozzles tilted at 60° directs the LNG vapors most effectively to the atmosphere, which prevents the vapors from traveling back to the ground level or being pushed to sideways away from the water spray region.

5.3.5 Nozzle Angle Sizes

The effects of various air entrainments on LNG vapor behavior were investigated using nozzles with different angle sizes. Fig. 82 shows the vapor concentration contour ([v/v] %) for different conical nozzle angles (30°, 45°, 60°, and 75°).

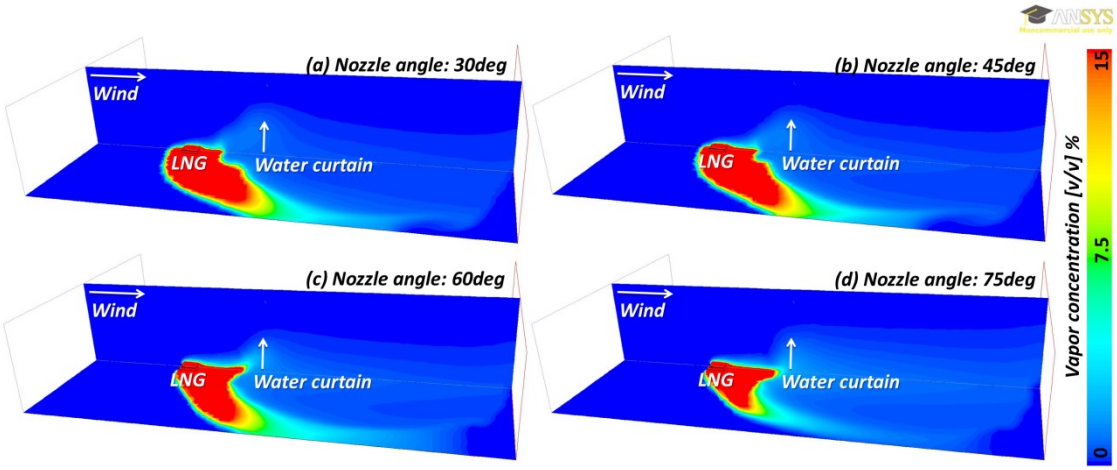

Fig. 82. Vapor concentration contour ([v/v] %) of LNG forced dispersion with different nozzle angle size; 30°, 45°, 60°, and 75°

The concentration contours for nozzle angle size 30°, 45°, and 60° show vapors being lifted around the water spray region, however, the vapors travel back to the lower

level as the vapors propagated in the downwind region. For the nozzle angle size of 75°, the vapors are dispersed more effectively in the atmosphere and shows less vapors traveling at the ground level. This implies that the LNG vapors are well mixed with the air and diluted to become more buoyant with 75° application.

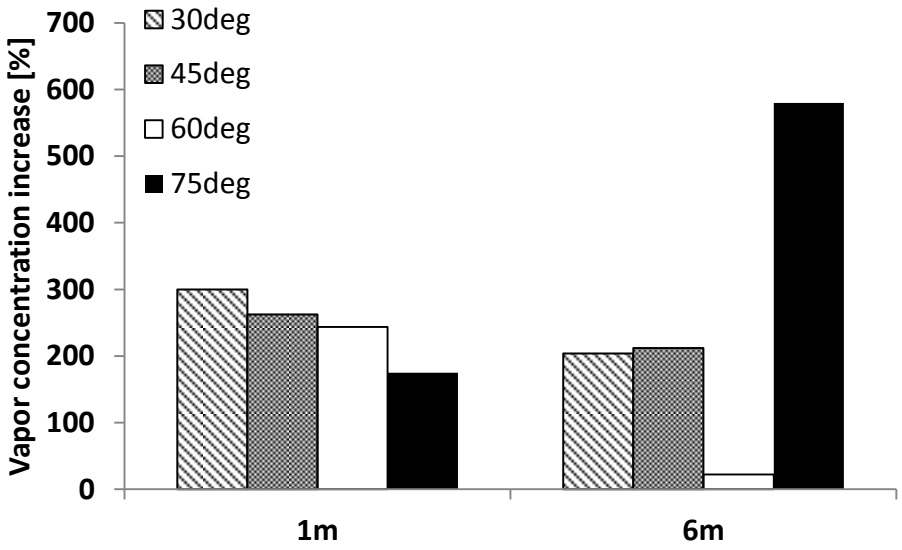

Fig. 83. Vapor concentration increase (%) at 1m and 6m with different nozzle angle size; 30°, 45°, 60°, and 75°

Fig. 83 quantifies the vapor concentration increase (%) of the forced mitigation application at two elevations (1 m and 6 m) for different nozzle angle sizes. At 1 m elevation, the smallest nozzle angle application (30°) shows the largest increase of 300 %, and the concentration increase declines as the size of the angle increases. This may be due to the high-entrained air velocity induced from smaller angle size applied, which allows more LNG vapors to be lifted instantly after spray region. The

concentration at 6 m elevation show approximately similar increase, around 210 % to 220 % for the nozzles with the angle size 30°, 45°, and 60°. The 75° application shows approximately a 580 % increase at 6 m elevation, which is more than double the increase observed for other cases. The significant increase for the nozzle angle at 75° can be explained by the air entrainment rates as the rest of the conditions were set constant. As the 75° nozzle entrains more air into the spray, the mixing effects become more dominant. More vapors travel to higher elevation as sufficient mixing promotes buoyancy of the LNG vapors.

The concentration increase at different heights clearly demonstrated that the nozzles that could provide sufficient air entrainment could dilute the air-vapor mixture and disperse the vapors to higher elevation. The effectiveness of tilted installation designs and different air entrainment rate cases were evaluated by comparing the behavior of LNG vapors and concentration increases at different elevations. Additional forces introduced from the water droplets to the air-vapor mixture induce distinct turbulent flows, which will result in different level of mixing within the air-vapor mixture. A further investigation on various turbulent effects from different spray applications is required to understand the underlying physical mechanisms of the modified configurations and various design applications.

5.4 Conclusion

The CFD modeling provides a promising solution in addressing the gaps from the limited experimental results. This work uses the multiphase flow model, which has

evolved significantly in providing an intricate description of the droplet interaction with the gas flows. The integral-type models provided limited predictions of water spray applications that were bounded by the predetermined parameters, such as barrier porosity. The CFD modeling also provided a promising solution in addressing the gaps from the limited experimental results. The Eulerian-Lagrangian spray model coupled with the LNG gas flow showed the detailed prediction of the vapor behavior, which had been unavailable through applying the integral-type modeling. The CFD code integrated the influence of the water droplets dispersed in the LNG gas flow in the fundamental calculation of fluid flow and provided intrinsic description of the flow prediction. The prediction of how LNG vapors may behave after applying certain level of mitigation measures will assist in predicting any unforeseen hazards that may caused by the under-sized mitigation.

The effectiveness of a water spray application depends on multiple parameters, such as potential LNG release sizes, atmospheric conditions, and site-specified criteria. The spray model coupled with validated CFD code can provide wide applications in terms of understanding the complex LNG vapor interaction with water droplets. The results of this work can provide a robust analogy in determining the impact of an LNG spill and can alleviate the concerns over the public safety and security around LNG facilities.

CHAPTER VI

CONCLUSIONS AND RECOMMENDATIONS

6.1 Conclusions

A numerical simulation approach using CFD code has been proposed to investigate the forced dispersion of LNG vapor clouds using a water curtain application. The model was calibrated with experimental data from the MKOPSC outdoor LNG spill experiment of March 2009. The measured concentration data were compared with the prediction results to calibrate some of the physical parameters for the LNG natural dispersion. The dilution factor evaluated from the experimental results was used to calibrate the physical parameters, such as the parcels produced from the nozzle, as well as the initial droplet velocity, for forced dispersion modeling using the Eulerian-Lagrangian approach.

The CFD codes provide detailed flow movement of LNG vapors, which can assist in designing a site-specified mitigation system. Various physical mechanisms involved in the forced dispersion of LNG vapors were evaluated. The mass flow rates showed the direct correlation to how much vapors were lifted from the ground level, while sufficient droplet velocity ensured the LNG vapors dispersed to atmosphere. Also, the overall momentum transfer results indicate that the effectiveness of the LNG forced dispersion will be limited when either mass flow rate or droplet velocity was set at inadequate level. The minimum operating conditions for this research were mass flow rate set above 3 kg/s and droplet velocity higher than 12–15 m/s per nozzle. The effects

of various thermal transfers from the droplets to the vapors were compared using different water droplet temperatures. The higher droplet temperatures allowed the LNG vapors to be sufficiently warm up to disperse to higher elevations. The vapor behaviors indicated that the thermal effects induced significant turbulence within the air-vapor mixture. For the air entrainments, the dilution effects improved with larger amount of entrained air, which allowed more vapor clouds to be dispersed into higher elevation. However, the turbulence effects played less significant role in air entrainments compared to the thermal effects, and the mixing mainly enhanced the dilution effects.

A parametric study has been conducted on different operating variables for designing an effective LNG forced dispersion system using water sprays. The Eulerian-Lagrangian approach integrates the influence from various droplet characteristics in the governing equations of momentum and energy to account for the spray effects. The CFD codes captured the subtle differences of heat transfer rates induced from various droplet sizes, which subsequently influenced the overall vapor dispersion. The optimum droplet size was verified, which induces the maximum thermal effects with the minimum water flow. Also, the effects of various air entrainments, configurations, installation distances, and droplet temperatures were investigated by integrating the spray characteristics directly to the constitutive equations of LNG flows.

The work presented here shows a promising solution for conducting a detailed parametric study of design parameters needed to optimize the water spray mitigation system for LNG facilities. The Eulerian-Lagrangian approach using a CFD code is capable of taking into account the forced dispersion parameters in detail, such as the

droplet size, flow rate, and initial spray velocity for various configurations. Sensitivity analysis on the key design parameters can provide guidance for defining the optimal operation conditions for an effective water curtain system. Also, the analysis from this work can serve as an engineering guideline in determining the level of risk reduction when applying a water curtain system for a LNG facility.

6.2 Recommendations for Further Research

This research proposed an alternative methodology in evaluating the forced mitigation effects using the water spray application on LNG vapors. The CFD modeling in this research applied k-ϵ turbulence model, which is one of the recommended turbulence models for simulating the LNG vapor dispersion. It was chosen to optimize the simulation time with the accuracy by simplifying the complex LNG turbulence motion. Further study is required to verify critical physical parameters involved in the forced dispersion of LNG vapors, which could help provide the model prediction more accurately.

This research applied the LNG source term adopted from experimental design used in March 2009 test. The main focus of this research was to investigate the interaction of droplet-LNG vapor system, and the effects of the LNG source size had not been evaluated. The mitigation effects on the larger scale LNG release using water spray application may show different level of mitigation effects. The integral type models assume the dilution effects determined through semi-empirical function. Therefore, it is difficult to predict the mitigation effects for the particular scenarios that do not have

empirical data set. The larger LNG spill will generate more LNG vapors and threshold limit may exist for a certain water spray application. A larger LNG spill may show relatively less or even no dilution effects beyond certain level. The correlations of the LNG spill size and effectiveness of water curtain should be addressed. This analysis can provide the minimum capacity specifications of the mitigation system for a site-specific water spray application.

A parameter that could define the overall effectiveness of the LNG forced dispersion can assist in incorporating the water spray system as part of the protection layer. The NFPA 59A revised in 2013 requires a quantitative risk assessment for the newly proposed LNG facilities or for any existing facilities with major modifications. The risk assessment must prove that the LNG facility does not impose risk beyond the tolerable level to the communities around. NFPA 59A recommends additional safety measures to be considered to meet the risk criteria. The universal parameter that could define the risk reduction of the water spray application will allow the water spray system to be considered in the risk assessment procedures in more systematic approach.

A total of three different commercial water spray nozzles were tested during the March 2009 LNG spill experiment: conical, flat-fan, and fog type. The conical upward oriented nozzles were evaluated in this research, because it was concluded that the full cone applied upward was most effective in diluting the LNG vapors in all elevations. Also, the full-cone type has been widely studied to evaluate the air entrainment rates. The flat-fan type is widely used in the industry for covering broader range of area. The Eulerian-Lagrangian spray code could be modified using the specific inlet domain of

droplet to simulate the flat-fan type spray nozzle. Further clarification on the dilution effects and droplet interaction with the vapors using the flat-fan type application will allow better implementation of the various nozzle types in the LNG facility.

This research used the ANSYS Fluent CFD code to simulate the LNG vapor dispersion and spray interaction. There are other CFD codes available for simulating the Eulerian-Lagrangian spray model coupled with the LNG vapor dispersion. The Fire Dynamic Simulator (FDS) has been developed by the National Institute of Standards and Technology (NIST). The FDS is an open source code developed to evaluate different effects of fire and the suppression methods. The FDS code is also capable of simulating the gas dispersion and has been studied by many to investigate the effects of various passive mitigation systems. FDS is also equipped with the Eulerian-Lagrangian spray model that could evaluate the spray interaction with the LNG vapors. Once validated, the FDS can be widely used for the LNG industry with less complication.

NOMENCLATURE

A_p	surface area of the droplet (m^2)
c_{p_p}	heat capacity of the droplet [J/(kg-K)]
C_{pk}	specific heat of species *k*
C_D	drag coefficient (smooth particle)
d_p	droplet diameter (m)
D	pool diameter (m)
F_{ex}	external body forces
F_x	virtual mass force and additional acceleration force of droplet
g	gravitational acceleration
H_{pyrol}	heat of pyrolysis of droplet as volatiles are evolved (J/kg)
H_{latref}	latent heat of droplet at reference conditions (J/kg)
h	enthalpy
h_{ref}	reference height (m)
h_∞	convective heat transfer coefficient [W/(m^2-K)]
j_k	diffusive flux
k	turbulent kinetic energy
K	von Karman constant (≈ 0.4)
m_k	mass fraction of species *k*
m_p	mass of the droplet (kg)

$m_{p,0}$	initial mass of the droplet (kg)
$\dot{m}_p$	mass flow rate of the droplet (kg/s)
$\dot{m}_{p,0}$	initial mass flow rate of the droplet injection (kg/s)
$m_{p\text{in}}, m_{p\text{out}}$	mass of the droplet upon cell entry and exit (kg)
p	pressure
q	flux of enthalpy
Re	Reynolds number
S_h	volumetric source of enthalpy
S_k	mass production rate of species *k*
T_∞	local temperature of the continuous phase (K)
T_i	turbulence intensity (1–10 %)
$T_{p\text{in}}, T_{p\text{out}}$	temperature of the droplet upon cell entry and exit (K)
T_{ref}	reference temperature (K)
u	velocity of fluid phase (m/s)
U	wind velocity
u_*	friction velocity (m/s)
U_h	specified velocity at reference height (m/s)
u_p	velocity of droplet (m/s)
v_g	inlet pool velocity for LNG source (m/s)
z_0	surface roughness length (m)

Greek letters

δ_{ij}	Kronecker delta (δ_{ij} = 1 if $i = j$ and δ_{ij} = 0 if $i \neq j$)
ϵ	turbulent dissipation
ϵ_p	droplet emissivity
θ_R	radiation temperature
κ	coefficient of bulk viscosity
μ	coefficient of viscosity
μ_t	eddy viscosity
π	molecular flux of momentum
ρ_p, ρ	density of the droplet and fluid phase, relatively
$(\rho v)_{\text{liq}}$	mass flux of LNG (kg/m^2-s)
ρ_{g}	natural gas density (1.76 kg/m^3 at 111 K)
σ	Stefan-Boltzmann constant
τ	viscous stress tensor

Abbreviation

ALARP	As low as reasonably practicable
BFTF	Brayton Fire Training Field
BLEVE	Boiling liquid expanding vapor explosion
Btu	British thermal units
CPU	Central processing unit
CBM	Coal bed methane
CFR	Code of Federal Regulation
CNG	Compressed natural gas
CFD	Computational fluid dynamics
DPM	Discrete phase model
FERC	Federal Energy Regulatory Commission
GRI	Gas Research Institute
LFL	Lower flammability limit
LNG	Liquefied natural gas
MKOPSC	Mary Kay O'Connor Process Safety Center
NFPA	National Fire Protection Association
OD	Outer diameter
RANS	Reynolds-averaged Navier-Stokes
RKF45	Runge-Kutta-Fehlberg
RPT	Rapid phase transition

SMD	Sauter mean diameter
TKE	Turbulence kinetic energy
UFL	Upper flammability limit

REFERENCES

Abraham, J. (1997). What is adequate resolution in the numerical computations of transient jets? (SAE technical paper series: 970051). Warrendale, PA: Society of Automotive Engineers, Inc.

Alessandri, E., Buchlin, J. M., Cavallini, A., Patel, M. K., & Galea, E. (1996). *On the modelling of the thermal interactions between a spray curtain and an impinging cold gas cloud.* London, UK: CMS Press.

Alinot, C., & Masson, C. (2005). k-ϵ model for the atmospheric boundary layer under various thermal stratifications. *Journal of Solar Energy Engineering, 127,* 438-443.

ANSYS. (2009). *ANSYS Fluent 12.0 theory guide*. Canonsburg, PA: ANSYS Inc.

Atallah, S., Guzman, E., & Shah, J. N. (1988). Water spray barriers for LNG vapor mitigation (GRI-89/0008). Chicago, IL: Gas Research Institue.

Barry, R. G., & Chorley, R. J. (2003). *Atmosphere, weather, and climate (8th ed.).* New York, NY: Routledge.

BETE. (2007). *Nozzles for industry, pollution control and fire protection.* Greenfield, MA: BETE Fog Nozzle Inc.

BP. (2007). *LNG fire protection and emergency response (2nd ed.).* Rugby, UK: Institution of Chemical Engineers.

BP. (2012). *Statistical review of world energy 2012.* London, UK: BP p.l.c.

Brown, L., Martinsen, W., Muhlenkamp, S., & Puckett, G. (1976). Small scale tests on control methods for some liquefied natural gas hazards. Washington DC: US Coast Guard.

Brown, T. C., Cederwall, R. T., Chan, S. T., Ermak, D. L., Koopman, R. P., Lamson, K. C., McClure, J. W., & Morris, L. K. (1990). Falcon series data report 1987 LNG vapor barrier verification field trials. Livermore, CA: Gas Research Institute.

CCPS. (1997). *Guideline for postrelease mitigation technology in the chemical process industry*. New York, NY: Center for Chemical Process Safety, American Institute of Chemical Engineers.

Cormier, B. R., Qi, R., Yun, G., Zhang, Y., & Mannan, M. S. (2009). Application of computational fluid dynamics for LNG vapor dispersion modeling: A study of key parameters. *Journal of Loss Prevention in the Process Industries, 22*, 332-352.

Crowe, C. T. (2006). *Multiphase flow handbook*. Boca Raton, FL: CRC Taylor & Francis.

Crowe, C. T., Sharma, M. P., & Stock, D. E. (1977). The particle-source-in cell (PSI-CELL) model for gas-droplet flows. *Journal of Fluids Engineering, 99*, 325-332.

Crowe, C. T., Sommerfeld, M., & Tsuji, Y. (1998). *Multiphase flows with droplets and particles.* Boca Raton, FL: CRC Press.

Dawe, R. A., & Lucas, A. G. (2000). *Modern petroleum technology (6th ed.)*. Chichester; NY: John Wiley & Sons.

DOE. (2003a). Balancing natural gas policy: fueling the demands of a growing economy (Vol. V: Transmission & distribution task group report and LNG subgroup report). Washington, DC: National Petroleum Council.

DOE. (2003b). Balancing natural gas policy: fueling the demands of a growing economy (Vol. II: Integrated report). Washington, DC: National Petroleum Council.

Drube, T., Haukoos, B., Thompson, P., & Williams, G. (2012). An initial qualitative discussion on safety considerations for LNG use in transportation. Washington, DC: National Petroleum Council.

Dukowicz, J. K. (1980). A particle-fluid numerical model for liquid sprays. *Journal of Computational Physics, 35*, 229-253.

EIA. (2011). *International energy outlook 2011.* Washington, DC: US Energy Information Administration.

EIA. (2012). *Annual energy outlook 2012 with projections to 2035.* Washington, DC: US Department of Energy.

Ermak, D. L., Chan, S. T., Morgan, D. L., & Morris, L. K. (1982). A comparison of dense gas dispersion model simulations with burro series LNG spill test results. *Journal of Hazardous Materials, 6*, 129-160.

Forsythe, G. E., Malcolm, M. A., & Moler, C. B. (1977). *Computer methods for mathematical computation.* Englewood Cliffs, NJ: Prentice-Hall.

Foss, M. M. (2003). *LNG safety and security.* Houston, TX: Center for Energy Economics.

Foss, M. M. (2007). *Introduction to LNG: An overview on liquefied natural gas (LNG), its properties, organization of the LNG industry and safety considerations.* Houston, TX: Center for Energy Economics.

Gant, S. E. (2006). CFD modelling of water spray barriers (HSL/2006/79). Derbyshire, UK: Health & Safety Laboratory.

Gavelli, F., Bullister, E., & Kytomaa, H. (2008). Application of CFD (Fluent) to LNG spills into geometrically complex environments. *Journal of Hazardous Materials, 159*, 158-168.

Gavelli, F., Chernovsky, M. K., Bullister, E., & Kytomaa, H. K. (2009). Quantification of source-level turbulence during LNG spills onto a water pond. *Journal of Loss Prevention in the Process Industries, 22*, 809-819.

Hald, K. (2005). *Forced dispersion of heavy gas clouds by water curtain.* PhD dissertation, Department of Environmental and Applied Fluid Dynamics, von Karman Institute, Sint-Genesius-Rode, Belgium.

Hald, K., Buchlin, J. M., Dandrieux, A., & Dusserre, G. (2005). Heavy gas dispersion by water spray curtains: A research methodology. *Journal of Loss Prevention in the Process Industries, 18*, 506-511.

Heskestad, G., Kung, H. C., & Todtenkopf, N. F. (1981). Air entrainment into water sprays (Report No 22533). Norwood, MA: Factory Mutual Research Corporation.

Heskestad, G., Meroney, R. N., Kothari, K. M., & Neff, D. E. (1983). Effectiveness of water spray curtains in dispersing LNG vapor clouds (Paper No 83-T-69). Paper presented at *The American Gas Association Transmission Conference, Seattle, WA.*

Hightower, M., Gritzo, L., Luketa-Hanlin, A., Covan, J., Tieszen, S., Wellman, G., Irwin, M., Kaneshige, M., Melof, B., Morrow, C., & Ragland, D. (2004). Guidance on risk analysis and safety implications of a large liquefied natural gas (LNG) spill over water (SAND2004-6258). Albuquerque, NM: Sandia National Laboratories.

IEA. (2011). *World energy outlook 2011: Are we entering a golden age of gas?* Paris, France: International Energy Agency.

ISGINTT. (2010). *International safety guide for inland navigation tank-barges and terminals.* Strasbourg, France: Central Commission for the Navigation of the Rhine.

Ivings, M. J., Jagger, S. F., Lea, C. J., & Webber, D. M. (2007). Evaluating vapor dispersion models for safety analysis of LNG facilities. Derbyshire, UK: Health Safety Laboratory.

Jiang, X., Siamas, G., Jagus, K., & Karayiannis, T.G. (2010). Physical modelling and advanced simulations of gas-liquid two-phase jet flows in atomization and sprays. *Progress in Energy and Combustion Science, 36*, 131-167.

Kim, B. K., Ng, D., Mentzer, R. A., & Mannan, M. S. (2012). Modeling of water spray application in the forced dispersion of LNG vapor cloud using a combined Eulerian-Lagrangian approach. *Industrial & Engineering Chemistry Research, 51*, 13803-13814.

Kumar, S., Kwon, H. T., Choi, K., Cho, J., Lim, W., & Moon, I. (2011). Current status and future projections of LNG demand and supplies: a global prospective. *Energy Policy, 39*, 4097-4104.

Lane, W. R. (1951). Shatter of drops in streams of air. *Industrial & Engineering Chemistry Research, 43*, 1312-1317.

Lom, W. L. (1974). *Liquefied natural gas*. New York, NY: John Wiley & Sons.

Lopez, J. P., Badin, J., Lieto, J., & Grollier-Baron, R. (1989). Water spray and steam curtain design: a common research programme. Paper presented at *The Control of Accidental Releases of Hazardous Gases, AICHE, Philadelphia, PA.*

Luketa-Hanlin, A., Koopman, R. P., & Ermak, D. L. (2007). On the application of computational fluid dynamics codes for liquefied natural gas dispersion. *Journal of Hazardous Materials, 140*, 504-517.

Mannan, M. S. (2012). *Lees' loss prevention in the process industries (4th ed.).* Waltham, MA: Elsevier.

Martinsen, W. E., Muhlenkamp, S. P., & Olson, J. (1977). Disperse LNG vapors with water. *Hydrocarbon Processing*, 260-267.

McQuaid, J. (1977). The design of water-spray barriers for chemical plants. Paper presented at *The 2nd International Symposium on Loss Prevention and Safety Promotion in the Process Industries, Heidelberg, Germany.*

McQuaid, J., & Fitzpatrick, R. D. (1981). The uses and limitations of water-spray barriers. In the Containment and Dispersion of Gases by Water Sprays, North Western Branch Papers, Manchester, UK: Institution of Chemical Engineers.

McQuaid, J., & Fitzpatrick, R.D. (1983). Air entrainment by water sprays: strategies for application to the dispersion of gas plumes. *Journal of Occupational Accidents, 5*, 121-133.

Meroney, R., & Neff, D. (1985). Numerical modelling of water spray barriers for dispersing dense gases. *Boundary-layer meteorology, 31*, 233-247.

Meroney, R., & Shin, S. H. (1992). Depth-integrated dispersion model prediction of dense gas dispersion in the presence of barriers and water spray curtains. Paper presented at *The Measurement and modeling of environmental flows, ASME, Anaheim CA*.

MKOPSC. (2010). Data report of MKOPSC LNG spill tests: 2005-2009. College Station, TX: Mary Kay O'Connor Process Safety Center, Texas A&M University.

Mokhatab, S., Poe, W. A., Speight, J. G., Zatzman, G., Islam, M. R., & Wassenhove, W. (2006). *Handbook of natural gas transmission and processing*. Burlington, MA: Gulf Professional Pub.

Moore, P., & Rees, W. D. (1981). Forced dispersion of gases by water and steam. In the Containment and Dispersion of Gases by Water Sprays, North Western Branch Papers, Manchester, UK: Institution of Chemical Engineers.

Morsi, S. A., & Alexander, A. J. (1972). An investigation of particle trajectories in two-phase flow systems. *Journal of Fluid Mechanics, 55*, 193-208.

NFPA. (2013). *NFPA 59A: standard for the production, storage, and handling of liquefied natural gas (LNG).* Quincy, MA: National Fire Protection Agency.

Nijdam, J. J., Guo, B., Fletcher, D.F., & Langrish, T.A.G. (2004). Challenges of simulating droplet coalescence within a spray. *Drying Technology: An International Journal, 22*, 1463-1488.

Qi, R., Ng, D., Cormier, B. R., & Mannan, M. S. (2010). Numerical simulations of LNG vapor dispersion in Brayton Fire Training Field tests with ANSYS CFX. *Journal of Hazardous Materials, 183*, 51-61.

Rana, M. (2009). *Forced dispersion of liquefied natural gas vapor clouds with water spray curtain application.* PhD Dissertation, Department of Chemical Engineering, Texas A&M University, College Station, TX.

Rana, M., Guo, Y., & Mannan, M. S. (2010). Use of water spray curtain to disperse LNG vapor clouds. *Journal of Loss Prevention in the Process Industries, 23*, 77-78.

Rana, M., & Mannan, M. S. (2010). Forced dispersion of LNG vapor with water curtain. *Journal of Loss Prevention in the Process Industries, 23*, 768-772.

Ranade, V. (2002). *Computational flow modeling for chemical reactor engineering*. Waltham, MA: Elsevier Academic Press.

Reid, R. C. (1983). Rapid phase transitions from liquid to vapor. *Advances in Chemical Engineering, 12*, 105-208.

Richards, P. J., & Hoxey, R. P. (1993). Appropriate boundary conditions for computational wind engineering models using the k-ϵ turbulence model. *Journal of Wind Engineering and Industrial Aerodynamics, 46*, 145-153.

Spicer, T. O., & Havens, J. A. (1987). Field test validation of the DEGADIS model. *Journal of Hazardous Materials, 16*, 231-245.

St-Georges, M., & Buchlin, J. M. (1994). Detailed single spray experimental measurements and one-dimensional modelling. *International Journal of Multiphase Flow, 20*, 979-992.

Title 49 Code of Federal Regulations Part 193 (2000). Liquefied natural gas facilities: Federal safety standards (49-CFR-193). Washington DC: US Government Printing Office.

Tu, J., Yeoh, G., & Liu, C. (2008). *Computational fluid dynamics: a practical approach.* Boston, MA: Butterworth-Heinemann.

Uzanski, D.T., & Buchlin, J.M. (1998). Mitigation of industrial hazards by water spray curtains. Paper presented at *The International Emergency Management Conference 1998: disaster and emergency management, international challenges for the next decade, Washington, DC.*

Yun, G. W., Ng, D., & Mannan, M. S. (2011a). Key findings of liquefied natural gas pool fire outdoor tests with expansion foam application. *Industrial & Engineering Chemistry Research, 50*, 2359-2372.

Yun, G. W., Ng, D., & Mannan, M. S. (2011b). Key observations of liquefied natural gas vapor dispersion field test with expansion foam application. *Industrial & Engineering Chemistry Research, 50*, 1504-1514.

Zalosh, R., Alpert, R. L., & Heskestad, G. (1983). Dispersal of LNG vapor clouds with water spray curtains: annual report - phase 1 (Report No. GRI-80/0107). Chicago, IL: Gas Research Institute.